Transportation Consortium of South-Central States

Solving Emerging Transportation Resiliency, Sustainability, and Economic Challenges through the Use of Innovative Materials and Construction Methods: From Research to Implementation

Self-Healing Microcapsules as Concrete Aggregates for Corrosion Inhibition in Reinforced Concrete

Project No. 17CLSU08

Lead University: Texas A&M University

Collaborative Universities: Louisiana State University

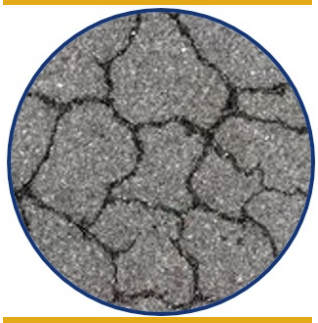

Enhancing Durability and Service Life of Infrastructure

Final Report

November 2018

Disclaimer

The contents of this report reflect the views of the authors, who are responsible for the facts and the accuracy of the information presented herein. This document is disseminated in the interest of information exchange. The report is funded, partially or entirely, by a grant from the U.S. Department of Transportation's University Transportation Centers Program. However, the U.S. Government assumes no liability for the contents or use thereof.

Acknowledgments

The authors would like to acknowledge the laboratory support from the Louisiana Transportation Research Center (LTRC), and the technical expertise of Dr. William Daly and Dr. Ioan Negulescu. The authors would also like to acknowledge the work and contributions from Reece Goldsberry, and Melvin McElwee. This study is part of the project 17CLSU08 funded by the Transportation Consortium of South-Central States (Tran-SET).

TECHNICAL DOCUMENTATION PAGE

1. Project No.	2. Government Accession No.	3. Recipient's Catalog No.
17CLSU08		

4. Title and Subtitle	5. Report Date
Self-healing Microcapsules as Concrete Aggregates for Corrosion Inhibition in Reinforced Concrete	Nov. 2018
	6. Performing Organization Code
7. Author(s) PI: Homero Castaneda https://orcid.org/0000-0002-9252-7744 Co-PI: Marwa Hassan https://orcid.org/0000-0001-8087-8232 Co-PI: Miladin Radovic https://orcid.org/0000-0003-4571-2848 Post-Doc: Jose Milla https://orcid.org/0000-0001-9144-8545 Post-Doc: Ahmad Karayan https://orcid.org/0000-0002-2945-3324	**8. Performing Organization Report No.**
9. Performing Organization Name and Address Transportation Consortium of South-Central States (Tran-SET) University Transportation Center for Region 6 3319 Patrick F. Taylor Hall, Louisiana State University, Baton Rouge, LA 70803	**10. Work Unit No. (TRAIS)**
	11. Contract or Grant No. 69A3551747106
12. Sponsoring Agency Name and Address United States of America Department of Transportation Research and Innovative Technology Administration	**13. Type of Report and Period Covered** Final Research Report Jul. 2017 – Jul. 2018
	14. Sponsoring Agency Code

15. Supplementary Notes

Report uploaded and accessible at: Tran-SET's website (http://transet.lsu.edu/)

16. **Abstract**

Reinforced Concrete (RC) structures are vital to the US's civil infrastructure for their strength and versatility. Unfortunately, RC elements deteriorate rapidly when exposed to corrosive environments. One possible solution is to extend the life of RC elements and systems using microencapsulated corrosion inhibitors to reduce the rebar corrosion rate. The capsules house an anodic corrosion inhibitor agent including calcium nitrate (CN) and triethanolamine (TEA). The integration of such microencapsulated materials will enhance the durability and extend the useful life by controlling the corrosion precursors and the corrosion process during damage evolution. Therefore, this work aims to develop and characterize the performance of microcapsules containing corrosion inhibitors (CN-C and TEA-C) in comparison to those introduced as admixtures (CN-A and TEA-A) for reinforced concrete applications.

For the corrosion tests, all samples were subjected to continuous ponding, wet/dry cycles, and fog chamber exposure to simulate different environments. The results showed that TEA-C is more effective in giving a corrosion protection than TEA-A and the Control. In contrast, the corrosion protection performance of both CN-A and CN-C was alike. The corrosion kinetics was slightly reduced on inhibited rebars compared to unprotected rebars (the Control). When comparing TEA-C and CN-C, in the presence of each stimulus (pH changes for TEA-C, cracks for CN-C), TEA-C protected the rebar better than CN-C. For the admixture samples (TEA-A and CN-A) that do not need stimuli in the concrete, a stable and better corrosion protection was provided by CN-A. The outcome of this proof-of-concept study in the laboratory validates the merit of the proposed technology for corrosion control in RC structures.

17. Key Words	18. Distribution Statement
Corrosion, Microcapsules, Durability, Concrete, Modeling	No restrictions.

19. Security Classif. (of this report)	20. Security Classif. (of this page)	21. No. of Pages	22. Price
Unclassified	Unclassified	78	

Form DOT F 1700.7 (8-72) **Reproduction of completed page authorized.**

SI* (MODERN METRIC) CONVERSION FACTORS

APPROXIMATE CONVERSIONS TO SI UNITS

Symbol	When You Know	Multiply By	To Find	Symbol
		LENGTH		
in	inches	25.4	millimeters	mm
ft	feet	0.305	meters	m
yd	yards	0.914	meters	m
mi	miles	1.61	kilometers	km
		AREA		
in^2	square inches	645.2	square millimeters	mm^2
ft^2	square feet	0.093	square meters	m^2
yd^2	square yard	0.836	square meters	m^2
ac	acres	0.405	hectares	ha
mi^2	square miles	2.59	square kilometers	km^2
		VOLUME		
fl oz	fluid ounces	29.57	milliliters	mL
gal	gallons	3.785	liters	L
ft^3	cubic feet	0.028	cubic meters	m^3
yd^3	cubic yards	0.765	cubic meters	m^3
		NOTE: volumes greater than 1000 L shall be shown in m^3		
		MASS		
oz	ounces	28.35	grams	g
lb	pounds	0.454	kilograms	kg
T	short tons (2000 lb)	0.907	megagrams (or "metric ton")	Mg (or "t")
		TEMPERATURE (exact degrees)		
^oF	Fahrenheit	5 (F-32)/9 or (F-32)/1.8	Celsius	^oC
		ILLUMINATION		
fc	foot-candles	10.76	lux	lx
fl	foot-Lamberts	3.426	$candela/m^2$	cd/m^2
		FORCE and PRESSURE or STRESS		
lbf	poundforce	4.45	newtons	N
lbf/in^2	poundforce per square inch	6.89	kilopascals	kPa

APPROXIMATE CONVERSIONS FROM SI UNITS

Symbol	When You Know	Multiply By	To Find	Symbol
		LENGTH		
mm	millimeters	0.039	inches	in
m	meters	3.28	feet	ft
m	meters	1.09	yards	yd
km	kilometers	0.621	miles	mi
		AREA		
mm^2	square millimeters	0.0016	square inches	in^2
m^2	square meters	10.764	square feet	ft^2
m^2	square meters	1.195	square yards	yd^2
ha	hectares	2.47	acres	ac
km^2	square kilometers	0.386	square miles	mi^2
		VOLUME		
mL	milliliters	0.034	fluid ounces	fl oz
L	liters	0.264	gallons	gal
m^3	cubic meters	35.314	cubic feet	ft^3
m^3	cubic meters	1.307	cubic yards	yd^3
		MASS		
g	grams	0.035	ounces	oz
kg	kilograms	2.202	pounds	lb
Mg (or "t")	megagrams (or "metric ton")	1.103	short tons (2000 lb)	T
		TEMPERATURE (exact degrees)		
^oC	Celsius	1.8C+32	Fahrenheit	^oF
		ILLUMINATION		
lx	lux	0.0929	foot-candles	fc
cd/m^2	$candela/m^2$	0.2919	foot-Lamberts	fl
		FORCE and PRESSURE or STRESS		
N	newtons	0.225	poundforce	lbf
kPa	kilopascals	0.145	poundforce per square inch	lbf/in^2

TABLE OF CONTENTS

LIST OF FIGURES VI

LIST OF TABLES X

ACRONYMS, ABBREVIATIONS, AND SYMBOLS XI

EXECUTIVE SUMMARY XII

IMPLEMENTATION STATEMENT XIII

1. INTRODUCTION 1

1.1. Literature Review 2

1.1.1. Microencapsulation Techniques 2

1.1.2. Corrosion in Reinforced Concrete 5

1.1.3. Corrosion Inhibitors for Reinforced Concrete 5

2. OBJECTIVE 8

3. SCOPE 9

4. METHODOLOGY 10

4.1. Microcapsule Preparation 10

4.1.1. Encapsulation of Calcium Nitrate 10

4.1.2. Encapsulation of Triethanolamine 11

4.2. Concrete Mix Design 13

4.3. Concrete Testing 14

4.4. Corrosion Characterization 17

4.4.1. Exposure of Concrete Beams 17

4.4.2. Electrochemical Testing of the Concrete Beams 18

4.4.3. Electrochemical Data and analysis 19

5. FINDINGS 21

5.1. Characterization of Microencapsulated Corrosion Inhibitors 21

5.1.1. Calcium Nitrate 21

5.1.2. Triethanolamine 24

5.2. Concrete Testing 26

5.2.1. Fresh Concrete Properties 26
5.2.2. Compressive Strength 28
5.3. Corrosion Testing 30
5.3.1. Open Circuit Potential Results 30
5.3.2. Macrocell Corrosion Current 34
5.3.3. EIS Results 36
5.3.4. Corrosion Rate and Percent Inhibition 65
6. CONCLUSIONS 68
6.1 Current Findings 70
6.1.1 Encapsulation of Calcium Nitrate 70
6.1.2 Concrete Mix Design 70
6.1.3 Exposure of Concrete Samples 71
6.1.4 Electrochemical Testing 71
6.1.5 Discussion 72
7. RECOMMENDATIONS 75
REFERENCES 76

LIST OF FIGURES

Figure 1. Corrosion inhibition mechanism of microencapsulated calcium nitrate (image adapted from White et al. *(6)*). 2

Figure 2. Encapsulation procedure of triethanolamine (TEA), (image from Choi et al. *(12)*). 4

Figure 3. Free radical polymerization (image from Encyclopedia Britannica, Inc. (*13*)). 4

Figure 4. Process for the microencapsulation of calcium nitrate. 10

Figure 5. Procedure for seed latex particles. 12

Figure 6. Procedure for shell latex particles. 13

Figure 7. Average mortar compressive strength results for mortar cubes cured for 7 days. .. 14

Figure 8. (a) crack sample cylinders, (b) crack beams samples. 15

Figure 9. Potential difference set-up for ponding samples. 18

Figure 10. Three-electrode set-up for the ponding samples. 18

Figure 11. Three electrode system set-up for the fog chamber samples. 19

Figure 12. Equivalent circuit used for fitting. 20

Figure 13. Electron microscope images of microcapsules synthesized with varying production parameters. 22

Figure 14. Influence of production parameters: (a) Temperature, and (b) Sulfonic acid concentration on mean microcapsule diameter. 23

Figure 15. Thermogravimetric analysis of (a) calcium nitrate tetrahydrate (green); (b) urea-formaldehyde microcapsules containing water (blue); and (c) urea-formaldehyde microcapsules containing calcium nitrate tetrahydrate healing agent (red and black). 24

Figure 16. Influence of initiator concentration on seed latex solids content (as a percentage by weight). 25

Figure 17. Influence of sodium hydroxide wash concentration on the shell's solid contents (as percentage by weight). 25

Figure 18. TEM Image of: (a) Seed-Shell latex particles with no TEA, (b) Seed-Shell latex particles with TEA, before separation, and (c) Seed-Shell latex particles with TEA, after separation. 26

Figure 19. Honeycombing observed in TEA-C 5.0% specimens. 28

Figure 20. Compressive strength test results. 28

Figure 21. Compressive strength results for: (a) CN-C Group, (b) CN-A Group, (c) TEA-C Group, and (d) TEA-A Group. The CN-A and CN-C samples were fiber reinforced, while the TEA-A and TEA-C samples were not fiber reinforced. 29

Figure 22. OCP values of the Control and encapsulated calcium nitrate (CN-I) samples in the first set exposed to: (a) continuous-then-cyclic, and (b) ASTM G109 cycle exposure. 31

Figure 23. Open circuit potential for: (a) Control with fiber and calcium nitrate (admixed and encapsulated), and (b) Control without fiber and triethanolamine in the ponding exposure. 34

Figure 24. Open circuit potential for Control (with fiber) and calcium nitrate (admixed and encapsulated) in the fog chamber exposure. 34

Figure 25. Macrocell corrosion current values for the Control and encapsulated calcium nitrate samples (CN-I) in the first set exposed to: (a) continuous-then-cyclic, and (b) ASTM G109 cycle exposure. 35

Figure 26. Macrocell corrosion current values for: (a) Control with fiber and calcium nitrate (admixed and encapsulated) and (b) Control without fiber and triethanolamine in the ponding exposure. 36

Figure 27. (a) Nyquist, (b) Bode, and (c) phase angle plots for the Control without fiber exposed to continuous-then-cyclic exposure. 37

Figure 28. (a) Nyquist, (b) Bode, and (c) phase angle plots for microencapsulated calcium nitrate 0.25% exposed to continuous-then-cyclic exposure..... 38

Figure 29. (a) Nyquist, (b) Bode, and (c) phase angle plots for microencapsulated calcium nitrate 0.50% exposed to continuous-then-cyclic exposure..... 39

Figure 30. (a) Nyquist, (b) Bode, and (c) phase angle plots for microencapsulated calcium nitrate 2.00% exposed to continuous-then-cyclic exposure..... 40

Figure 31. (a) Nyquist, (b) Bode, and (c) phase angle plots for microencapsulated calcium nitrate 0.25% exposed to ASTM G109 cyclic exposure. 41

Figure 32. (a) Nyquist, (b) Bode, and (c) phase angle plots for microencapsulated calcium nitrate 0.50% exposed to ASTM G109 cyclic exposure. 42

Figure 33. (a) Nyquist, (b) Bode, and (c) phase angle plots for microencapsulated calcium nitrate 2.00% exposed to ASTM G109 cyclic exposure. 43

Figure 34. (a) Nyquist, (b) Bode, and (c) phase angle plots for the Control with fiber exposed to Ponding exposure..... 44

Figure 35. (a) Nyquist, (b) Bode, and (c) phase angle plots for microencapsulated calcium nitrate 0.50% exposed to Ponding exposure. 45

Figure 36. (a) Nyquist, (b) Bode, and (c) phase angle plots for microencapsulated calcium nitrate 2.00% exposed to Ponding exposure. 46

Figure 37. (a) Nyquist, (b) Bode, and (c) phase angle plots for microencapsulated calcium nitrate 5.00% exposed to Ponding exposure. 47

Figure 38. (a) Nyquist, (b) Bode, and (c) phase angle plots for admixed calcium nitrate 0.50% exposed to Ponding exposure. 48

Figure 39. (a) Nyquist, (b) Bode, and (c) phase angle plots for admixed calcium nitrate 2.00% exposed to Ponding exposure. 49

Figure 40. (a) Nyquist, (b) Bode, and (c) phase angle plots for admixed calcium nitrate 5.00% exposed to Ponding exposure. 50

Figure 41. (a) Nyquist, (b) Bode, and (c) phase angle plots for the Control without fiber exposed to Ponding exposure..... 51

Figure 42. (a) Nyquist, (b) Bode, and (c) phase angle plots for microencapsulated triethanolamine 0.50% exposed to Ponding exposure. 52

Figure 43. (a) Nyquist, (b) Bode, and (c) phase angle plots for microencapsulated triethanolamine 2.00% exposed to Ponding exposure. 53

Figure 44. (a) Nyquist, (b) Bode, and (c) phase angle plots for microencapsulated triethanolamine 4.00% exposed to Ponding exposure. 54

Figure 45. (a) Nyquist, (b) Bode, and (c) phase angle plots for microencapsulated triethanolamine 5.00% exposed to Ponding exposure. 55

Figure 46. (a) Nyquist, (b) Bode, and (c) phase angle plots for admixed triethanolamine 0.50% exposed to Ponding exposure. 56

Figure 47. (a) Nyquist, (b) Bode, and (c) phase angle plots for admixed triethanolamine 2.00% exposed to Ponding exposure. 57

Figure 48. (a) Nyquist, (b) Bode, and (c) phase angle plots for admixed triethanolamine 5.00% exposed to Ponding exposure. 58

Figure 49. (a) Nyquist, (b) Bode, and (c) phase angle plots for the Control with fiber exposed to fog chamber exposure. 59

Figure 50. (a) Nyquist, (b) Bode, and (c) phase angle plots for the microencapsulated calcium nitrate 0.50% exposed to fog chamber exposure. 60

Figure 51. (a) Nyquist, (b) Bode, and (c) phase angle plots for the microencapsulated calcium nitrate 2.00% exposed to fog chamber exposure. 61

Figure 52. (a) Nyquist, (b) Bode, and (c) phase angle plots for the microencapsulated calcium nitrate 5.00% exposed to fog chamber exposure. 62

Figure 53. (a) Nyquist, (b) Bode, and (c) phase angle plots for the admixed calcium nitrate 0.50% exposed to fog chamber exposure. 63

Figure 54. (a) Nyquist, (b) Bode, and (c) phase angle plots for the admixed calcium nitrate 2.00% exposed to fog chamber exposure. 64

Figure 55. (a) Nyquist, (b) Bode, and (c) phase angle plots for the admixed calcium nitrate 5.00% exposed to fog chamber exposure. 65

Figure 56. Corrosion rate for: (a) Control and microencapsulated nitrate exposed to continuous-then-cyclic exposure, and (b) only microencapsulated calcium nitrate exposed to ASTM G109 cyclic exposure. 66

Figure 57. Corrosion rate for: (a) microencapsulated and admixed calcium nitrate and (b) microencapsulated and admixed triethanolamine exposed to ponding exposure. 66

Figure 58. Corrosion rate for microencapsulated calcium nitrate exposed to fog exposure... 66

Figure 59. Percent inhibition for: (a) microencapsulated and admixed calcium nitrate, (b) and microencapsulated and admixed triethanolamine exposed to ponding exposure. 67

Figure 60. Experimental set-up for open circuit and electrochemical impedance spectroscopy measurement. 72

Figure 61. OCP change over the experimental period. 72

Figure 62. Nyquist plots for (a) Control and (b) CN C 2%. 73

Figure 63. Bode plots for (a) Control and (b) CN C 2%..... 74

Figure 64. Phase angle plots for (a) Control and (b) CN C 2%. 74

LIST OF TABLES

Table 1. Encapsulation techniques (adapted from Ghosh (8)). 2

Table 2. The influence of the encapsulation method on the ranges of microcapsule sizes produced (adapted from Ghosh (*8*)). 3

Table 3. Matrix parameters used for the synthesis of calcium nitrate microcapsules. 11

Table 4. Concrete mix design. 14

Table 5. Description of initial specimen groups. 15

Table 6. Description of calcium nitrate and triethanolamine specimen groups. 16

Table 7. Description of the samples prepared for study. 17

Table 8. Circuit elements. 20

Table 9. Slump and air test results for initial concrete specimens with microencapsulated calcium nitrate. 26

Table 10. Slump and air test results for concrete specimens reinforced with polymer fibers, including microencapsulated calcium nitrate, and calcium nitrate added as an admixture at varying concentrations, respectively. 27

Table 11. Slump and air test results for concrete specimens with microencapsulated triethanolamine, and triethanolamine added as an admixture at varying concentrations, respectively. 27

Table 12. Corrosion condition for OCP values (*34*). 30

Table 13. Concrete mix design. 71

Table 14. Samples tested in current results. 71

ACRONYMS, ABBREVIATIONS, AND SYMBOLS

AASHTO	American Association of State Highway and Transportation Officials
ASTM	American Society for Testing and Materials
BA	Butyl Acrylate
BSE	Backscattered Electron
CN	Calcium Nitrate
EGDMA	Ethylene Glycol Dimethyl Acrylate
EIS	Electrochemical Impedance Spectroscopy
MAA	Methacrylic Acid
MMA	Methyl Methacrylate
OCP	Open Circuit Potential
PD	Potential Difference
RC	Reinforced Concrete
SCE	Saturated Calomel Electrode
SDBS	Sodium Dodecyl Denzene Sulphonate
SEM	Scanning Electron Microscope
TEA	Triethanolamine
TGA	Thermogravimetric Analysis

EXECUTIVE SUMMARY

Microencapsulated corrosion inhibitors embedded in concrete were tested for their basic principle and efficiency to mitigate corrosion in rebar and thus extend the durability of reinforced concrete (RC) structures. Two corrosion inhibition mechanisms are proposed, where (a) calcium nitrate microcapsules rupture during a cracking event and thereby release the core material; and (b) triethanolamine (TEA) microcapsules that release the core material due to pH changes in the local environment. These compounds were selected as they are reportedly known to retard the corrosion of steel, and are also known to be compatible with concrete materials.

Calcium nitrate (CN) was encapsulated in a urea-formaldehyde shell, and the production parameters (i.e., sulfonic acid concentration, temperature, and agitation rate) were varied to optimize the capsule size and morphology. On the other hand, triethanolamine (TEA) was encapsulated in a four-step process, requiring (1) the production of the seed latex material, (2) the formation of an amphiphilic first shell, (3) the formation of a hydrophobic second shell, and (4) the neutralization of the seed materials with TEA (and thus loading the seed latex particles with TEA). The production parameters were adjusted to maximize the yield and the amount of TEA infused onto the seed latex particles. The synthesized microcapsules were embedded into concrete in concentrations of 0.25%, 0.50%, 2.00%, and 5.00% by weight of cement for calcium nitrate, and 0.50%, 2.00%, and 5.00% by weight of the cement for triethanolamine.

For corrosion tests, four types of samples were investigated: (i) microencapsulated TEA (TEA-C), (ii) admixed TEA (TEA-A), (iii) microencapsulated CN (CN-C), and (iv) admixed CN (CN-A). TEA-A and CN-A samples were included in this study to evaluate which form (either microencapsulated or admixed) was more effective for corrosion mitigation of the steel reinforcement. The Control samples that had no corrosion inhibitors were also tested as a reference. This work presents the interfacial characterization of such corrosion-inhibiting agents by exposing the concrete specimens to continuous ponding, wet/dry cycles (and a combination of both), and fog chamber during the electrochemical tests such as open circuit potential (OCP), potential difference, and electrochemical impedance spectroscopy (EIS).

As such, the feasibility of the proposed microcapsules for corrosion control in RC was tested, and the experimental data obtained by electrochemical methods shed light on the initiation mechanisms in detail at the micro-interface level. Based on the corrosion test results, it can be concluded that TEA gave better corrosion protection to rebar when it was housed in microcapsules rather than distributed directly in the concrete (admixture). TEA-C was also found to be more corrosion resistant than the Control that had no corrosion inhibitor. This is evident by the impedance modulus of TEA-C that was four times as high as the one for TEA-A and the Control. For the CN samples, both admixture and microcapsule technique slightly improved the corrosion resistance of inhibited rebars compared to unprotected rebars (the Control). When comparing TEA-C and CN-C, in the presence of each stimulus (pH changes for TEA-C, cracks for CN-C), TEA-C protected the rebars better than CN-C. For the admixture samples (TEA-A and CN-A) that do not need stimuli in the concrete, corrosion resistance of rebars was slightly improved.

IMPLEMENTATION STATEMENT

This project has successfully demonstrated the benefit of microencapsulated triethanolamine (TEA-C) compared to admixed triethanolamine (TEA-A) for protecting rebars from corrosion in the concrete applications. This benefit was also observed for microencapsulated calcium nitrate (CN-C) and admixed calcium nitrate (CN-A) but at a lesser degree. The success of TEA-C in protecting the rebars more effectively and efficiently has opened a potential technology that can be transferred in the real world. This technology would be able to reduce the resources and costs related to the application of triethanolamine (TEA) as a corrosion inhibitor. However, to fully implement the proposed technology, more results and evidence is needed to explore the mechanisms and performance of encapsulated TEA for corrosion protection in reinforced concrete. Similarly, although both CN-C and CN-A offered the similar level of corrosion protection, further research is required to explain these results, and explore alternatives to improve the performance. Since the performance of corrosion inhibitor strongly depends on the concentration, the optimum concentration of TEA and CN in the microcapsule must also be determined.

In order to achieve the implementation of this technology, future work is needed on the inhibition mechanisms, in particular for encapsulated TEA, since the results determined this sample group was the most efficient. Corrosion inhibition will be studied from the macro and microscale in order to better understand the performance and mechanisms. In the future study, the testing environments for TEA-C and CN-C will be designed differently. For TEA-C specimens, the carbonation process will be simulated more quickly by introducing simulated pore simulation with different pH values. The main advantage of performing the corrosion tests in this simulated solution instead of concrete is the actual optimum pH can be easily and more quickly monitored, so that the mechanisms could be more accurately predicted.

For the CN-C specimens, cracked concrete samples will still be used. The concentrations of TEA will be kept the same as the ones in the current project. However, for CN, different concentrations will be tested since the current results show that both CN-C and CN-A did not significantly improve the corrosion resistance. In addition, the encapsulation procedure will be revisited to increase the encapsulation efficiency of calcium nitrate. Two types of corrosion measurements will be performed in the next phase: (i) global, and (ii) local measurements. The global measurements that mainly consist of polarization and electrochemical impedance spectroscopy will provide information about the overall performance of corrosion inhibitors while the local measurements that consist of scanning vibrating electrode technique and local electrochemical impedance spectroscopy will give information about the mechanism in more detail. Implementation for this phase includes a proof-of-concept study in laboratory conditions that can be used for next phase, where the making of these materials can help in the departments of transportation (DOTs) mission of reliability and integrity of concrete structures.

1. INTRODUCTION

Reinforced Concrete (RC) structures are vital to the US's infrastructure due to their high durability and strong mechanical properties when used for bridges, superstructures, and other civil engineering applications. However, the durability and reliability of RC infrastructure is largely affected by corrosion-induced deterioration of the steel reinforcement. A recent cost-of-corrosion study by the Federal Highway Administration (FHWA) has estimated the annual cost of corrosion to US bridges to be approximately $30 billion, not including indirect costs incurred by the traveling public due to infrastructural closures (*1*).

Steel reinforcement in concrete is generally in a passive state due to the surface oxide layer in a highly alkaline environment. However, such passive layer may be deteriorated by the ingress of aggressive agents (e.g., chlorides ions) and thus lead to the corrosion of the steel reinforcement. The deterioration mechanism follows the evolution concept under steady state conditions including three different stages: (1) mass transport of the ionic corrosive precursors (chlorides) within the concrete layer, (2) activation of the metallic rebar due to charge transfer mechanism, and (3) charge transfer with possible mass transfer due to the growth of corrosion products at the rebar surface. This concept can lead to the current inadequate performance levels of infrastructure elements in Region 6; for example, bridges in Region 6 are below the national average of C+, which is already significantly low (*2*).

In order to minimize corrosion, researchers have proposed embedding microencapsulated corrosion inhibitors in the concrete matrix. Zuo et al. prepared polymer/metal hydroxide microcapsules that steadily released the encapsulated materials over time (*3*). Using calcium hydroxide and barium hydroxide as corrosion inhibitors, the results showed the microcapsules successfully delayed the decline on the pH values of concrete, thus decreasing the corrosion rate of the rebar. Dong et al. prepared polystyrene microcapsules containing sodium monofluorophosphate. The results showed strong corrosion inhibition in a simulated concrete environment, measured with an Electrochemical Impedance Spectroscopy (EIS) technique (*4*).

In the present study, microencapsulated corrosion inhibitors (calcium nitrate and triethanolamine) embedded in concrete will be tested for their efficiency to mitigate corrosion in rebars and thus extend the durability of reinforced concrete structures. Both compounds are reportedly known to retard the corrosion of steel and will be encapsulated in polymeric shells and admixed into concrete at different concentrations (as a % by weight of cement). Through microencapsulation, it is expected that the corrosion protection of RC structures will be extended by controlling the release of corrosion inhibitor only when needed, and thus prevent any potential leaching.

The calcium nitrate corrosion inhibition mechanism will be initiated during a cracking event, causing the microcapsules to rupture and subsequently release the core material. This will initiate the corrosion inhibition process, as calcium nitrate will act as an anodic inhibitor against chloride-induced corrosion (*5*). The proposed corrosion inhibition mechanism with calcium nitrate is illustrated in Figure 1.

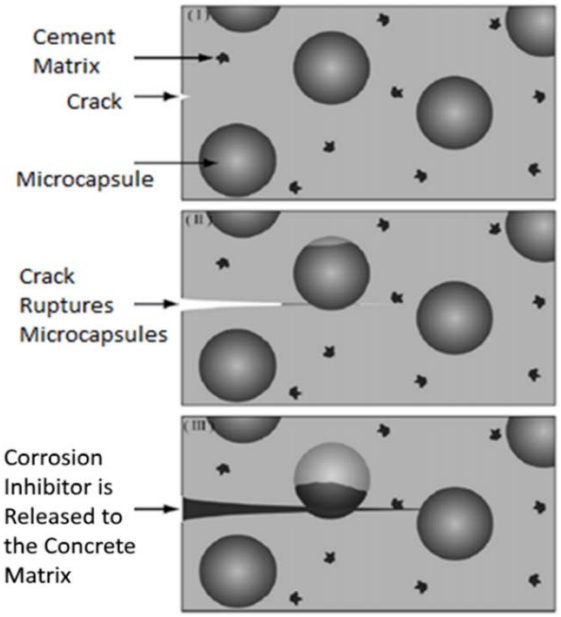

Figure 1. Corrosion inhibition mechanism of microencapsulated calcium nitrate (image adapted from White et al. *(6)*).

Triethanolamine (TEA) capsules, on the other hand, release the corrosion inhibitor based on pH changes of the surrounding environment, and thus it does not necessarily require a cracking event to rupture the capsules and release the corrosion inhibitor. Choi et al. tested the release behavior of encapsulated TEA, and verified that the core material was effectively released when the pH of the surrounding environment was changed to a pH of 10.85 (*7*). This is particularly useful for corrosion mitigation in RC structures, since the corrosion of the steel reinforcement begins when the pH of the concrete is lowered from 10 to 11, due to the destabilization of the passive film on the rebar.

1.1. Literature Review

1.1.1. Microencapsulation Techniques

Microencapsulation is a process by which a core material (in either solid, liquid, or gas form) is enclosed by an inert shell or coating. Depending on the desired application, microcapsules can be used to protect the core material from its surroundings, or to provide a controlled release of the core material based on the shell's permeability. There are three main methods used for encapsulation, involving either chemical, physico-chemical, or physico-mechanical processes. Table 1 shows the most commonly used encapsulation techniques sorted by their corresponding manufacturing processes.

Table 1. Encapsulation techniques (adapted from Ghosh *(8)*).

Chemical Processes	Physico-Chemical Processes	Physico-Mechanical Processes
In situ polymerization	Supercritical CO_2 assisted microencapsulation	Multiple nozzle spraying
Polycondensation	Layer-by-layer assembly	Spray-drying
Interfacial polymerization	Sol-gel encapsulation	Fluid-bed coating
Miniemulsion polymerization	Coacervation	Centrifugal techniques

The selected encapsulation process controls the shell wall's properties, yield rates, and the type

of core material that can be encapsulated. In general, the size of the produced microcapsules can range from the millimeter to the nanometer scale. Table 2 summarizes the typical particle sizes that result from each respective encapsulation technique (*8*).

Table 2. The influence of the encapsulation method on the ranges of microcapsule sizes produced (adapted from Ghosh (*8*)).

Microencapsulation Process	Particle Size (μm)
Extrusion	250-2500
Spray-drying	5-5000
Fluid bed coating	20-1500
Rotating disk	5-1500
Coacervation	2-1200
Solvent evaporation	0.5-1000
Phase separation	0.5-1000
In situ polymerization	0.5-1000
Interfacial polymerization	0.5-1000
Miniemulsion	0.1-0.5
Sol-gel encapsulation	2-20
Layer-by-layer assembly	0.02-20

In this study, calcium nitrate is encapsulated using an in-situ polymerization process adapted from Rodson et al. and Milla et al. (*9*, *10*). The encapsulation procedure was influenced by the following parameters: (a) the temperature at which the suspension or emulsion is heated; (b) the type of acid catalyst used and its concentration; (c) reaction time; (d) agitation rate; (e) water-oil ratio; and (f) choice of core material, and thus its water solubility and its compatibility with the shell materials (*9*, *11*). The selection of the acid catalyst is critical as it must be soluble in an organic solvent and also act as a surfactant. The temperature and surface-active acid catalyst concentration controls the polymerization reaction rate, and thus define the reaction time needed. The agitation rate influences the droplet size of the suspension or emulsion, and thus controls the microcapsule diameter. Similarly, the surface-active acid catalyst concentration controls the particle size and distribution.

On the other hand, triethanolamine is encapsulated with a free-radical mini-emulsion polymerization technique adapted from Choi et al. (*7*, *12*). Thus, the polymerization reaction is carried out in a reactor under a nitrogen atmosphere to prevent early termination caused by airborne oxygen. It involves a four-step process, requiring the production of the seed latex material, the formation of an amphiphilic first shell, the formation of a hydrophobic second shell, and the neutralization of the seed materials with TEA (and thus loading the seed latex particles with TEA). The first shell layer with intermediate hydrophilicity was added to facilitate the encapsulation of the hydrophobic, outer polystyrene shell. Figure 2 describes the steps required to encapsulate TEA.

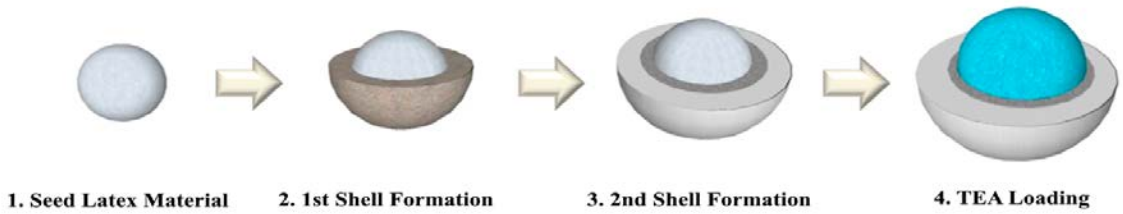

Figure 2. Encapsulation procedure of triethanolamine (TEA), (image from Choi et al. *(12)*).

The seed latex production is influenced by (a) the temperature at which the seed latex emulsion is heated; (b) the ratio of the seed latex components (i.e., methyl methacrylate, butyl actylate, and methacrylic acid); (c) choice and concentration of surfactants; and (d) the choice and concentration of initiator (to remove the polymerization inhibitors that are used in commercial monomer solutions to prevent premature polymerization before use). These parameters control the seed latex's emulsion, yield (based on the total solids content), and to maximize the seed latex's neutralization degree to entrap triethanolamine. Figure 3 shows a free radical polymerization reaction to form latex particles.

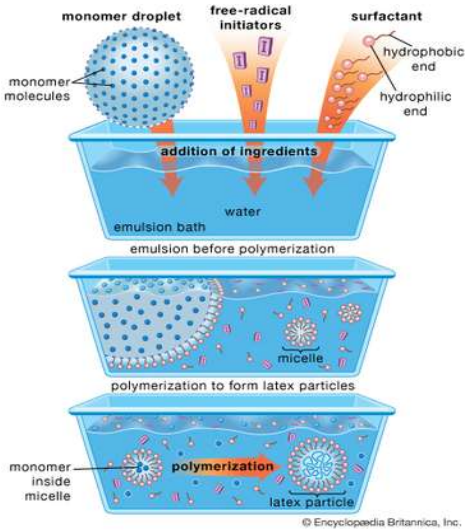

Figure 3. Free radical polymerization (image from Encyclopedia Britannica, Inc. (*13*)).

The first shell's formation is controlled by: (a) the de-ionized water content used to disperse the seed latex in the emulsion; (b) the ratio of the first shell's components (i.e., methyl methacrylate, butyl actylate, and methacrylic acid – differs from the ratios used for the seed latex); (c) the temperature at which the seed latex emulsion is heated; and (d) the choice and concentration of initiator. Similarly, the second shell's formation (made from polystyrene) is influenced by the following: (a) the temperature at which the monomer pre-emulsion is heated; (b) ratio of styrene to monomer pre-emulsion; (c) choice and concentration of surfactants; and (d) the choice and concentration of initiator. All of the aforementioned parameters control their respective monomer emulsion and the reaction rate. It is important to note that the triethanolamine must be introduced simultaneously with the styrene pre-emulsion mixture; otherwise, the styrene shell will prevent the penetration of triethanolamine to reach the acidic seed latex particles.

1.1.2. Corrosion in Reinforced Concrete

Corrosion of the reinforcing steel inside of concrete structures is one of the main causes of structure degradation and eventual failure of the concrete structure. The corrosion of steel reinforcement can be due to multiple process such as: chloride ingress, carbonation, or other changes in the local area of the embedded steel (*14*). The ingress of these aggressive agents will break down a protective passive that is formed on the steel reinforcing bar due to the high alkalinity of the concrete.

Chloride ingress is one of the major leading causes for corrosion of the rebar in reinforced concrete in marine environments and in places were de-icing salts are used. Initially, the rebar is in a passive state that protects the rebar from corrosion. This passive layer is due the high alkalinity of local environment, with pH values ranging from 12.5 to 14 depending on the properties of the concrete (*15*). Corrosion due to chlorides occurs when the concentration of chlorides at the rebar surface rises to a critical threshold to break down the passive layer. The cathodic and anodic reactions for the corrosion process at the rebar interface are as follows:

$$Fe \rightarrow Fe^{2+} + 2e^{-} \text{ (anodic)} \quad [1]$$

$$O_2 + 2H_2O + 2e^{-} \rightarrow 2OH^{-} \text{ (cathodic)} \quad [2]$$

These reactions can only occur once the protective passive layer has been destroyed. Once these processes start, the electrons from the anodic reactions at the anodic sites will flow through metal to the cathodic sites. Then, the hydroxide ions from the cathodic reaction will flow through the concrete due to an electric field to the anodic sites. The ions from the cathodic sites react to the ferrous ions to form ferrous hydroxide. When oxygen is still present after ferrous hydroxide is formed, it can be further oxidized to higher volume insoluble rust.

1.1.3. Corrosion Inhibitors for Reinforced Concrete

To extend the service life of reinforced concrete structure, it has been shown that the addition of corrosion inhibitors into the concrete matrix may minimize corrosion. In principle, the direct addition of these types of corrosion inhibitors is to bind or combine chloride for reducing the $[Cl^-]/[OH^-]$ ratio. The most common ways corrosion inhibitors are added to reinforced concrete are: added to fresh concrete as an admixture, applied on the hardened concrete surface also known as migrating corrosion inhibitor or surface-applied corrosion inhibitor, added to repair mortars, and as a surface treatment on the reinforcement bars (*16*). Adding corrosion inhibitors to the concrete is known to extend the life of the reinforced concrete structures since the time to initiation (t_i) of the corrosion process at the rebar is delayed due to the addition of these inhibitors. Examples of corrosion inhibitors used for reinforcing steel are calcium nitrate and triethanolamine.

Calcium Nitrate: Calcium nitrate is an anodic corrosion inhibitor that was found to be effective in delaying the onset of rebar corrosion in concrete specimens incorporating seawater, chloride solution or chloride plus sulfate solution (*17*). Calcium nitrate passivates the steel reinforcement's surface against the chloride ion stacks. When measuring the efficiency of calcium nitrate as a corrosion inhibitor, it is important to note that any measured corrosion potentials are not reliable in evaluating corrosion. When anodic inhibitors are included in the concrete mix, their oxidation abilities will shift the potential to lower values without actually having an on-going severe corrosion of the rebar (*5*).

It is generally believed that calcium nitrate corrosion-inhibiting effect is degenerative in nature. The unbound nitrate ions diminish in concentration as they stabilize the passive layer of rebar. Since the admixture is relatively small in concrete, it tends to be dispersed in the mass rather than at the concrete/steel interface (*18*). It was also reported that calcium nitrate only provides sufficient corrosion protection when used in combination with good quality concrete (*19*, *20*). This type of inhibitor failed to protect the reinforcing steel even in uncracked concrete (*19*, *21*).

Triethanolamine: Triethanolamine (TEA), a tertiary alkanolamine, is well-known as a multifunctional chemical admixture for concrete and an effective grinding aid for cement manufacturing in addition as an corrosion inhibitor (*22*). TEA has been previously used in concrete as a set accelerator (which may also enhance early strength) at very low dosages, ranging from 0.02% to 0.05% by weight of cement (*23*, *24*). The setting time is decreased by TEA's ability to accelerate the hydration of tricalcium aluminates and ettringite formation (*25*). However, at higher dosages (particularly higher than 0.1%), TEA may cause strength deficiencies as it has been reported to retard the hydration of tricalcium silicate, a main component of Portland cement's binder strength (*26*).

Based on the report on an European patent application (*27*) that tested several amines alkanolamines having molecular weights ranging from 48 to about 500, triethanolamine was considered to be one of the most three efficient inhibitors. Ormellese et al. studied the performance of some organic corrosion inhibitors to mitigate chloride-induced corrosion in concrete and found that triethanolamine showed a significant increase of pitting potential for chloride concentration equal or higher than 0.3 mol/L (*28*).

Need for Microencapsulated Corrosion Inhibitors: Generally, there are two main drawbacks of the direct applications of corrosion inhibitors. The first one is associated with the solubility of corrosion inhibitors themselves. If the solubility is low, there is a lack of active agent to provide a corrosion protection to rebar. However, if the solubility is high, corrosion inhibitors can cause premature reactions during hydration of the cement, which could then negatively affect the microstructure and composition of the hydration products. Secondly, it is very likely that a certain amount of corrosion inhibitor is consumed at an early age, which could lead to less availability of active agent to inhibit corrosion or bind the chloride at later stages (*29*).

To address these problems, a research team from Shenzhen University developed microencapsulated corrosion inhibitors (*29*, *30*). Their self-healing ethyl cellulose/calcium hydroxide microcapsule has successfully provided a high-efficient corrosion protection of rebar on the pH self-regulation to decrease the $[Cl^-]/[OH^-]$ ratio (*4*, *29*, *31*, *32*). The core agent in the microcapsule contains hydroxyl ions is encapsulated in order to prevent premature reactions with other components. A pH sensitive shell material is selected to control the release of hydroxyl ions. This microcapsule releases the active agents (i.e., calcium hydroxide), when there is a pH gradient, which is monitored by a micro-plate spectrophotometer (*29*). A continuous release of calcium hydroxide promotes the stability of passive film when the pH decreases. When the pH increases, the release rate of calcium hydroxide is inhibited. Another type of microcapsule with polystyrene resin/sodium monofluorophosphate was also fabricated and studied by the same team (*4*, *30*).

It is worth mentioning that corrosion on steel reinforcement usually does not occur

immediately at the beginning of concrete service life, but rather happens after a certain period of time. This suggests that corrosion protection may not be necessary during the early time of service. Microcapsules with corrosion inhibitors can prevent the premature reaction between the active agent of corrosion inhibitor and the cement when corrosion protection is not needed during the beginning of service by isolating this agent inside the microcapsule. In this study, the effectiveness of microencapsulated corrosion inhibitors embedded into the concrete was measured based on their ability to slow down the corrosion process and to extend the service life of the reinforced concrete structures. The two corrosion inhibitors and mechanism used in this study were calcium nitrate and triethanolamine.

2. OBJECTIVE

The objective of this study is to evaluate the feasibility of embedded encapsulated corrosion inhibitors (i.e., calcium nitrate and triethanolamine) in polymeric shells for corrosion control in reinforced concrete. Specific objectives:

- Optimize the design parameters needed to produce single and/or double-walled corrosion inhibiting microcapsules to be used in concrete structures.
- Design an electrochemical set up for qualitative/qualitative characterization of concrete additives/microcapsules.
- Perform method of advanced laboratory techniques based on electrochemical and transport phenomena principles.
- Validation of the methodology by testing several conditions and samples with different microcapsules concentrations and formulations.

3. SCOPE

The proposed research will develop a technology for corrosion-damaged reinforced concrete elements so that the current degradation management system can be improved. In addition, an important class of physical asset, reinforced concrete bridges, can be preserved by mitigating corrosion induced damages. One of the center's stated objectives is to extend the life of the existing or new transportation infrastructure through the application of emerging materials.
In this work, two corrosion inhibitors (calcium nitrate and triethanolamine) were encapsulated and evaluated. The inhibition mechanism is initiated by a concrete cracking event causing the microcapsules to rupture and subsequently release the core material to initiate the corrosion inhibition process. Therefore, once these corrosion inhibitors were encapsulated, they were admixed into reinforced concrete beams to study the corrosion resistance and self-healing properties of these admixed microcapsules in a corrosive environment. The microcapsules were tested for their efficiency to mitigate corrosion in rebars and thus extend the durability of reinforced concrete structures.

4. METHODOLOGY

The aim of this study was to encapsulate calcium nitrate and triethanolamine, which are known corrosion inhibitors. Once these corrosion inhibitors were encapsulated, they were admixed into reinforced concrete beams to study the corrosion resistance and self-healing properties of these admixed microcapsules in a corrosive environment. The methodology and characteristics for each element of the concrete system and the microcapsules are described as follows:

4.1. Microcapsule Preparation

4.1.1. Encapsulation of Calcium Nitrate

The microencapsulation procedure for calcium nitrate was adapted from a previous study (*10*), albeit with minor modifications. The process is based on a water-in-oil suspension polymerization reaction of polyurea-formaldehyde, where the temperature and acid catalyst concentration control the rate of reaction *(9)*. Kerosene was selected as an organic solvent as it is more economical than hexane. Moreover, the calcium nitrate solution concentration was increased from 16.7% to 25%. Once the microcapsules were synthesized, it was important to neutralize the microcapsules' surface as it has been found to contain traces of sulfonic acid, based on a previous study (*11*, *33*). Therefore, the microcapsules were decanted, washed with 150 ml of a 1% sodium bicarbonate solution, and subsequently washed with 150 ml of DI water and vacuum filtered. The details of the microencapsulation procedure are shown in Figure 4.

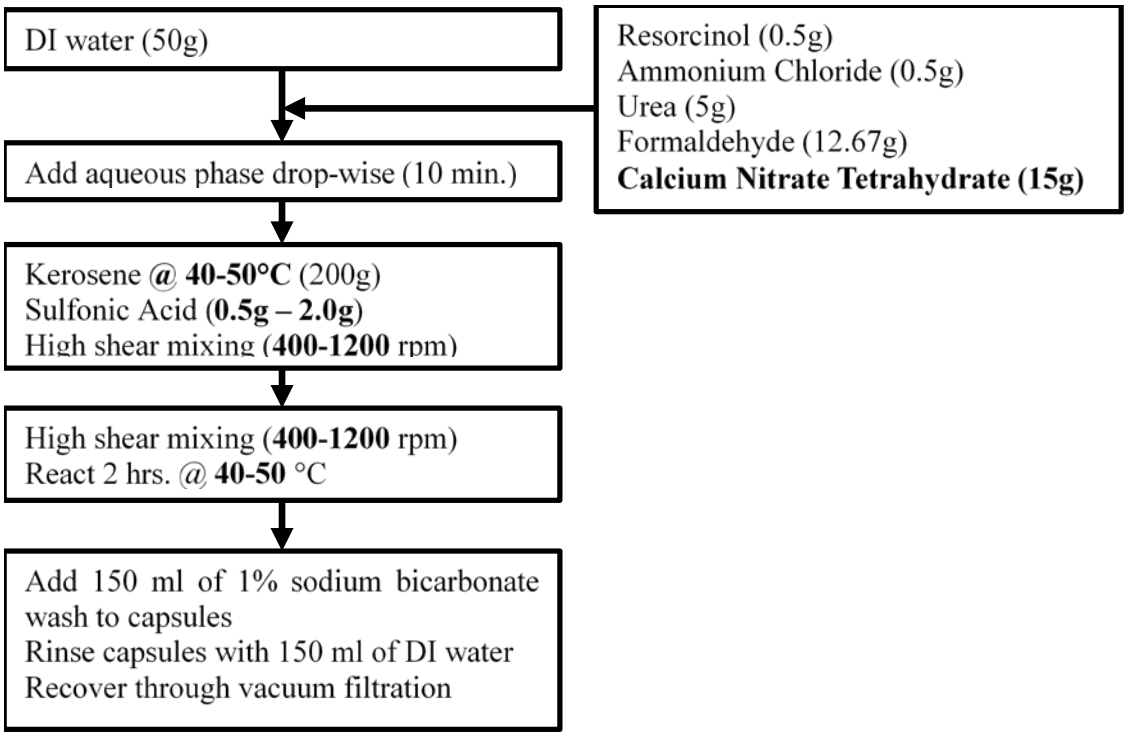

Figure 4. Process for the microencapsulation of calcium nitrate.

The suspension polymerization reaction was enabled by heating at a high temperature (> 40 °C) for 2 hours. The production parameters, including the temperature, agitation rate, and acid

catalyst concentrations (% by wt. of organic solvent) were varied to investigate the effects on the microcapsule's diameter, and morphology. The samples were then characterized using a Scanning Electron Microscope (SEM). Table 3 illustrates the parameters that were investigated in this study.

Table 3. Matrix parameters used for the synthesis of calcium nitrate microcapsules.

Sample No.	Agitation Rate (RPM)	Acid Catalyst Conc. (%)	Temp. (°C)
1	400	0.25	45
2	400	0.50	45
3	400	1.00	45
4	400	0.25	40
5	400	0.25	50
6	800	0.25	45
7	800	0.50	45
8	800	1.00	45
9	800	0.25	40
10	800	0.25	50
11	1200	0.25	45
12	1200	0.50	45
13	1200	1.00	45
14	1200	0.25	40
15	1200	0.25	50

4.1.2. Encapsulation of Triethanolamine

The procedure for the encapsulation of triethanolamine (TEA) was adapted from Choi et al. (*7*). It involves a four-step process, requiring the production of the seed latex material, the formation of an amphiphilic first shell, the formation of a hydrophobic second shell, and the neutralization of the seed materials with TEA (and thus loading the seed latex particles with TEA).

The method selected for the encapsulation of TEA was a free-radical polymerization micro-emulsion. Through this emulsion procedure, different parameters were changed to influence the seed latex such as the initiator and molecular weight. Sodium hydroxide, triethanolamine, and water content were changed in order to influence the shell particles. The equipment utilized in the development phase are the following; resin kettle equipped with condenser, a nitrogen inlet, an overhead mechanical stirrer, a heating mantle with a thermocouple, and a pressure equalizing funnel.

Seed Latex: The seed latex consists of four central monomers: methyl methacrylate (MMA), methacrylic acid (MAA), butyl acrylate (BA), and ethylene glycol dimethyl acrylate (EGDMA). The monomers were treated with sodium hydroxide in order to remove the polymerization inhibitors. This is because inhibitors are placed in monomer solutions in order to prevent premature polymerization while shipping. MAA, BA, and MMA have a ratio of 28:9:63 with mean particle sizes of 130 nm. Using this ratio, the infusion of TEA onto the seed latex was optimized.

EGDMA monomer was used as a cross linker, potassium persulphate was used as the initiator, and sodium dodecyl denzene sulphonate (SDBS) was used as the surfactant. Sodium Bicarbonate was used as a buffer to prevent possible hydrolysis reactions within the solution at acidic pH levels. Sodium hydroxide was adjusted at different concentrations in order to

control the activity amongst the monomers which in return increased the solid content. The initiator was varied at multiple concentrations in order to affect solid content of the resulting polymer. Utilizing initiators at different concentrations directly impacted infusion of TEA as well.

Surfactants, monomers, and initiators are added to a water base solution. Micelles are formed due to the hydrophilic and hydrophobic properties of surfactants. Monomers attach to the hydrophobic tail of the micelle. The initiator reacts with the monomers and produce seed latex particles. Figure 5 illustrates the procedure for seed latex particles.

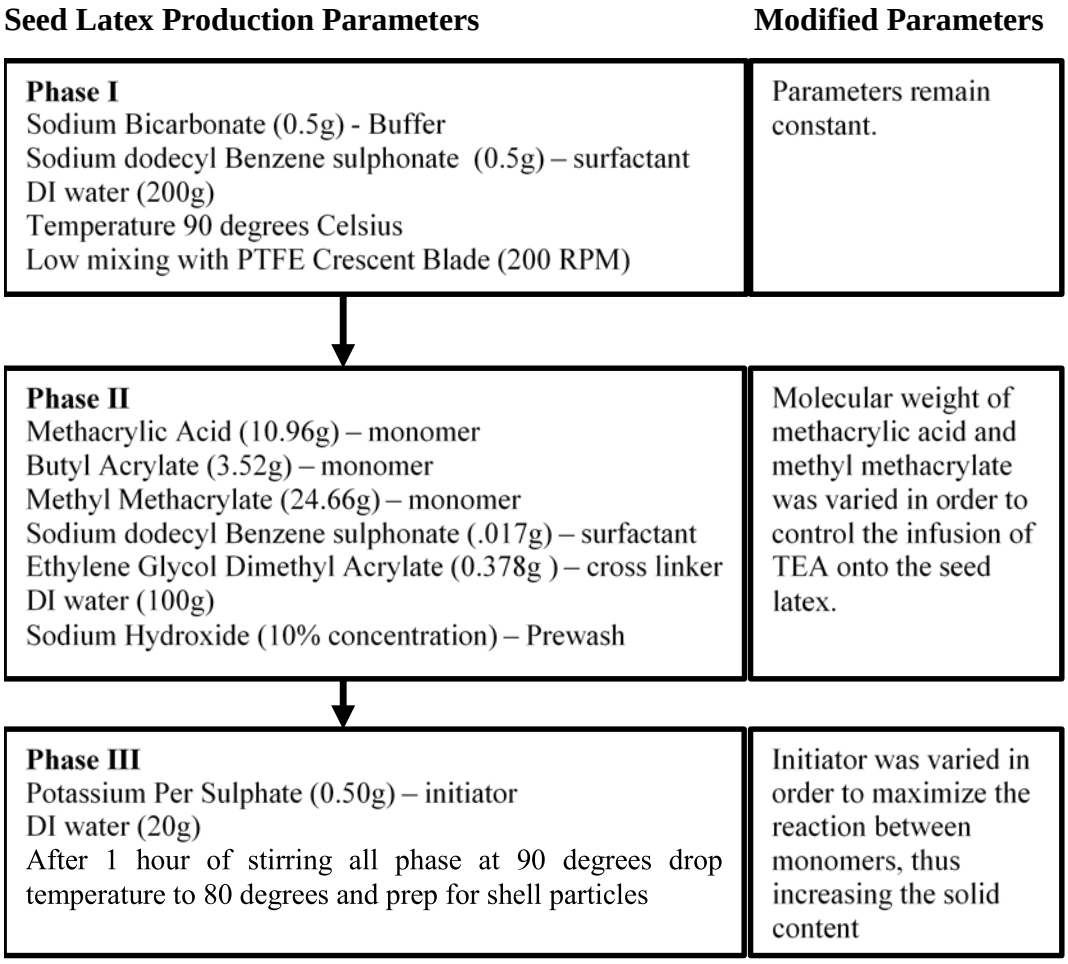

Figure 5. Procedure for seed latex particles.

Shell Particles: The TEA nanocapsules contain two shell walls. The first shell was deployed for affinity increase between the hydrophilic seed latex and the hydrophobic polystyrene shell (second shell). This first shell and the ratio of the seed latex allowed for a well-regulated fabrication of the hydrophobic polystyrene shell (second shell) with concentric shell particle morphology. The neutralization of the seed latex with triethanolamine is contingent on the balance between the first and second shell.

Before the second shell is positioned, triethanolamine must be infused onto the seed latex. The neutralization of triethanolamine helps insure the maximal inhibition efficiency. The maximal

inhibition efficiency in the shell phase was also aided by altering the following parameters: triethanolamine, water content, and sodium hydroxide. Figure 6 illustrates the procedure of shell latex particles.

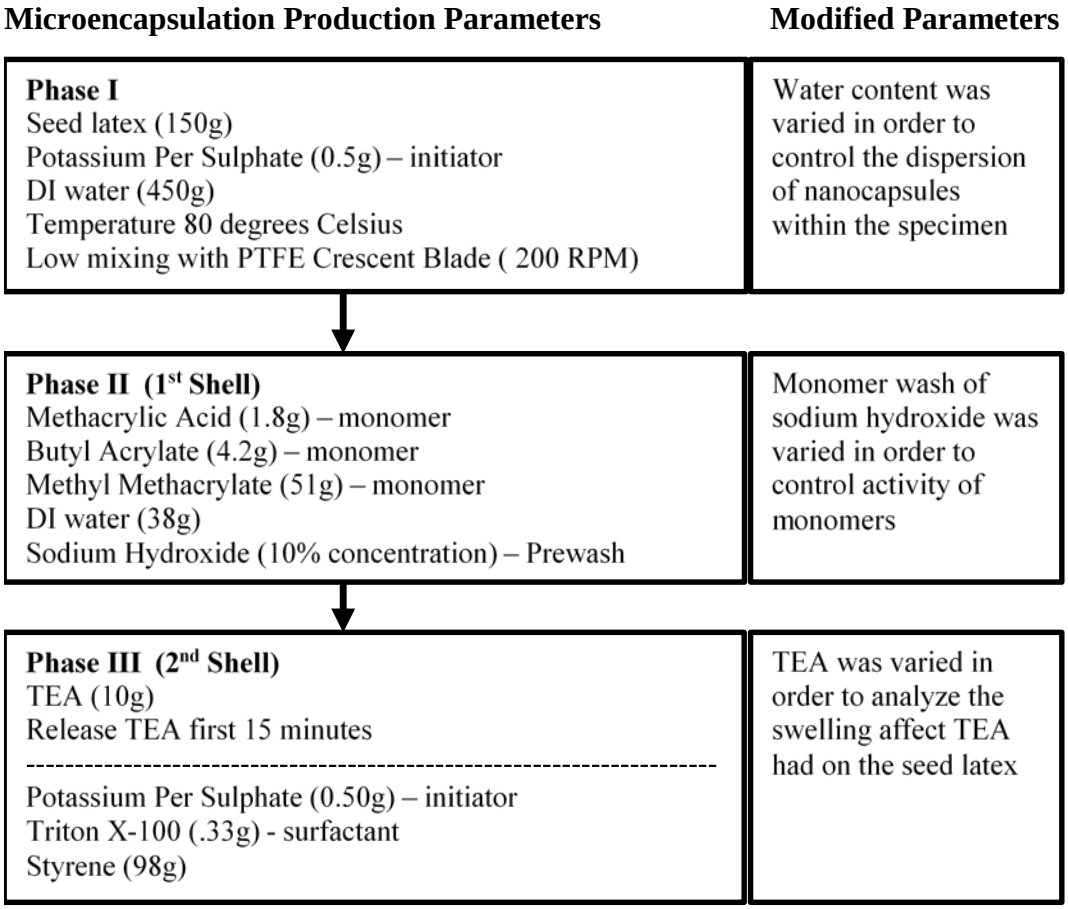

Figure 6. Procedure for shell latex particles.

4.2. Concrete Mix Design

After finalizing the calcium nitrate production, preliminary tests were conducted to investigate the influence of the microcapsules on the cementitious matrix with mortar specimens, and evaluated whether a defoaming agent is needed in the mix design to counter any potential strength reduction caused by the microcapsules in the sample's compressive strength. Therefore, four mortar mixes were poured for compression tests after 7-days of curing: (a) Control samples, with no defoamer [Ctrl-N]; (b) Control samples, with defoamer [Ctrl-D]; (c) Specimens loaded with microcapsules (2% by wt. of cement), with no defoamer [C2%-N]; and (d) Specimens loaded with microcapsules (2% by wt. of cement), with defoamer [C2%-D]. A water-cement ratio of 0.42 was selected, whereas a super plasticizer Adva 195 was added at 455 ml/100kg, and a defoaming agent concentration of 0.1% by weight of cement. These parameters were selected based on previous experience with other microcapsule-containing concrete mixes. The results plotted in Figure 7 indicate that the defoaming agent was crucial for minimizing any strength deficiencies.

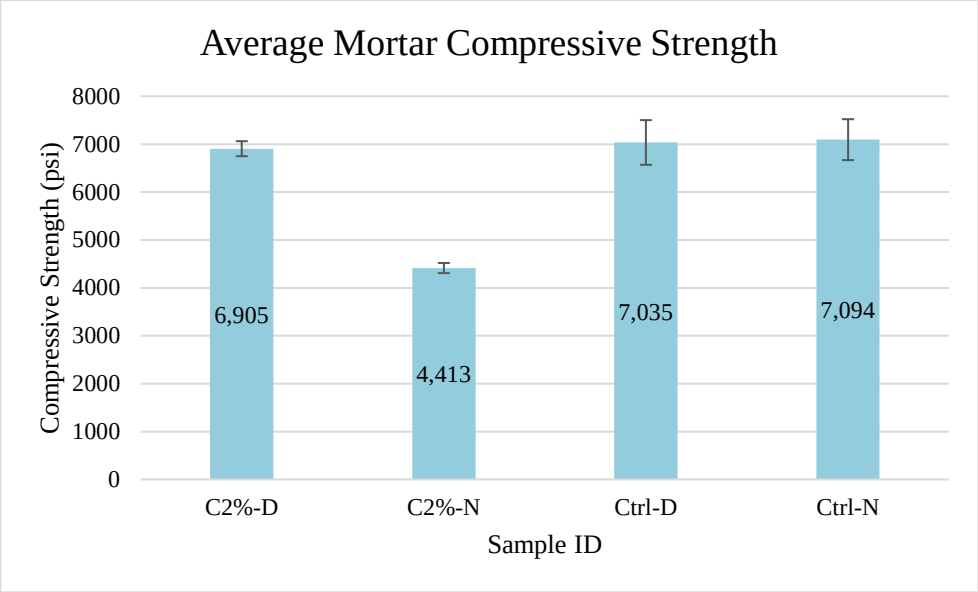

Figure 7. Average mortar compressive strength results for mortar cubes cured for 7 days.

The concrete mix design was therefore developed based on the mortar compression test results. A water-cement ratio of 0.42 was selected through preliminary laboratory tests. The nominal maximum aggregate size was 19 mm for the coarse aggregate, and 4.76 mm for the fine aggregate, respectively. The microcapsules were embedded at varying concentrations of microencapsulated corrosion inhibitors by weight of cement to determine the minimal dosage required to mitigate corrosion considerably. A superplasticizer was added to increase the workability of the concrete mix. A defoaming agent was also added at a dosage of 0.1% by weight of cement to counter the increases in air voids caused by the addition of microcapsules in concrete. The details of the concrete mix design are shown in Table 4.

Table 4. Concrete mix design.

Material Description	**Proportions (kg/m^3)**
Aggregate 1: Sand, Dennis Mills, LA	785
Aggregate 2: #67 Limestone, Martin Marietta	1110
Cement: Holcim Type I	326
Water: Mixing water	231
Air (%)	5.0
57 mm Polymer Fibers**	4.45
Admixture 1: Adva 195 (ml/100kg)	455
Admixture 2: Microcapsules* (%)	Varied
Admixture 3: TEGO Antifoam MR 1015* (%)	0.10

* By weight of cement; **Polymer fibers only added for certain concrete specimens containing calcium nitrate as a corrosion inhibitor.

4.3. Concrete Testing

Concrete cylinders were prepared for compressive strength (ASTM C39), and surface resistivity tests (AASHTO TP 95), while concrete beams were prepared for corrosion testing (ASTM G109). The concrete samples were cast and cured in laboratory settings per ASTM C192 guidelines. The concrete beams in particular were cast in custom-made molds using a vibrating table to compact and consolidate the fresh concrete. The influence of the corrosion inhibitor admixtures on the fresh concrete properties was measured with slump and air tests

per ASTM C143 and ASTM C231, respectively. A total of three 100 mm x 200 mm cylinders as illustrated in Figure 8a and three 150 mm x 150 mm x 280 mm beams were poured per specimen group as illustrated in Figure 8b. Table 5 shows characteristics of the specimens used in this study. All beam specimens associated with calcium nitrate were subjected to a 3-point loading system, where a displacement rate of 0.005 in/sec was applied until a crack was induced. The crack sizes induced ranged from 0.20 to 0.45 mm.

(a) (b)

Figure 8. (a) crack sample cylinders, (b) crack beams samples.

Table 5. Description of initial specimen groups.

Sample ID	Corrosion Inhibitor	Mechanism of Protection	Microcapsule Concentration (% by wt. of cement)	Corrosion Inhibitor Concentration (% by wt. of cement)	Fiber Reinforced?	Pre-Cracked?
Ctrl-I	Control	N/A	0.00 %	0.00 %	N	Y
CN-I 0.25	Calcium Nitrate	Microcapsule	0.25 %	0.06 %	N	Y
CN-I 0.50	Calcium Nitrate	Microcapsule	0.50 %	0.11 %	N	Y
CN-I 2.00	Calcium Nitrate	Microcapsule	2.00 %	0.44 %	N	Y

Given that the initial crack sizes were predominantly large for the initial specimen groups, additional samples were poured for the calcium nitrate groups to ensure that the cracks induced are smaller than 0.1 mm, in order to successfully rupture and release the corrosion inhibitor in the microcapsules, and prevent a substantial increase in the chloride diffusion coefficient. The additional specimens were useful in determining the efficiency of calcium nitrate microcapsules for corrosion mitigation under small (50-120 microns) and large cracks (200-500 microns). This was achieved by using a lower displacement rate (0.005 in/min) in the third-point loading test, and the addition of 25 mm polymer fibers to have more control on the crack width obtained.

Hence, the new calcium nitrate specimen groups were poured to be tested for corrosion inhibition when added as microcapsules, and when added as an admixture. This also required a new control specimen reinforced with fibers as reference. On the other hand, the

triethanolamine specimen groups were poured without polymer fiber reinforcement as they did not require pre-cracking to release the core material, and thus were poured with a control specimen group that was not cracked and did not have polymer fibers.

The concentrations of microencapsulated corrosion inhibitors were also changed to investigate whether a high capsule concentration is more effective, particularly because the encapsulation efficiencies were found to be 22% and 5.2% for calcium nitrate and triethanolamine, respectively. Hence, the corrosion inhibitor concentrations to be tested were 0%, 0.50%, 2.00%, and 5.00% for both the calcium nitrate specimen groups and the triethanolamine specimen groups. It should be noted that due to the difficulties in casting the TEA-C 5% samples (caused by a significant decrease in workability), TEA-C 4% samples were cast and did not result in honeycombing, unlike the TEA-C 5% samples. The details of the experimental matrix are shown in Table 6.

Table 6. Description of calcium nitrate and triethanolamine specimen groups.

Sample ID	Corrosion Inhibitor	Mechanism of Protection	Microcapsule Concentration (% by wt. of cement)	Corrosion Inhibitor Concentration (% by wt. of cement)	Fiber-Reinforced?	Pre-Cracked?
Ctrl-F	Control, with Fibers	N/A	N/A	0.00%	Y	Y
CN-C 0.50	Calcium Nitrate	Microcapsule	0.50 %	0.11 %	Y	Y
CN-C 2.00	Calcium Nitrate	Microcapsule	2.00 %	0.44 %	Y	Y
CN-C 5.00	Calcium Nitrate	Microcapsule	5.00 %	1.10 %	Y	Y
CN-A 0.50	Calcium Nitrate	Admixture	N/A	0.11 %	Y	Y
CN-A 2.00	Calcium Nitrate	Admixture	N/A	0.44 %	Y	Y
CN-A 5.00	Calcium Nitrate	Admixture	N/A	1.10 %	Y	Y
Ctrl-NF	Control, No Fibers	N/A	0.00 %	0.00 %	N	N
TEA-C 0.50	Triethanolamine	Microcapsule	0.50 %	0.03 %	N	N
TEA-C 2.00	Triethanolamine	Microcapsule	2.00 %	0.10 %	N	N
TEA-C 4.00	Triethanolamine	Microcapsule	4.00 %	0.21%	N	N
TEA-C 5.00	Triethanolamine	Microcapsule	5.00 %	0.26 %	N	N
TEA-A 0.50	Triethanolamine	Admixture	0.50 %	0.03 %	N	N
TEA-A 2.00	Triethanolamine	Admixture	2.00 %	0.10 %	N	N
TEA-A 5.00	Triethanolamine	Admixture	5.00 %	0.26 %	N	N

Table 7 describes all of the samples prepared for this study, with their respective corrosion tests (i.e., through wet-dry cycles and fog chamber conditions).

Table 7. Description of the samples prepared for study.

Sample ID	Corrosion inhibitor	Mechanism of Protection	Microcapsule Concentration (% by wt. of cement)	Corrosion Inhibitor Concentration (% by wt. of cement)	Total Number of Replicas poured	Replicas for Fog Chamber	Replicas for Wet-Dry Cycles
Ctrl-I	Control, no Fibers	N/A	Control, no fibers	0.00 %	3	0	3
CN-I 0.25	Calcium Nitrate	Microcapsule	0.25 %	0.06 %	3	0	3
CN-I 0.50	Calcium Nitrate	Microcapsule	0.50 %	0.11 %	3	0	3
CN-I 2.00	Calcium Nitrate	Microcapsule	2.00 %	0.44 %	3	0	3
Ctrl F	Control, with Fibers	N/A	Control with fibers	0.00 %	4	2	2
CN-C 0.50	Calcium Nitrate	Microcapsule	0.50 %	0.11 %	3	2	1
CN-C 2.00	Calcium Nitrate	Microcapsule	2.00 %	0.44 %	3	2	1
CN-C 5.00	Calcium Nitrate	Microcapsule	5.00 %	1.10 %	4	2	2
CN-A 0.50	Calcium Nitrate	Admixture	N/A	0.11 %	3	2	1
CN-A 2.00	Calcium Nitrate	Admixture	N/A	0.44 %	3	2	1
CN-A 5.00	Calcium Nitrate	Admixture	N/A	1.10 %	4	2	2
Ctrl NF	Control, no Fibers	N/A	Control, no fibers	0.00 %	4	2	2
TEA-C 0.50	Triethanolamine	Microcapsule	0.50 %	0.03 %	3	2	1
TEA-C 2.00	Triethanolamine	Microcapsule	2.00 %	0.10 %	3	2	1
TEA-C 4.00	Triethanolamine	Microcapsule	4.00 %	0.21%	3	2	1
TEA-C 5.00	Triethanolamine	Microcapsule	5.00 %	0.26 %	4	2	2
TEA-A 0.50	Triethanolamine	Admixture	0.50 %	0.03 %	3	2	1
TEA-A 2.00	Triethanolamine	Admixture	2.00 %	0.10 %	3	2	1
TEA-A 5.00	Triethanolamine	Admixture	5.00 %	0.26 %	4	2	2

4.4. Corrosion Characterization

4.4.1. Exposure of Concrete Beams

For the exposure of the concrete beams, three different types of accelerating testing cycles were selected to simulate the different environments that a reinforced concrete structure could be exposed to during its service life. The details of the electrochemical measurements are outlined in section 4.4.2. The first set of samples were continuously ponding in a 3.5% NaCl solution for 12 weeks and then subject to weekly cycles of wetting and drying for another 12 weeks in the same solution as the first part of the cycle. Electrochemical measurements were performed on the samples once a week for the first 6 weeks of continuous ponding and then once every 2 weeks for the next 6 weeks, and then measurements were performed once a cycle during the next 12 weeks.

The second type of cycles used is the same wetting and drying cycles based on the ASTM G109 standard, where the samples were ponded for 2 weeks in a 3.5% NaCl solution with measurements in the second week of ponding, and then drying to open air and room temperature for another 2 weeks. The samples were exposed for 24 weeks total with a total 6 electrochemical measurements performed. These two cycles were used for reinforced samples with admixed calcium nitrate microcapsules with varying percentages of 0.25, 0.50, and 2.00% by weight of the cement.

The third cycle used was a 48-hour wetting and drying cycle with a 5% NaCl solution. Samples inside a fog chamber and ponding used this cycle and solution, the samples inside the fog chamber was also subject to a raised temperature of 35 °C for both the wetting and drying phases of the cycle.

4.4.2. Electrochemical Testing of the Concrete Beams

The electrochemical testing performed on the concrete beams during the test were open circuit potential (OCP), potential difference, and electrochemical impedance spectroscopy (EIS). The set-up for potential difference measurements is shown in Figure 9.

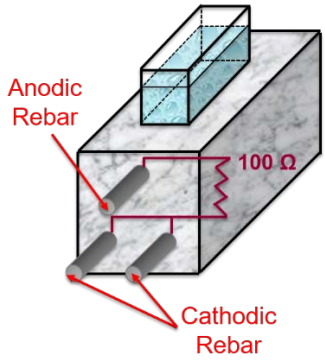

Figure 9. Potential difference set-up for ponding samples.

Potential difference is the measurement of the microcell current from the anodic top bar to the two cathodic bottom bars across a 100 Ω resistor. Potential difference is recorded every time measurements are made during the test duration. For OCP and EIS, the tests are run with a three-electrode system (Figure 10), where the working electrode is the top rebar, the counter electrode is a platinum mesh, and the reference electrode is a saturated calomel electrode (SCE) reference electrode.

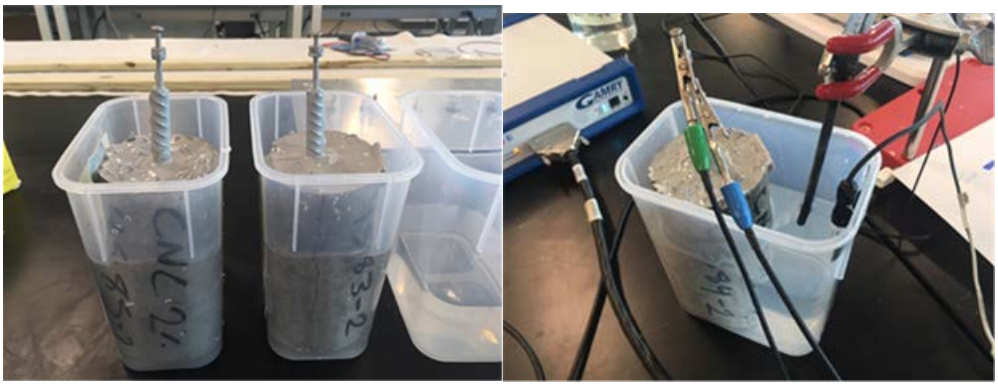

Figure 10. Three-electrode set-up for the ponding samples.

For the measurements inside the fog chamber the connections to the three electrodes are isolated and must be waterproofed. The set-up for the three-electrode system inside the fog chamber is shown in Figure 11.

Figure 11. Three electrode system set-up for the fog chamber samples.

OCP and EIS are both non-destructive techniques that can be used to determine the interfacial mechanisms at the rebar interface and these two tests are run every time that measurements are made during the test duration. OCP measures the potential difference between the reference electrode and the working electrode. EIS is the frequency response of the system when a sinusoidal potential is sent into the system at frequencies ranging from 100 kHz to 0.01 Hz.

4.4.3. Electrochemical Data and analysis

The following descriptions include the formulas and definitions of parameters that were quantified during the experimental results. Electrochemical methods are analyzed by the magnitudes obtained from the formulas and concepts. The potential difference between the anodic bar and the cathodic bar can be used to calculate the macrocell corrosion current by using Ohm's law (Equation 3):

$$I = \frac{V}{R} \qquad [3]$$

where, I = macrocell corrosion current, V = potential difference, and R = 100 Ω. If the anodic and cathodic Tafel slopes are known for the steel reinforcing bars in concrete then the microcell corrosion current density can be calculated by Equation 4:

$$i_{corr} = \left(\frac{\beta_a * \beta_c}{2.3 * (\beta_a + \beta_c)}\right) * \frac{1}{R_P} = \frac{B}{R_P} \qquad [4]$$

where, i_{corr} = corrosion current density (A/cm^2), β_a= anodic Tafel slope (V), β_c = cathodic Tafel slope (V), and R_P = polarization resistance (Ω-cm^2). EIS data can be used to characterize different elements of the system formed in the laboratory conditions. The common procedure to determine physical properties and mechanisms occurring from this technique is to fit a theoretical electrical circuit to the experimental impedance data. The equivalent circuit (EC) that is used in this study is shown in Figure 12 and the circuit elements are defined in Table 8.

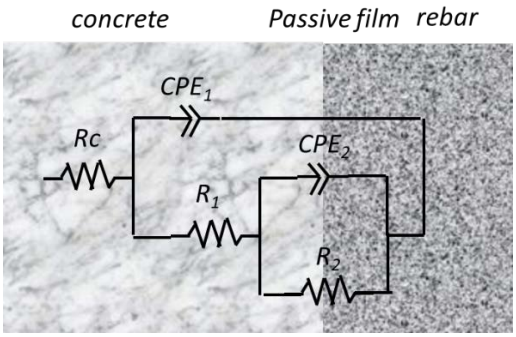

Figure 12. Equivalent circuit used for fitting.

Table 8. Circuit elements.

Element	Description
Rc	Pore network resistance, including the contribution of the disconnected pore network and solid phase
CPE_1	CPE of connected pore network only
RIF	Resistance of connected pore network
CPE_2	CPE of double layer at rebar-concrete interface
Rct	Charge Transfer Resistance

Once a circuit has been fit to the experimental data the Rct (in this case is equivalent to $R_{P)}$ value can calculated. This Rp value is used to determine the microcell corrosion current density (Equation 4) and characterize the corrosion and dissolution behavior based on the magnitudes for each element.

5. FINDINGS

5.1. Characterization of Microencapsulated Corrosion Inhibitors

5.1.1. Calcium Nitrate

Size and Morphology: In general, the agitation rate is known to control the mean microcapsule diameter, while the temperature and acid catalyst concentration both control the polymerization kinetics (i.e. the rate of reaction) *(9)*. As such, these production parameters were investigated to observe their effects on the microcapsule's size and morphology. The samples were characterized using a Scanning Electron Microscope (SEM) as shown in Figure 13.

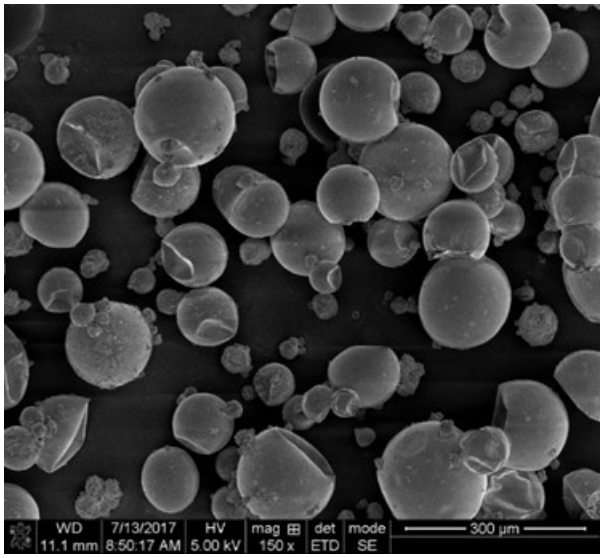

(a) 400 rpm, 0.25% SA, 45 °C

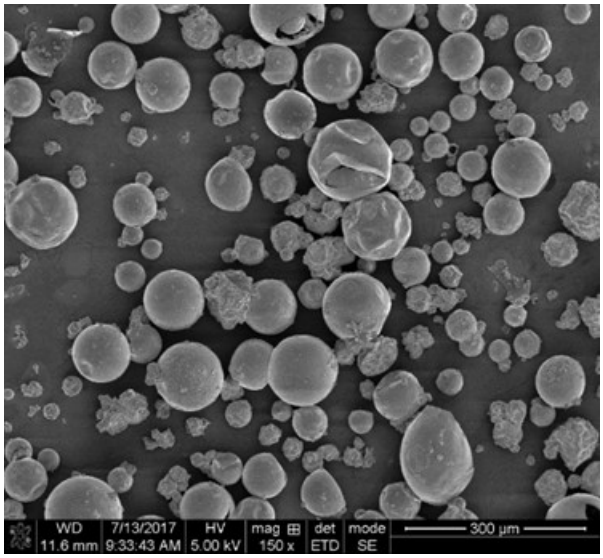

(b) 400 rpm, 1.00% SA, 45 °C

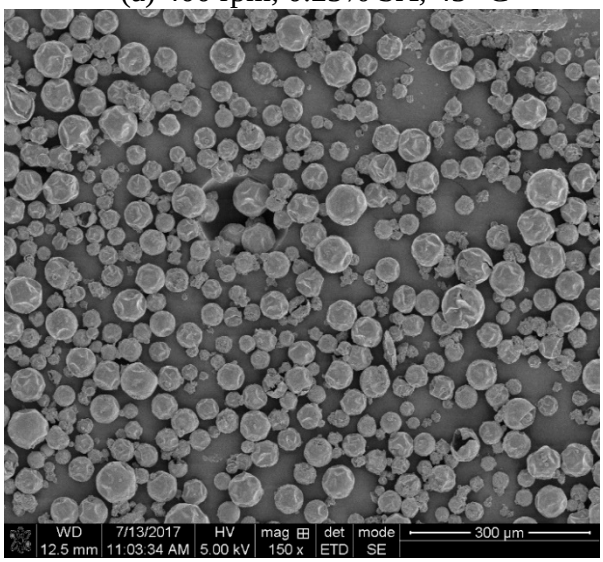

(c) 800 rpm, 1.00% SA, 45 °C

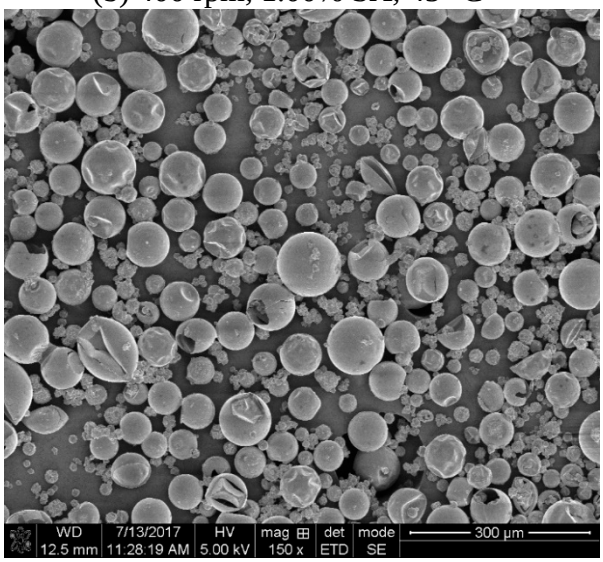

(d) 800 rpm, 0.25% SA, 45 °C

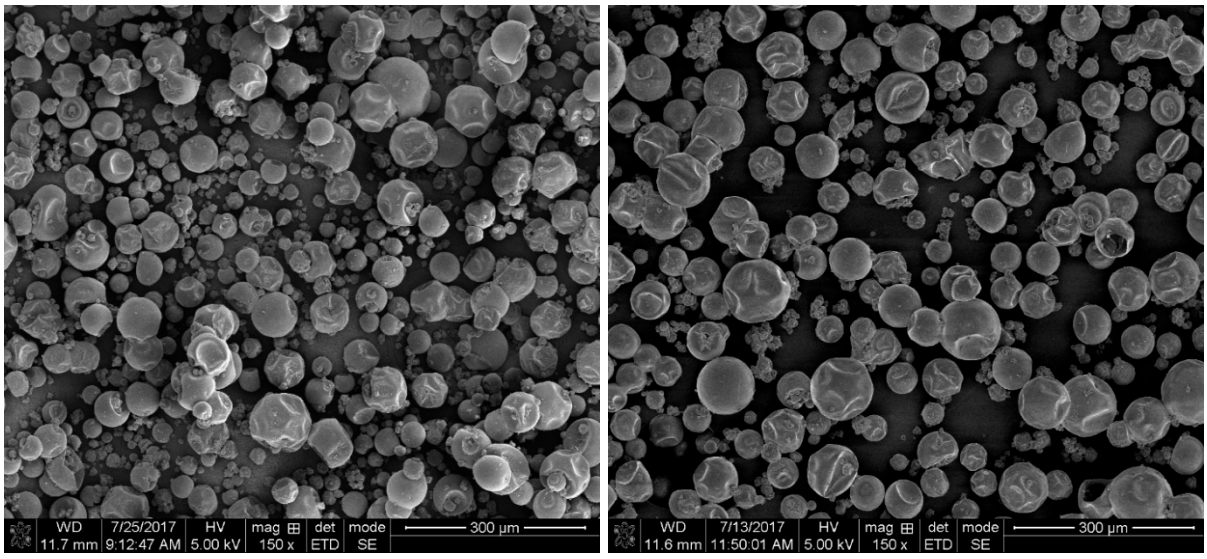

(e) 1200 rpm, 0.25% SA, 50 °C (f) 1200 rpm, 0.25% SA, 45 °C

Figure 13. Electron microscope images of microcapsules synthesized with varying production parameters.

In general, the synthesized microcapsules had a smooth outer surface and a spherical shape. Some microcapsules, however, seem to be deflated and this may be attributed to the sodium bicarbonate wash that was used to neutralize the traces of sulfonic acid in the microcapsules' shell. This is because it was observed that a prolonged exposure of sodium bicarbonate and/or a strong solution of sodium bicarbonate was prone to deflate the microcapsules significantly when compared to samples that were not rinsed with a sodium bicarbonate wash.

Based on a qualitative analysis, it is apparent that higher agitation corresponds to smaller microcapsules, given that all the electron micrographs were taken at the same magnification of 150x. In addition, the microcapsules appear to be smaller when a larger sulfonic acid concentration has been added. To confirm these observations, at least 250 measurements were taken for each sample produced from the experimental matrix shown in Table 3. Figure 14 illustrates the influence of the microcapsule production parameters to the mean capsule diameter. For comparison purposes, one production parameter was varied at a time while the others were kept constant. Therefore, to evaluate the influence of temperature, the sulfonic acid concentration was kept at 0.25%. Similarly, to understand how the sulfonic acid concentration affects the mean capsule diameter, the temperature was kept constant at 45 °C.

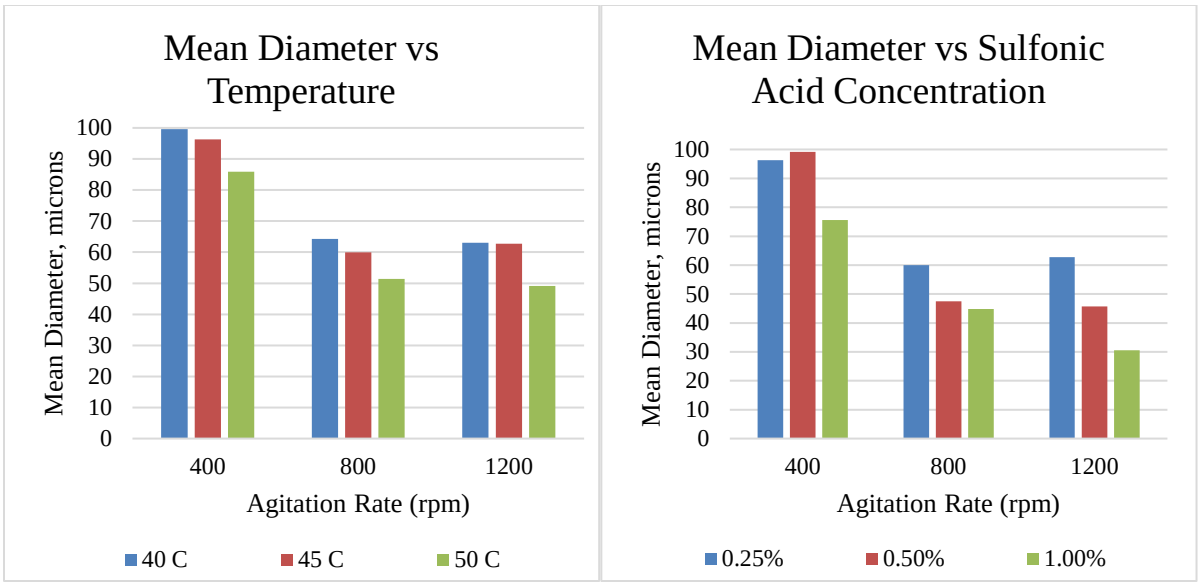

(a) (b)

Figure 14. Influence of production parameters: (a) Temperature, and (b) Sulfonic acid concentration on mean microcapsule diameter.

A statistical analysis using Fisher's Least Square Difference (LSD) at the 5% level was used to evaluate whether the production parameters had a significant effect on the microcapsule diameter. A variation in temperature produced significant differences, where a higher temperature corresponding to a smaller mean diameter between those samples produced at 50 °C and those produced at 40 °C and 45 °C. The sulfonic acid concentration also had a significant effect on the mean microcapsule diameter, where a higher sulfonic acid concentration corresponded to a smaller particle size. The exception was found on the sample produced at 400 rpm, 45 °C, where both 0.25% and 0.50% had no significant differences. Based on these observations, the selected production parameters for synthesizing microcapsules were the following: Temperature of 40 °C, an agitation rate of 800 rpm, and an acid catalyst concentration of 0.25%.

Encapsulation Efficiency: The encapsulation efficiency was determined using a Thermogravimetric analysis (TGA) technique at a heating rate of 10 °C /minute and stopped at 600 °C. The following samples were prepared for analysis: (a) calcium nitrate tetrahydrate (core material); (b) urea-formaldehyde microcapsules containing water only; and (c) urea-formaldehyde microcapsules containing calcium nitrate tetrahydrate healing agent. The temperature of interest is 500 °C, where the thermal degradation of urea-formaldehyde occurs. The TGA curve is shown in Figure 15.

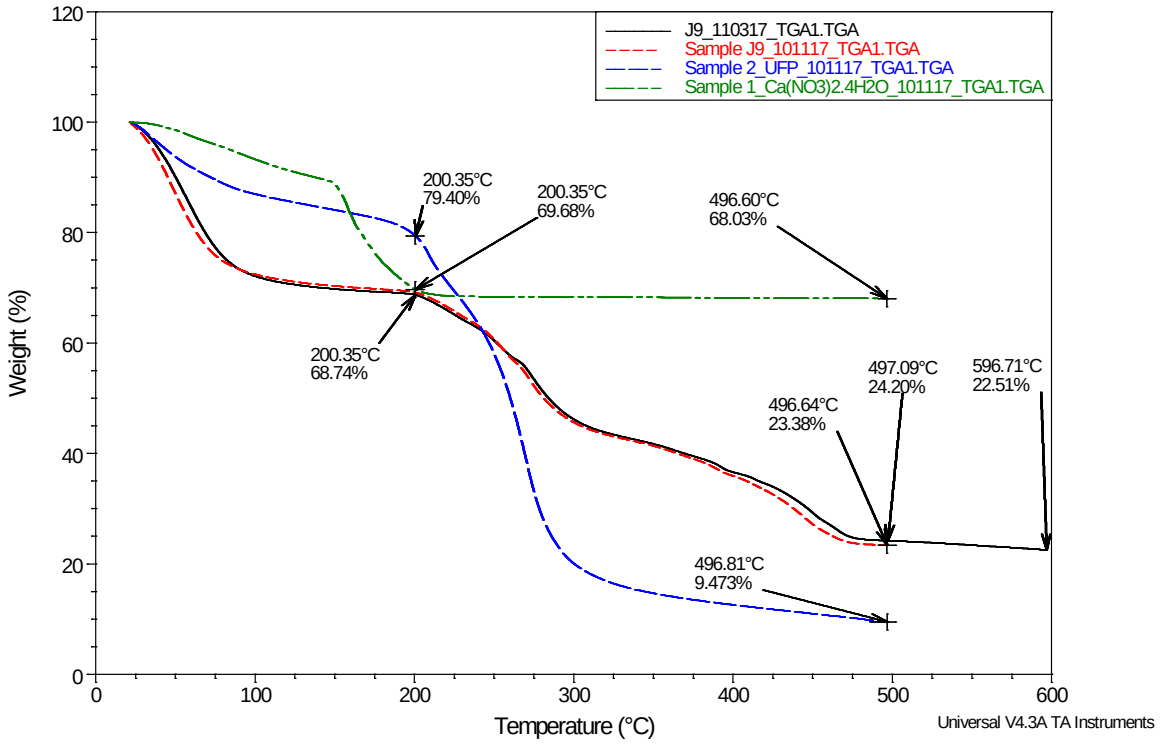

Figure 15. Thermogravimetric analysis of (a) calcium nitrate tetrahydrate (green); (b) urea-formaldehyde microcapsules containing water (blue); and (c) urea-formaldehyde microcapsules containing calcium nitrate tetrahydrate healing agent (red and black).

The sample with microencapsulated water had a weight loss of 21.6% at 200 °C, a temperature that indicates the total decomposition of absorbed water, and any water that is less able to diffuse to the surface. Next, the urea-formaldehyde polymer continues to decompose until 500 °C, indicating a weight loss of 90.6%. In contrast, the sample with microencapsulated calcium nitrate had a weight loss of 31.3% at 200 °C, and a weight loss of 75-76% at 500 °C.

The theoretical water content of calcium nitrate tetrahydrate ($Ca(NO_3)_2 \cdot 4H_2O$) is 28% by weight, yet in the TGA curve, the water weight is approximately 31.3% while the amorphous calcium nitrate was observed to be 68.7%. It is worth mentioning that amorphous calcium nitrate does not degrade at 500 °C, and therefore, any differences in weight from the analyzed microcapsule samples can be attributed to the amount of calcium nitrate successfully encapsulated. Thus, the encapsulation efficiency of amorphous calcium nitrate is estimated to be 13.9% - 14.7%. However, given that the amorphous calcium nitrate is 68% of the total mass of calcium nitrate tetrahydrate, the actual encapsulation efficiency ranges from 20 to 22%.

5.1.2. Triethanolamine

Seed Latex - Initiator: Initiator concentration was evaluated. Dense concentration of initiators facilitated growth of polymers while increasing the seed latex solid content. A 2-hour of polymerization time was chosen for the seed latex. It was observed that the longer the polymerization was carried out, an inverse consequence on the growth of polymers occurred. Figure 16 shows the influence of the initiator's concentration on the growth of polymers (measured as the percentage of seed latex solid content) over time.

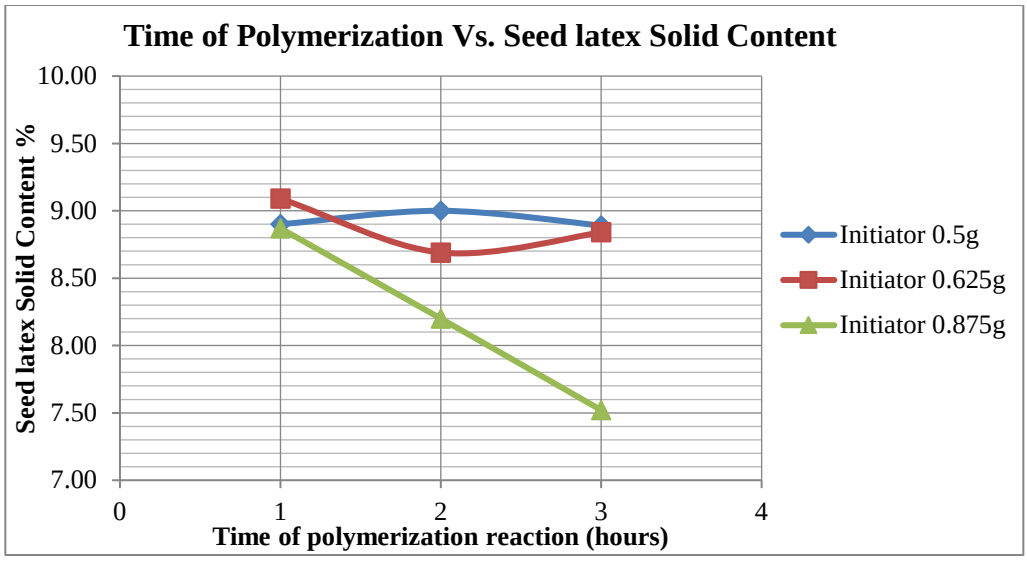

Figure 16. Influence of initiator concentration on seed latex solids content (as a percentage by weight).

Seed Latex – Molecular Weight: Seed latex was composed of MAA, BA, and MMA in the ratio of 28:9:63, respectively. By developing a seed latex at maximal carboxylic acid content, this heavily influenced the concentration of triethanolamine that can be attached onto the seed latex. Keeping the BA constant, the carboxylic acid content was manipulated by changing the molecular weight of the seed latex through MAA and MA. Two different monomer ratios were evaluated at 28:9:63 and 36:9:55. The 36:9:55 was not chosen due to the failure of this ratio being able to produce spherical seed latex particles.

Shell Particles - Sodium Hydroxide Concentration: Shell particle monomers were treated with sodium hydroxide at different concentrations, as shown in Figure 17. This allowed for maximum activity amongst monomers prompting a high conversion of shell particles. Based on the experimental results, the highest sodium hydroxide concentration yielded the highest solid content, and thus 10% sodium hydroxide was chosen for the shell particle wash.

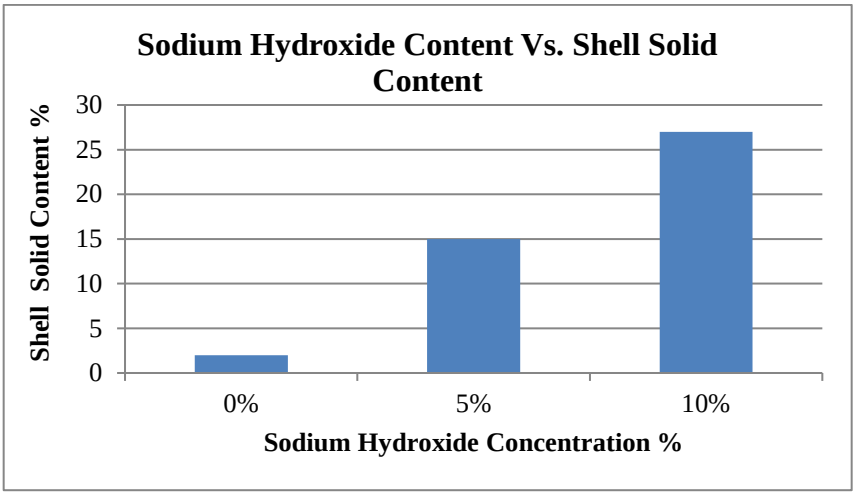

Figure 17. Influence of sodium hydroxide wash concentration on the shell's solid contents (as percentage by weight).

Shell Particles – Water Content: Shell particles were starved of water in order to impact the physical properties of the nanocapsules. As water content was altered, nanocapsules appeared to experience more amalgamation, which made separation of nanocapsules extremely difficult. Separating nanocapsules are imperative to distributing the corrosion inhibitor uniformly. Nanocapsules are well distributed throughout the concrete specimen to combat the aggressive behavior of corrosion.

Having capsules distributed uniformly aids in the dispersion of corrosion inhibitors. If all capsules are concentrated in small areas, the corrosion mitigation system will be ineffective. The water content was varied at 10%, 40%, and 90%. A water content of 10% produced shell particles that were coarse and had a high presence of amalgamation. A water content of 40% produced shell particles that were fine but also had a high presence of amalgamation. Water content of 90% was chosen, and this produced shell particles whose characteristics were fine with no amalgamation. The 90% water content allowed the capsules to be distributed uniformly, which aided in the corrosion mitigation system being effective. Figure 18 illustrates seed-shell latex particles with no TEA, with TEA, and with TEA after separation, respectively.

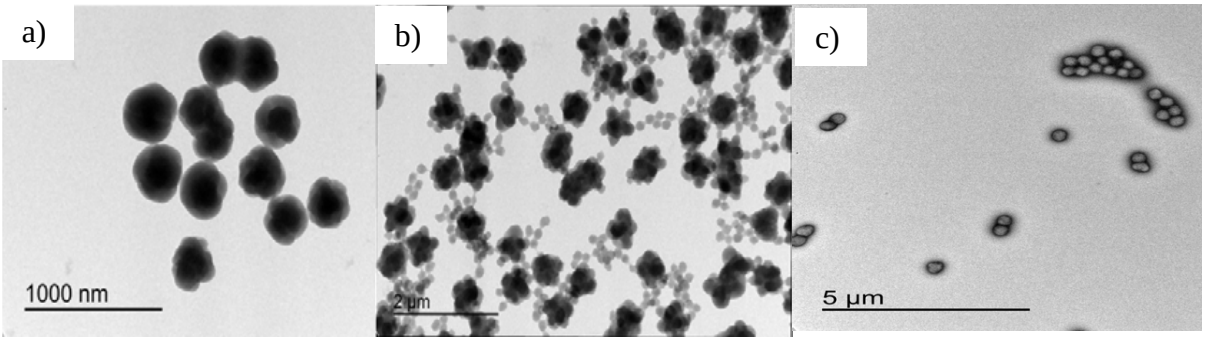

Figure 18. TEM Image of: (a) Seed-Shell latex particles with no TEA, (b) Seed-Shell latex particles with TEA, before separation, and (c) Seed-Shell latex particles with TEA, after separation.

5.2. Concrete Testing

5.2.1. Fresh Concrete Properties

The slump and air test results are shown in Table 9 for the initial calcium nitrate microcapsule group that was poured without polymer fiber reinforcement. The slump of the concrete increased as the microcapsule concentration increased, indicating that the microcapsules increased the workability. The air content test results showed low differences between each specimen group, indicating that the defoaming agent was successful in controlling the air content even when the microcapsule concentrations were increased.

Table 9. Slump and air test results for initial concrete specimens with microencapsulated calcium nitrate.

Sample ID	Concentration (% by wt. of cement)	Slump (mm)	Air Content (%)
Ctrl-I	N/A	15	2.6
CN-I 0.25	0.25	40	2.4
CN-I 0.50	0.50	50	2.0
CN-I 2.00	2.00	70	2.4

The slump and air test results are shown in Table 10 for the calcium nitrate specimen groups

that were poured with polymer fiber reinforcement, at concentrations of 0.5%, 2.0%, and 5.0% as a percentage by weight of cement. Virtually all specimens had a higher slump than the control specimen, thus indicating that the workability of the mixtures was improved when calcium nitrate was added through microcapsules or as an admixture. The only exception was for specimen group CN-A 2.0%, and this was attributed to the variability of the mix given that higher slumps were observed when calcium nitrate was admixed at higher and lower concentrations (CN-A 0.5% and CN-A 5.0%, respectively). The air content test results also showed low differences between each specimen group, although a higher calcium nitrate concentration (when added as an admixture or as microcapsules) caused a slightly higher air content.

Table 10. Slump and air test results for concrete specimens reinforced with polymer fibers, including microencapsulated calcium nitrate, and calcium nitrate added as an admixture at varying concentrations, respectively.

Sample ID	Concentration (% by wt. of cement)	Slump (mm)	Air Content (%)
Ctrl-F	Control with Fibers	20	2.0
CN-C 0.5%	0.50	65	1.5
CN-C 2.0%	2.00	75	2.1
CN-C 5.0%	5.00	65	2.4
CN-A 0.5%	0.50	25	2.3
CN-A 2.0%	2.00	15	2.2
CN-A 5.0%	5.00	135	2.9

With respect to the triethanolamine sample groups, the slump and air test results are shown in Table 11. The slump results indicate that the workability of the mix was not substantially changed when triethanolamine was added as an admixture. However, when the encapsulated triethanolamine was added, the consistency of the concrete mix was dramatically changed since the added microcapsules changed the viscosity of the mixing water.

Table 11. Slump and air test results for concrete specimens with microencapsulated triethanolamine, and triethanolamine added as an admixture at varying concentrations, respectively.

Sample ID	Concentration (% by wt. of cement)	Slump (mm)	Air Content (%)
Ctrl-NF	Control without fibers	95	3.0
TEA-A 0.5%	0.5	125	1.8
TEA-A 2.0%	2.0	75	2.6
TEA-A 5.0%	5.0	90	2.5
TEA-C 0.5%	0.5	40	2.0
TEA-C 2.0%	2.0	0	2.9
TEA-C 4.0%	4.0	0	3.2
TEA-C 5.0%**	5.0	0	5.3

**Specimen group was admixed with double the dosage of super plasticizer during the mixing process due to poor workability.

With the exception of TEA-C 0.5%, all samples with triethanolamine nanocapsules resulted in a stiff, dry mix with poor workability and no slump. At the highest nanocapsule concentrations (TEA-C 5.0%), the super plasticizer dosage was doubled to facilitate the concrete casting process. However, even with the use of the vibrating table, the compaction and consolidation of fresh concrete into the beam molds proved to be challenging and the hardened concrete cover's quality was poor, featuring honeycombing as shown in Figure 19. The air content was observed to increase with a higher dosage of triethanolamine, particularly when added as nanocapsules. In general, the air content did not change significantly between all specimen

groups shown in Table 11, with the exception of sample TEA-C 5%, due to the defoaming agent. This is because sample TEA-C 5% exhibited honeycombing, which caused a significant increase in air content.

Figure 19. Honeycombing observed in TEA-C 5.0% specimens.

Due to the difficulties in casting concrete specimens with embedded triethanolamine capsules at high concentrations (above 2%), it will be necessary to optimize the mix design to compensate the lack of workability observed for the samples cast at 4% and 5%. Otherwise, high concentrations of TEA capsules would be considered impractical for implementation, especially since the concrete cover suffered dramatically.

5.2.2. Compressive Strength

The compressive strength results shown in Figure 20 indicate that for the calcium nitrate specimens, an increase in microcapsule concentration has a negative impact on strength. The highest microcapsule concentration (2% by wt. of cement) resulted in an 18% strength reduction. A statistical test using Fisher's least squares difference (LSD) was used to determine if the addition of microcapsules had a significant effect on the compressive strength of concrete. The analysis shows that the control specimen group is significantly different from those samples admixed with microcapsules at 0.5% and 2.0%. Even though the defoaming agent was shown to improve dispersibility of the microcapsules in water, it is possible that with the defoamer concentration used, it was still insufficient to adequately disperse the capsules throughout the concrete matrix. Thus, any clusters of microcapsules would weaken the cementitious matrix and increase the variability of the compressive strength considerably as compared to the control specimens.

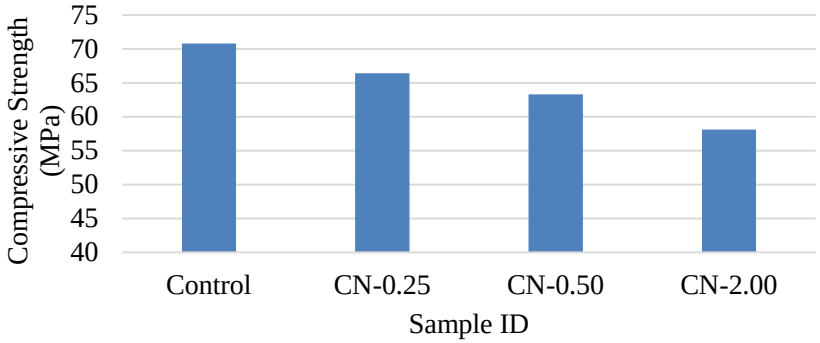

Figure 20. Compressive strength test results.

For the additional sample groups poured, the compressive strength results are shown in Figure 21.

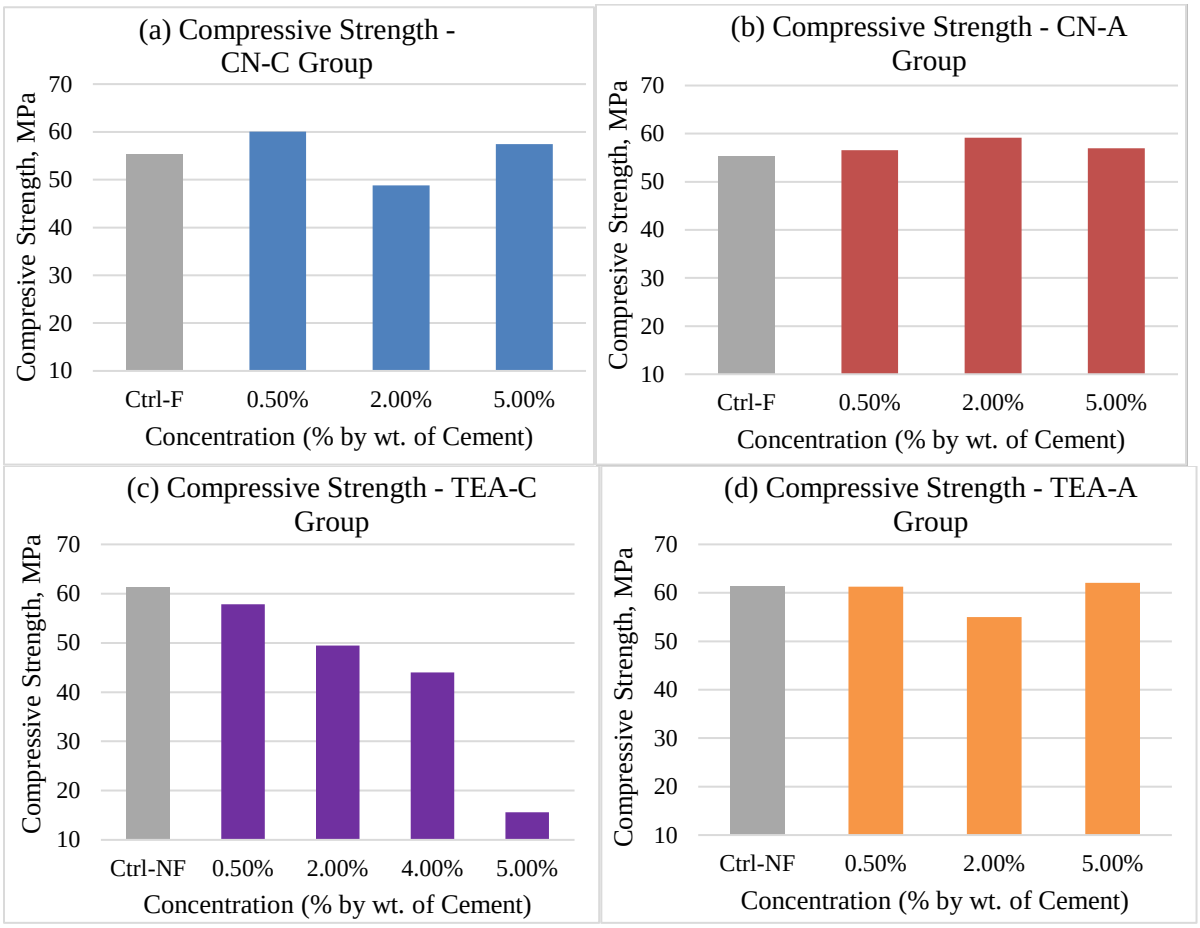

Figure 21. Compressive strength results for: (a) CN-C Group, (b) CN-A Group, (c) TEA-C Group, and (d) TEA-A Group. The CN-A and CN-C samples were fiber reinforced, while the TEA-A and TEA-C samples were not fiber reinforced.

The four sample groups tested include: (a) calcium nitrate, added through microcapsules [CN-C]; (b) calcium nitrate, added as an admixture [CN-A]; (c) triethanolamine, added through microcapsules [TEA-C]; and (d) triethanolamine, added as an admixture [TEA-A]. Since the calcium nitrate samples had an encapsulation efficiency of 22%, the CN-A groups had an equivalent amount of calcium nitrate admixed than the CN-C groups have encapsulated. Similarly, the triethanolamine samples had an assumed encapsulation efficiency of 5.2% (based on Choi et al. (*7*)), and therefore the TEA-A groups had an equivalent amount of triethanolamine admixed than the TEA-C groups have encapsulated.

The encapsulated calcium nitrate (CN-C) specimen group's compressive strength test results did not agree with the initial calcium nitrate microcapsule groups, since a higher concentration of microcapsules did not result in a weaker compressive strength (particularly at a 5% level). This may be attributed to the addition of 57 mm polymer fibers in the matrix, which may have added an extra level of variability depending on how well they were distributed in the 100 mm x 200 mm concrete cylinders. On the other hand, the CN-A groups did not have significant differences in compressive strength when compared to the control specimens, with the

exception of sample CN-A 2% which exhibited a stronger compressive strength. Thus, these results reaffirm that calcium nitrate as an admixture is compatible with concrete and does not negatively impact the mechanical properties.

The encapsulated triethanolamine (TEA-C) specimen group's compressive strength results showed that as the microcapsule concentration is increased, the concrete's strength decreased. However, there were no significant differences between the TEA-C 0.5% and the Control NF specimen groups. With respect to the TEA-A group, it was observed that triethanolamine is also compatible as an admixture with concrete as it did not cause any significant differences in compressive strength relative to the control specimens. The only difference was observed with the TEA-A 2% specimen groups, which resulted in a significantly weaker compressive strength (a 10% decrease in strength).

5.3. Corrosion Testing

There were two main sets of samples tested in this study. The first set consisted of trial samples named Ctrl-I, CN-I 0.25, CN-I 0.50, and CN-I 2.00. For the second set, all the samples listed earlier in Table 7 are included other than the first set of samples listed above.

5.3.1. Open Circuit Potential Results

First Set: Figures 22a and b shows the OCP values for the samples in the continuous-then-cyclic exposure, and samples subjected to only cyclic exposure, respectively. During 12 weeks of continuous ponding (Figure 22a), Ctrl-I and CN-I 0.25 (sample with the lowest microcapsule concentration, 0.25% by weight of cement) remained passive while CN-I 0.5 and CN-I 2.00 (samples with higher microencapsulated calcium nitrate concentrations) remained active even from the first measurement. CN-I 0.50 and 2.00 were found to be more electrochemically active than the Control and CN-I 0.25 during 12 weeks of continuous ponding exposure, as evident by more negative OCP values for CN-I 0.20 and 2.00. While the Control and CN-I 0.25 remained passive (low-corrosion risk), CN-I 0.50 and 2.00 were subject to intermediate-corrosion risk.

After 12 weeks of continuous ponding, the exposure was switched to the wet/dry cycles. This step was performed to simulate the condition when the actual environment surrounding the concrete changes from continuous immersion to wet/dry exposure due to environmental changes. During the 12 weeks of wet/dry cycles, Control and CN-I 0.25 samples kept passive while CN-I 0.50 tended to become more passive with time. On the other hand, CN-I 2.00 became more active. Its OCP values significantly dropped during 12 weeks of wet/dry cycles. The corrosion risk of CN-I 2.00 was close to 90% in the last weeks of testing. The interpretation of OCP values shown in all the OCP graphs in this study follows the interpretation made by Broomfield (*34*), as shown in Table 12.

Table 12. Corrosion condition for OCP values (*34*).

OCP (mV vs SCE)	Corrosion Condition
>-80 mV	Low (10% risk of corrosion)
-80 mV to -230 mV	Intermediate corrosion risk
<-230 mV	High (> 90% risk of corrosion)
<-380 mV	Severe corrosion

The OCP values for the encapsulated samples, which were exposed to ASTM G 109 cyclic exposure since the beginning of testing, are shown in Figure 22b. It can be seen that the sample with the highest concentration (i.e., CN-I 2.00) stayed within the passive region for the entire test. Samples CN-I 0.25 and CN-I 0.50 both showed activation in the first 2 weeks but then showed repassivation of the rebar as the test continued. The results from the cyclic test were in contrast with the continuous-then-cyclic test, where the highest concentration of microcapsules was more effective in the ASTM cyclic test, while the samples with the lowest concentration of microcapsule and no microcapsules performed the best in the continuous-then-cyclic test. The inconsistent finding in OCP trend in the ASTM cyclic and continuous-then-cyclic test could be attributed to the different mechanism of corrosion and diffusion of aggressive species occurring in the continuous ponding compared to that of the ASTM G 109 cyclic ponding. For instance, the Cl^- ions and O_2 are more limited in the continuous ponding environment due to the low diffusion rate of these species through the ponding solution (3.5% NaCl). In addition, the difference in the number of ruptured microcapsules in each same type of sample which affect the actual concentration of inhibitor released from capsules to concrete may also play a significant role in this inconsistent trend.

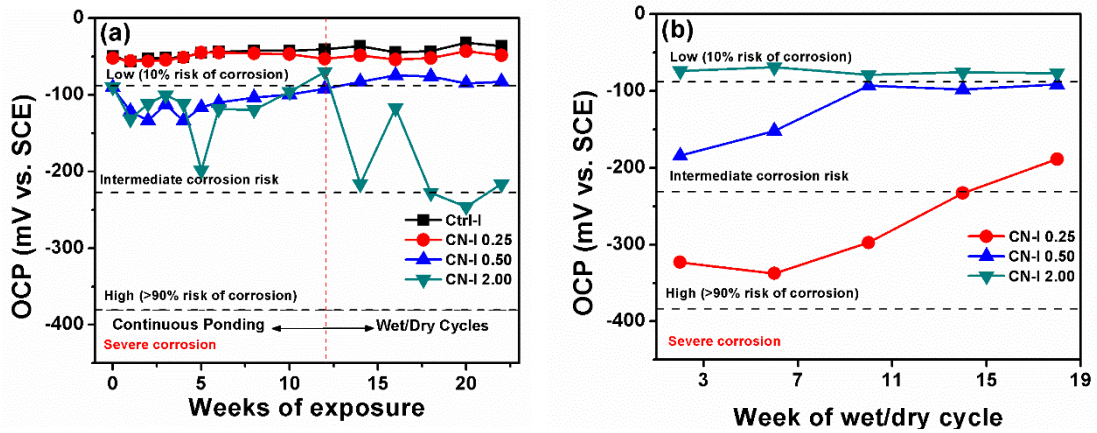

Figure 22. OCP values of the Control and encapsulated calcium nitrate (CN-I) samples in the first set exposed to: (a) continuous-then-cyclic, and (b) ASTM G109 cycle exposure.

Since the Control sample for ASTM G 109 cyclic exposure was completely broken during the 3-point bending to create cracks, the values of OCP, PD, macrocell corrosion current, EIS spectra, concrete resistance, corrosion rate, and % inhibition could not be reported in this study.

Second Set: In the second set, samples were subject to different exposures: (1) ponding and (2) fog chamber exposure. Both ponding and fog chamber exposures consisted of 2 days of wet cycle and 2 days of dry cycle. The difference is that the ponding exposure had the wet/dry cycles in the air while the fog chamber, as its name suggests, had them in the fog chamber.

In the first 26 days of ponding exposure, CN-C samples showed corrosion activation as indicated by their OCP values located in the intermediate-corrosion risk (Figure 23a). As time increases, their OCP values increased to the passive (low-corrosion risk) zone. This corrosion activation in the first 26 days of days could be associated with higher availability of aggressive species such as chloride diffusing more quickly into concrete due to cracks. Although calcium nitrate was already available in the concrete (released from ruptured microcapsule) before

corrosion testing, it took time for calcium nitrate to diffuse and reach the rebar and worked as an inhibitor. The calcium nitrate available at different depths of concrete from different positions of microcapsules took time to diffuse and reach the rebar. After 26 days, a sufficient amount of calcium nitrate released from microcapsules blocked the anodic areas and formed the passive films on the rebar, resulting in more positive OCP values. In contrast, CN-A samples that had no cracks, meaning lower concentration of aggressive species, were almost stable in the passive (low corrosion risk) zone (Figure 23a). Unlike in the CN-C samples, calcium nitrate in CN-A samples was readily available at the rebar – concrete interface to passivate the rebar. This made the OCP values of CN-A samples almost constant in the passive zone from the beginning until the end of testing.

For the TEA-C samples, the sample with the lowest concentration (0.50%) remained stable in the low corrosion risk zone while the higher concentrations (2.00, 4.00, and 5.00%) were in the intermediate corrosion risk (with more negative potentials) during the ponding exposure (Figure 23b). However, as can be seen, a slight increase in OCP values with increasing time were observed for those higher concentration samples. In contrast, all of TEA-A samples remained passive during the testing. The more negative potentials of TEA-C samples than the ones for TEA-A could be attributed to the fact that TEA in TEA-A samples was readily available in the concrete and even at the rebar/concrete interface to react and form the passive film while the TEA in TEA-C samples needed a pH change to be released form microcapsule to the concrete. Considering the diffusion of aggressive species was faster than the speed of TEA release from microcapsules due to pH change in the laboratory wet/dry cycles, the concentration of TEA in TEA-C might be ineffective compared to TEA-A sample case.

All Control samples (no corrosion inhibitors) for both CN and TEA samples remained passive during 68 days of testing without showing any corrosion activation while some CN-C and TEA-C samples did show an activation in the early days (26 days) of exposures. CN-A and TEA-A also remained passive like Control samples did during 68 days the testing, but they were slightly more noble than the Control samples. After 68 days of exposure, the OCP values for CN-C and TEA-C became more noble, locating in the passive (low corrosion risk) zone. However, their OCP values were still lower than the ones for CN-A, TEA-A and Control. These phenomena could be related to the effective concentration of corrosion inhibitor in each type of samples. The CN and TEA are anodic corrosion inhibitors. The CN and TEA react with the metal ions to form a passive layer on the metal surface that is able to slow down the corrosion process. For an anodic inhibitor, the concentration must be high enough to cover the anodic sites on the metal. If the concentration is low, only a few anodic sites are covered by the passive film. This condition is worse compared to the situation where a metal has no passive film at all. When a metal is not fully covered by a passive film or in other words, only few areas are covered by the passive film, localized corrosion may occur. This localized corrosion is more active than the uniform corrosion.

For CN-C samples, at the early stages (less than 26 days) the actual amount of released corrosion inhibitor from ruptured microcapsules might not be sufficient at the rebar/concrete interface to form the passive film. This is because the released corrosion inhibitor took time to diffuse and reach the rebar. As a result, only small areas of anodic sites were initially covered by the passive film. This left some sites of metal uncovered which then led to localized corrosion. After 26 days, most of the released corrosion inhibitors had reached the rebar surface and covered the surface, leading to more noble OCP values located in the passive zone (Figure

23a). For CN-A, in contrast, since sufficient concentration of corrosion inhibitor was readily available at the rebar/concrete interface, this corrosion inhibitor instantaneously formed the passive film, even from the beginning of testing. This is evident by constant passive OCP values during the testing. For the Control, since localized corrosion induced by incomplete passive film coverage did not happen, corrosion was expected to be less active. This is proved by the constant passive OCP value. As can be seen in Figure 23a, the most noble OCP values were achieved by CN-A samples that had readily sufficient concentration of corrosion inhibitor at the rebar/concrete interface, followed by the Control and lastly by CN-C. It is well know that the use of insufficient concentration of anodic inhibitor leads to worse corrosion process on the metal compared to the case where no corrosion inhibitor is present. These explanations for CN-C samples apply to CN-I samples in Figure 22a where incomplete passive film coverage made OCP values of CN-I samples were more active.

For TEA, similarly, TEA-A had more noble OCP values than TEA-C because sufficient corrosion inhibitors might have been more readily available at the rebar/concrete interface in TEA-A samples. The pH change due to wet/dry cycles might have triggered the release of corrosion inhibitor in TEA-C as indicated by a slight increase in OCP with time but the concentration might not have been sufficiently at the early stages. The explanation why the OCP values of the Control was between TEA-A and TEA-C is the same as the one for CN samples. It is related to the absence of localized corrosion induced by incomplete passive film coverage.

However, it should be considered that the slightly more noble OCP values do not represent lower corrosion rates. The OCP is a thermodynamics parameter that does not provide information about the corrosion rate. It describes how likely corrosion to occur. In the corrosion field, the kinetics of corrosion in terms of corrosion rate is more important and practical. In order to evaluate the kinetics of corrosion of these rebars, the EIS was performed and analyzed.

In the fog chamber exposure, CN-C samples in the fog chamber were generally more electrochemically active than the CN-A ones. With the concentrations of encapsulated calcium nitrate being same as the ones in the ponding exposure, these encapsulated samples in the fog chamber had more negative OCP values (Figure 24), indicating more active corrosion. This suggests that the environment inside the fog chamber is more aggressive than the one in the ponding exposure. The corrosion activation on the rebar was followed by re-passivation process regardless small fluctuations in the OCP observed in all samples except for CN-C 0.50 and 2.00. While corrosion risk for microencapsulated CN-C 0.50 and 2.00 became higher with increasing exposure time, the rest of samples (for both CN-A and CN-C) tend to be stable and stayed in the same corrosion risk zone in the entire testing time although some small fluctuations were observed. In the fog chamber testing, the diffusion of harmful species especially Cl^- was faster than in the ponding exposure, making the pore solution is more conductive and more conducive for corrosion to occur.

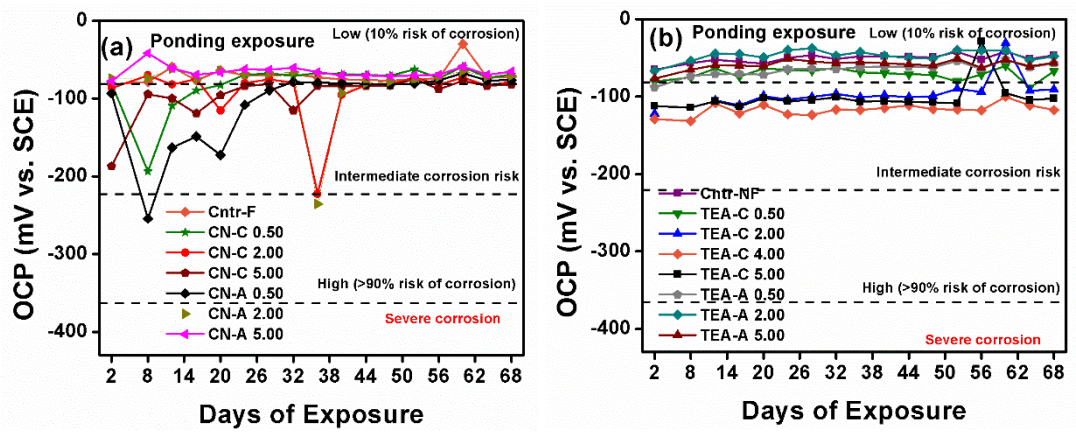

Figure 23. Open circuit potential for: (a) Control with fiber and calcium nitrate (admixed and encapsulated), and (b) Control without fiber and triethanolamine in the ponding exposure.

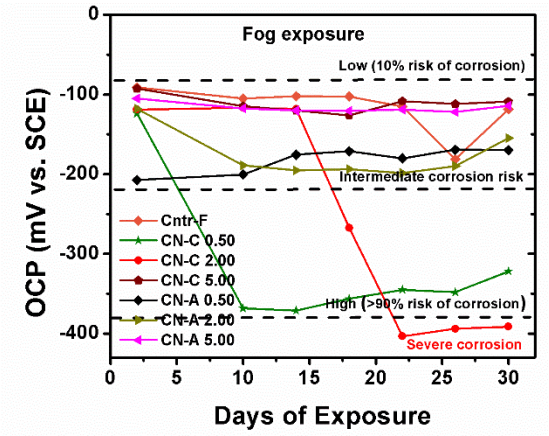

Figure 24. Open circuit potential for Control (with fiber) and calcium nitrate (admixed and encapsulated) in the fog chamber exposure.

5.3.2. Macrocell Corrosion Current

First Set: The corrosion process of reinforcing steel in concrete is complicated by the coexistence and mutual influence of micro and macro corrosion cells. Due to the multiscale and non-uniform phase of concrete, various spatial dimensions of microcell and macrocell corrosion exist in the corrosion process of steel in concrete. In this study, the measurement of these two types of corrosion enables us to evaluate which is more dominant. Microcell corrosion is defined as a corrosion process where active dissolution and the corresponding cathodic half-cell reaction take place in adjacent parts of the same metal. In this study, the microcell corrosion current was converted to and presented as corrosion rate (mm/year). Macrocell corrosion can occur when the active rebar is coupled to another/other rebars, which are passive or have a lower corrosion rate, either due to its different metal composition or different environments.

Figures 25a and b show the macrocell corrosion current for microencapsulated CN-I samples exposed to continuous ponding then wet/dry cycles and ASTM G109 cyclic exposure, respectively. For CN-I samples exposed to continuous then wet/dry cycles (Figure 25a), the highest current was found in CN-I 2.00 (the highest concentration of calcium nitrate in

microcapsule) while the lowest one belonged to CN-I 0.50, followed by the Control. This suggests that the most active corrosion was found on the anode of CN-I 2.00 while the lowest one was in CN-I 0.25. This trend is slightly different from the OCP results shown in Figure 22 where the least and most active samples were the Control and CN-I 2.00, respectively.

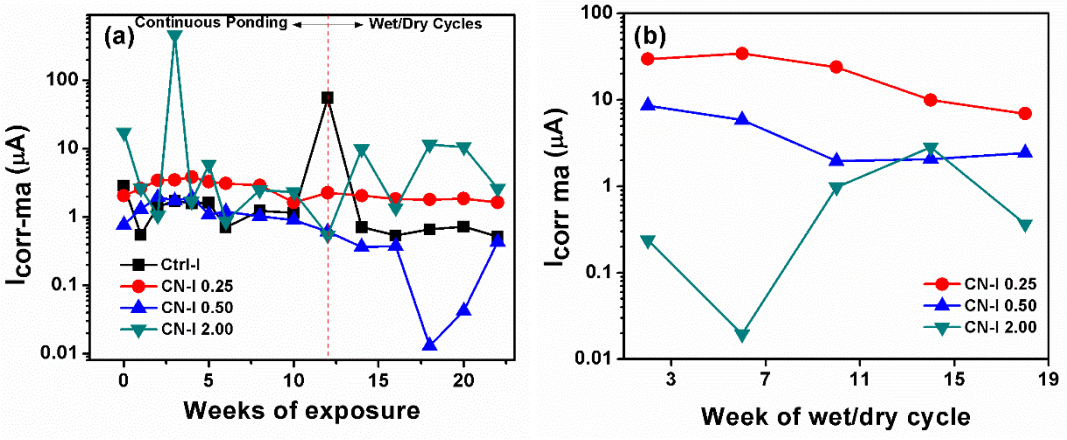

Figure 25. Macrocell corrosion current values for the Control and encapsulated calcium nitrate samples (CN-I) in the first set exposed to: (a) continuous-then-cyclic, and (b) ASTM G109 cycle exposure.

For the encapsulated samples exposed to ASTM G 109 cyclic exposure (Figure 25b), the trend is similar to the one of OCP (Figure 24) where increasing the concentration of calcium nitrate improved the corrosion resistance of rebar. The macrocell corrosion current that represents the total current flowing in the system show that for both exposures (continuous then cycles and ASTM G 109 cyclic exposure), its current values, in general, increased with decreasing the percentage of calcium nitrate (by the weight of cement). Since the OCP of the top rebar only depends on the electrochemical reactions while macrocell corrosion current gets contributions from electrochemical reactions from the bottom rebars; the trend in macrocell corrosion current does not have to be necessarily the same as the one in OCP. In some samples, the OCP values of the bottom rebars were found to be more active than the top one, making the bottom ones, which are expected to be cathodes become anodes.

No potential difference measurement was performed on the fog chamber due to the activation of bottom rebars.

Second Set: For the calcium nitrate (admixed and microencapsulated) and triethanolamine (admixed and microencapsulated), the macrocell corrosion current values were similar even when compared to the Control samples. There are two possible explanations. First, the corrosion inhibitor in both microcapsules and admixtures have not been activated. Second, although the triggering factors have activated the inhibitors, the difference in corrosion rate between the top rebar (anode) and bottom ones (cathode) was extremely small. For both samples (Figures 26a and b), the macrocell corrosion current tend to remain constant during 68 days of exposure, indicating that there is no significant corrosion process on the rebars. An abrupt increase in current observed for CN-A 0.50 and 2.00 was most likely caused by an interference in the measurement due to high impedance system, such as concrete, the currents are low and the measurement can pick up any random electric noise.

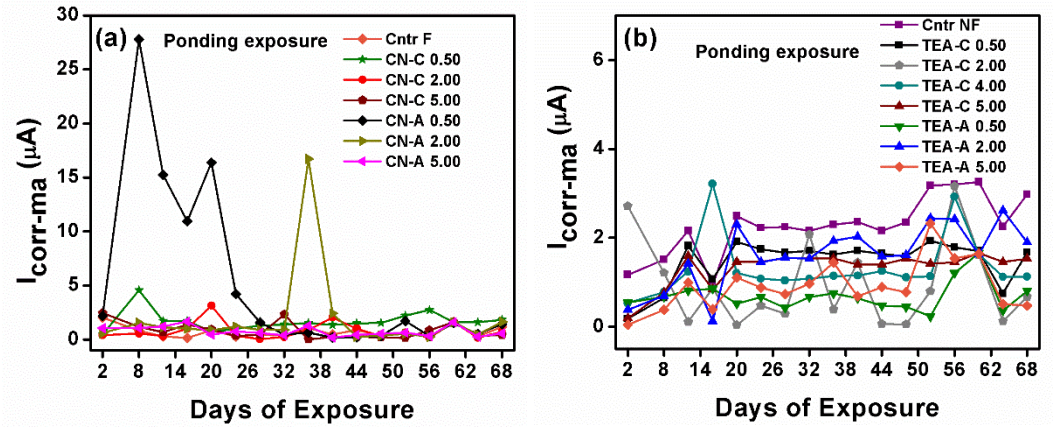

Figure 26. Macrocell corrosion current values for: (a) Control with fiber and calcium nitrate (admixed and encapsulated) and (b) Control without fiber and triethanolamine in the ponding exposure.

5.3.3. EIS Results

First Set of Samples: The electrochemical and chemical reactions occurring in the concrete and rebar/concrete interface was studied by EIS. EIS is a frequency domain technique that is able to extract of electrochemical and chemical reactions by correlating the kinetics degradation with the relation between input (potential) and output (current). For corrosion assessment in reinforced concrete, depending on the frequency range, mechanistic information in the concrete/rebar interface (pore network, isolated pore matrix), and rebar surface can be characterized in steady state conditions and as a non-destructive technique. EIS follows the lineal system theory in which electrical passive elements can be used to represent the electrochemical system from EIS signature. Three different representations resulted from EIS analysis are Nyquist, Bode and phase angle plots. The Nyquist or complex diagrams cover the mechanistic processes existing within the concrete/rebar system. Bode and Phase angle diagrams cover the quantitative or qualitative elements forming the electrochemical system, such as capacitors, resistances and mass transfer magnitudes.

Figures 27 to 30 are the EIS signatures for the CN-I samples exposed to continuous ponding then wet/dry cycles exposure while Figures 31 to 33 are for the samples exposed to ASTM G109 cyclic exposure. Two capacitive loops are observed at medium and low frequencies in the Nyquist plots (Figures 27a-30a and Figures 31a-33a), indicating two different processes in the system. The first process relates to the reaction in the connected and unconnected pore networks, and solid phase. This is observed at medium frequencies. At low frequencies, the process corresponds to the charge transfer reactions at the rebar/concrete interface. From the impedance modulus in the Bode plot (Figures 27-30b and Figures 31-33b), it can be seen that the modulus values range from 60 to 80 kΩ-cm^2 for all samples from week 1 to 22. This indicates that the corrosion rates were similar for the Control and all inhibited samples. In this case where the impedance modulus values for each sample is close to one another, another technique is required to more precisely calculate the corrosion rate. This technique is a polarization resistance obtained from the EIS spectra. A polarization resistance measurement using Equivalent Circuit (EC) in Figure 11 was used to evaluate the instantaneous corrosion rate on the rebars. From the high (10^5 Hz) to intermediate (10^0 Hz) frequencies (Figures 27-30c and Figures 31-33c), the phase angle is at 0°, indicating that concrete resistance factor is dominant in the electrochemical and chemical reaction in the system.

Based on these characteristics, the types of exposures were altered for the second set of samples. In order to speed up the tests and to increase the aggressiveness of the environment, the testing was conducted in the 2-2 day wet dry cycle in the ponding and fog exposure. These are the exposures that were used for the second set of samples, as described below.

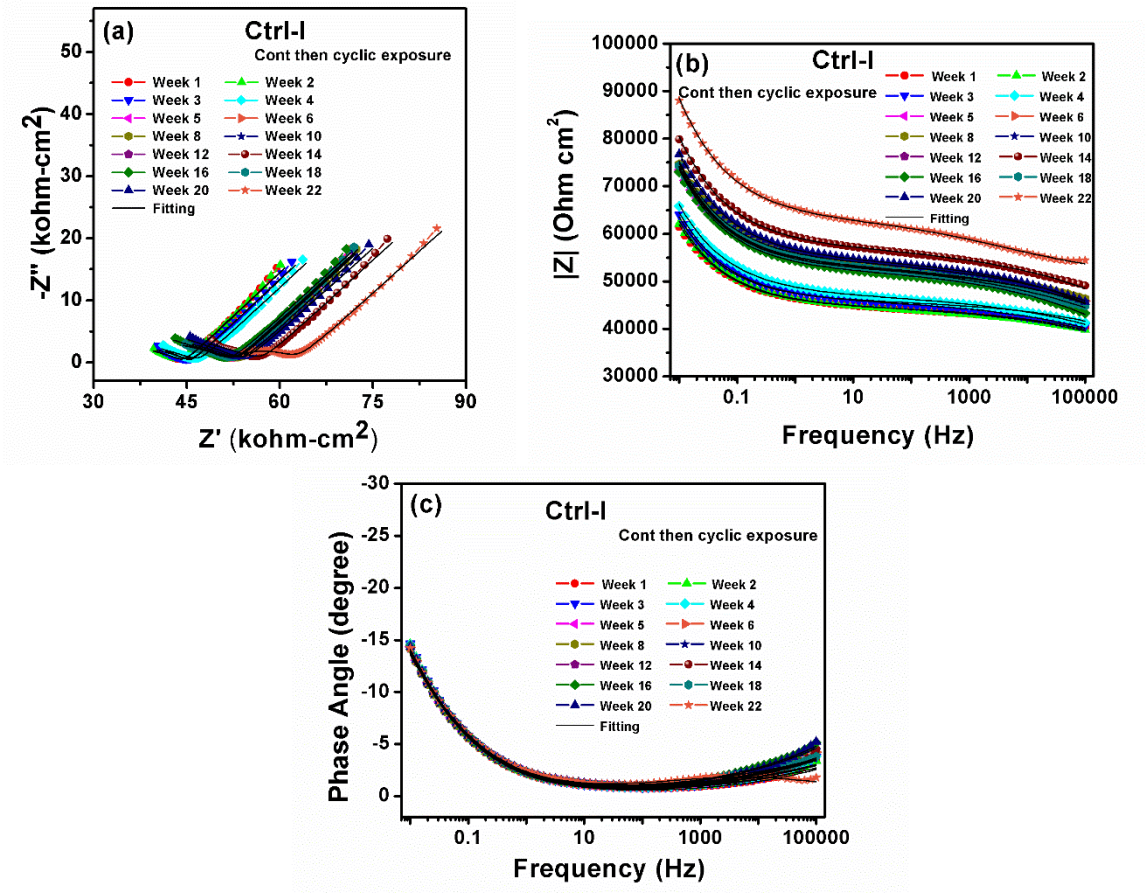

Figure 27. (a) Nyquist, (b) Bode, and (c) phase angle plots for the Control without fiber exposed to continuous-then-cyclic exposure.

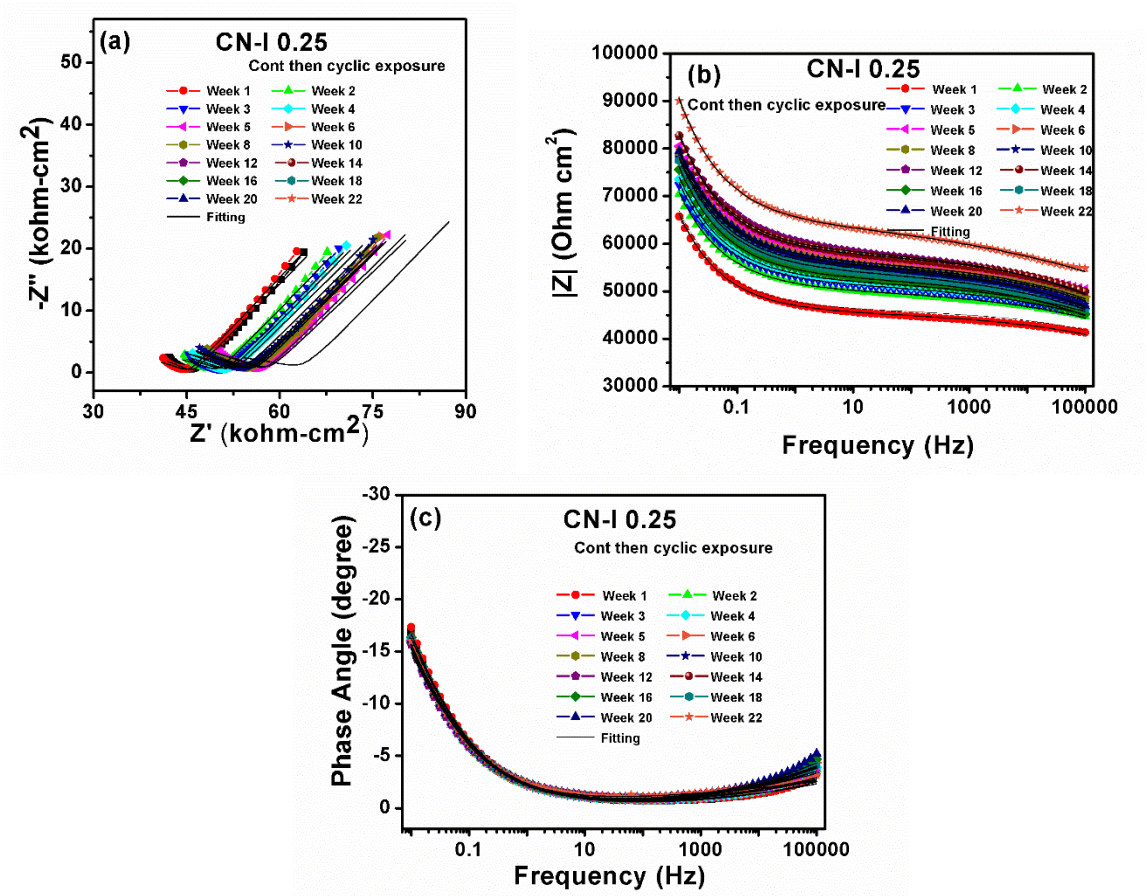

Figure 28. (a) Nyquist, (b) Bode, and (c) phase angle plots for microencapsulated calcium nitrate 0.25% exposed to continuous-then-cyclic exposure.

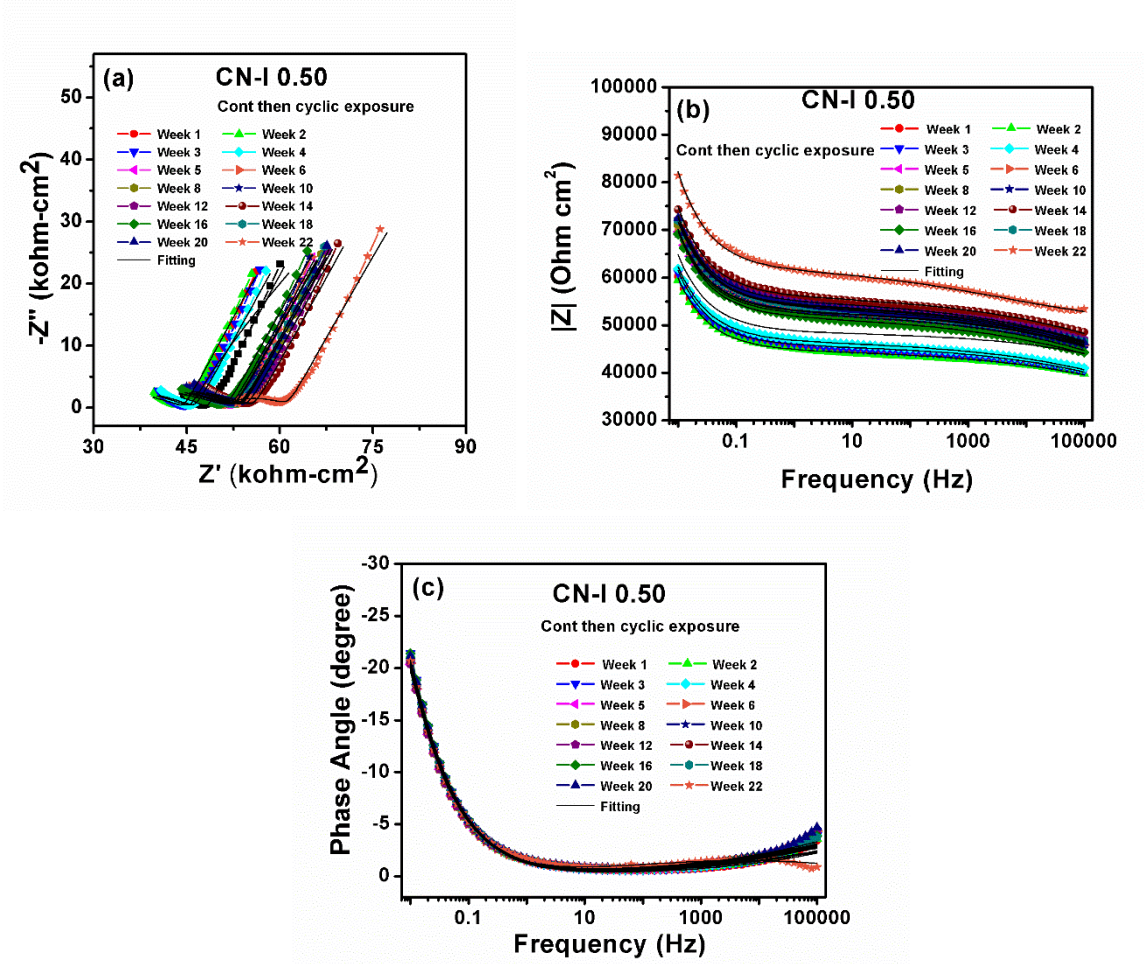

Figure 29. (a) Nyquist, (b) Bode, and (c) phase angle plots for microencapsulated calcium nitrate 0.50% exposed to continuous-then-cyclic exposure.

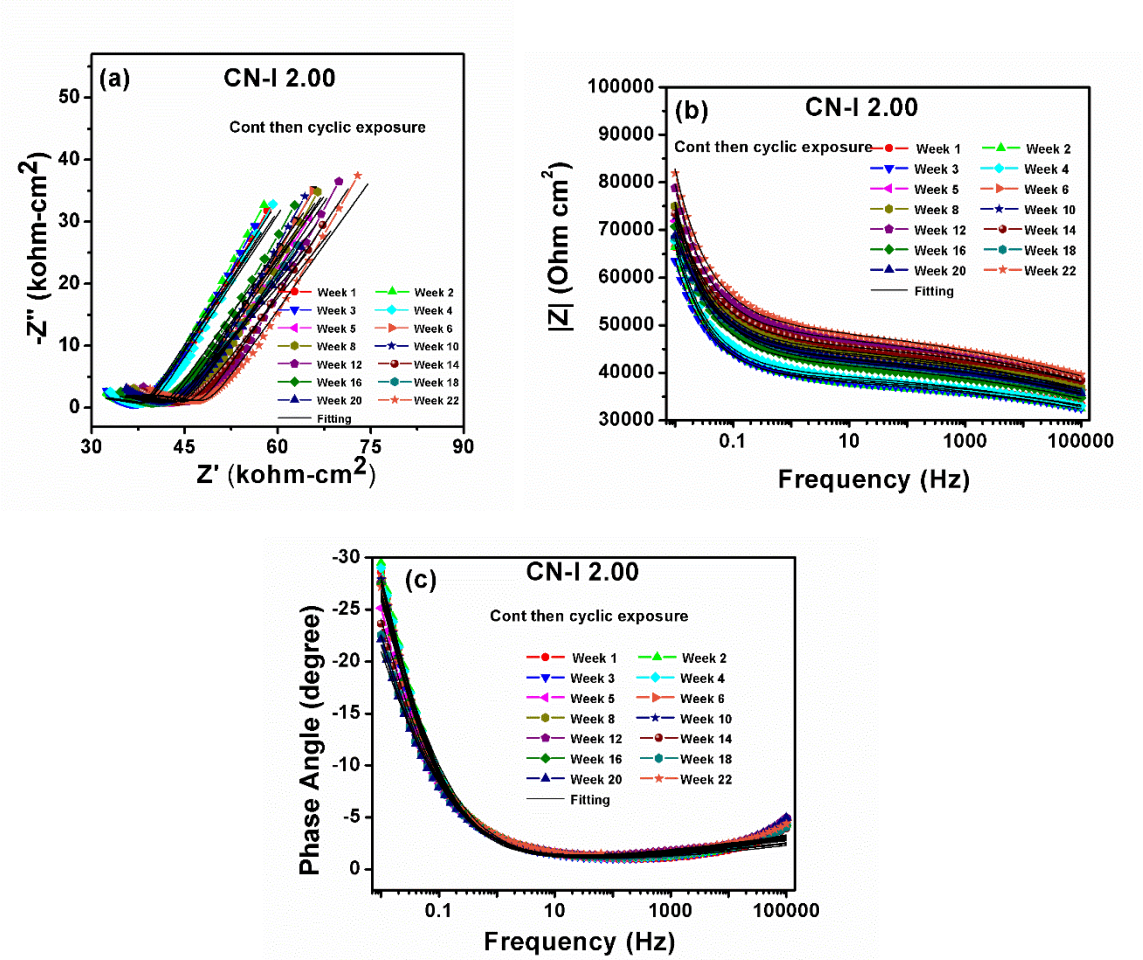

Figure 30. (a) Nyquist, (b) Bode, and (c) phase angle plots for microencapsulated calcium nitrate 2.00% exposed to continuous-then-cyclic exposure.

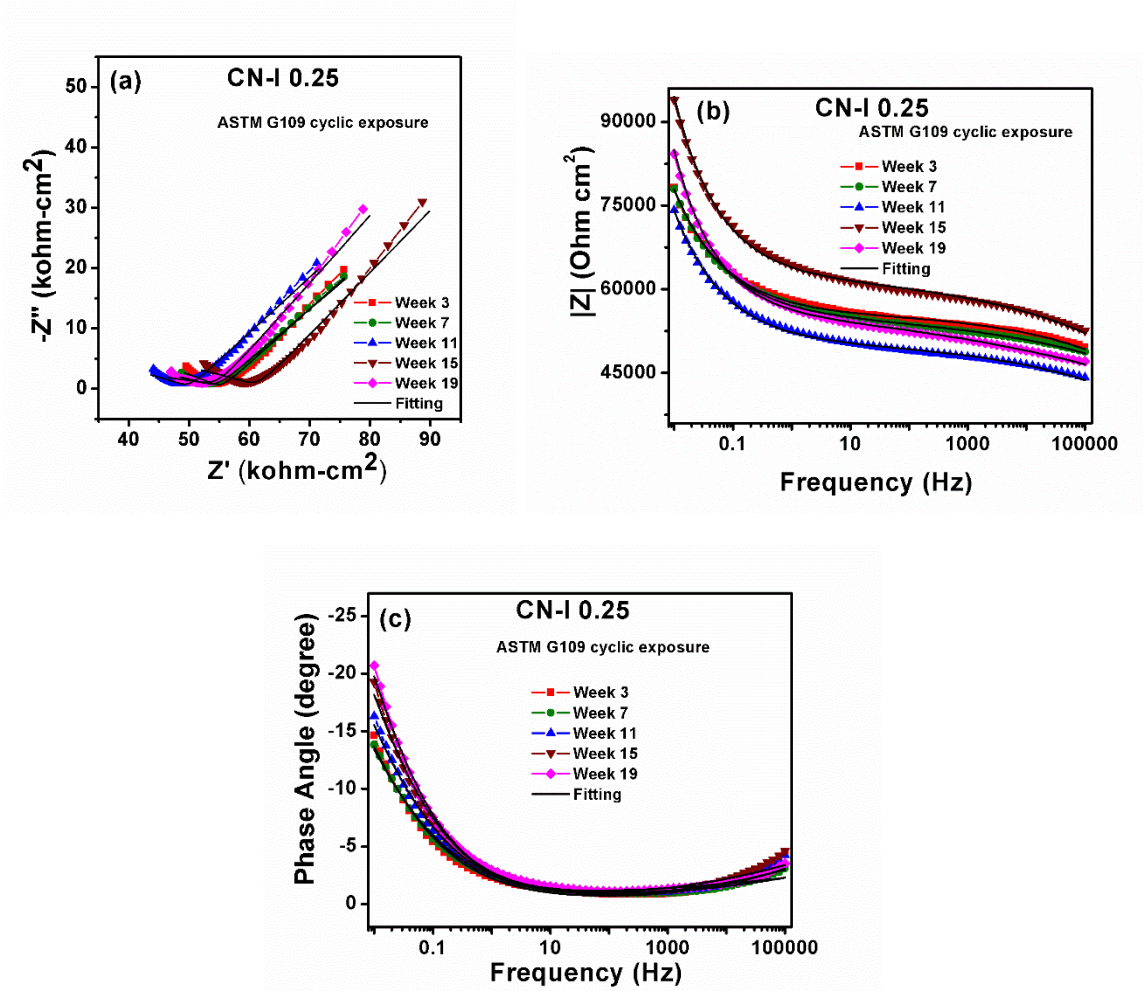

Figure 31. (a) Nyquist, (b) Bode, and (c) phase angle plots for microencapsulated calcium nitrate 0.25% exposed to ASTM G109 cyclic exposure.

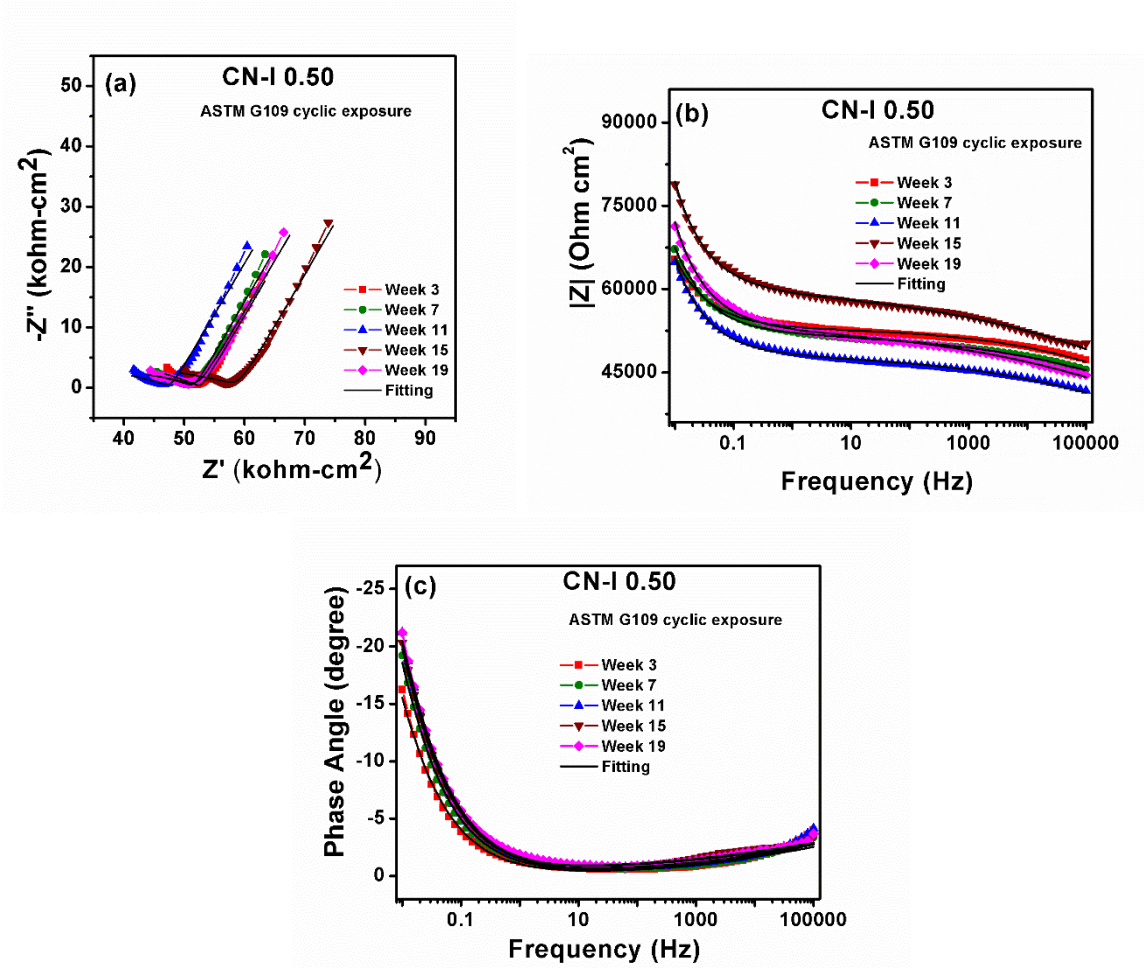

Figure 32. (a) Nyquist, (b) Bode, and (c) phase angle plots for microencapsulated calcium nitrate 0.50% exposed to ASTM G109 cyclic exposure.

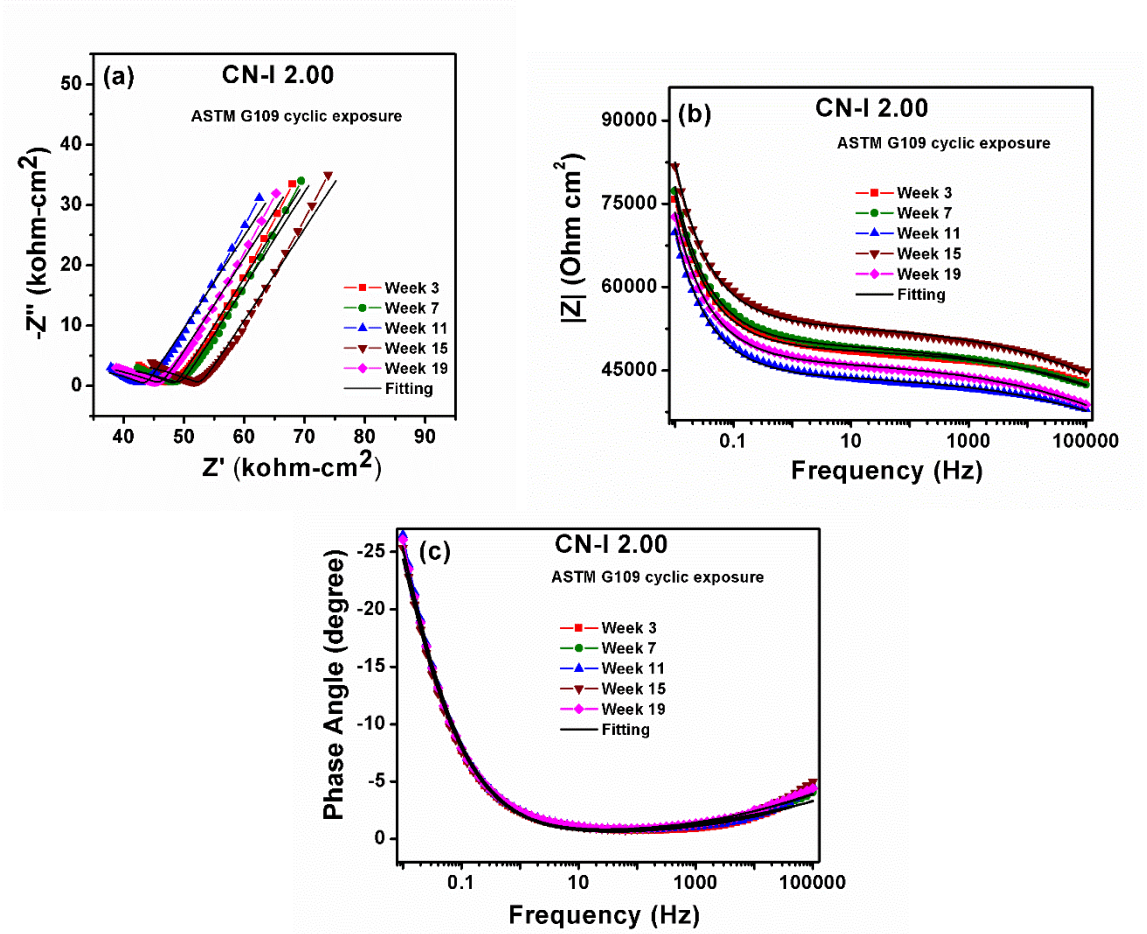

Figure 33. (a) Nyquist, (b) Bode, and (c) phase angle plots for microencapsulated calcium nitrate 2.00% exposed to ASTM G109 cyclic exposure.

Second Set: The EIS spectra of calcium nitrate (CN-A and CN-C) and triethanolamine (TEA-A and TEA-C) including their Control samples exposed to ponding exposures are shown in Figures 34 to 48. Quarter circles (poorly defined capacitive loops) at high frequencies are observed in all samples (Figures 34-48a). This is the characteristic that is also found in the samples exposed to continuous then cyclic and ASTM G109 cyclic exposures (Figures 27-33a). This typical quarter circle corresponds to a very high resistance of concrete.

The impedance modulus values in the CN-A and CN-C are, in general, slightly higher than the ones observed in the Control with fiber sample. This suggests that calcium nitrate slightly improved the corrosion resistance of rebars. When comparing CN-A to CN-C, it was observed that CN-C was more effective in decreasing the corrosion kinetics than CN-A as suggested by the higher impedance modulus of CN-C. This trend is different than the one observed in the OCP values, indicating that the OCP values cannot be solely used to predict corrosion resistance of rebars protected by corrosion inhibitors.

In contrast, the inhibiting effects can be seen clearly in the TEA-C. The impedance modulus values increase from around 60 kΩ-cm^2 in the Control sample to around 200 kΩ-cm^2 in the TEA-C samples except for 2% TEA-C. This suggests that the pH change that might be stimulated by wet/dry cycles successfully activated the release of triethanolamine and inhibited

corrosion on the rebars.

For the admixed triethanolamine, there is no significant change in the impedance modulus compared to the Control sample. The impedance modulus values for the Control and admixed triethanolamine samples are around 60–80 kΩ-cm^2. This finding proves that the microencapsulated triethanolamine is more effective in inhibiting corrosion than admixed triethanolamine.

From the phase angle plots (Figures 34-48c, the dominant process in the concrete can also be seen in phase angle at high to intermediate frequencies. This very high resistance might have slowed down the diffusion process of species to the concrete and rebar. The maximum peak angles for the TEA-C samples that have lower corrosion rate (based on the modulus impedance) are located at the higher frequencies (≈ 60°) than the ones for Controls, admixed triethanolamine, admixed calcium nitrate, and microencapsulated calcium nitrate.

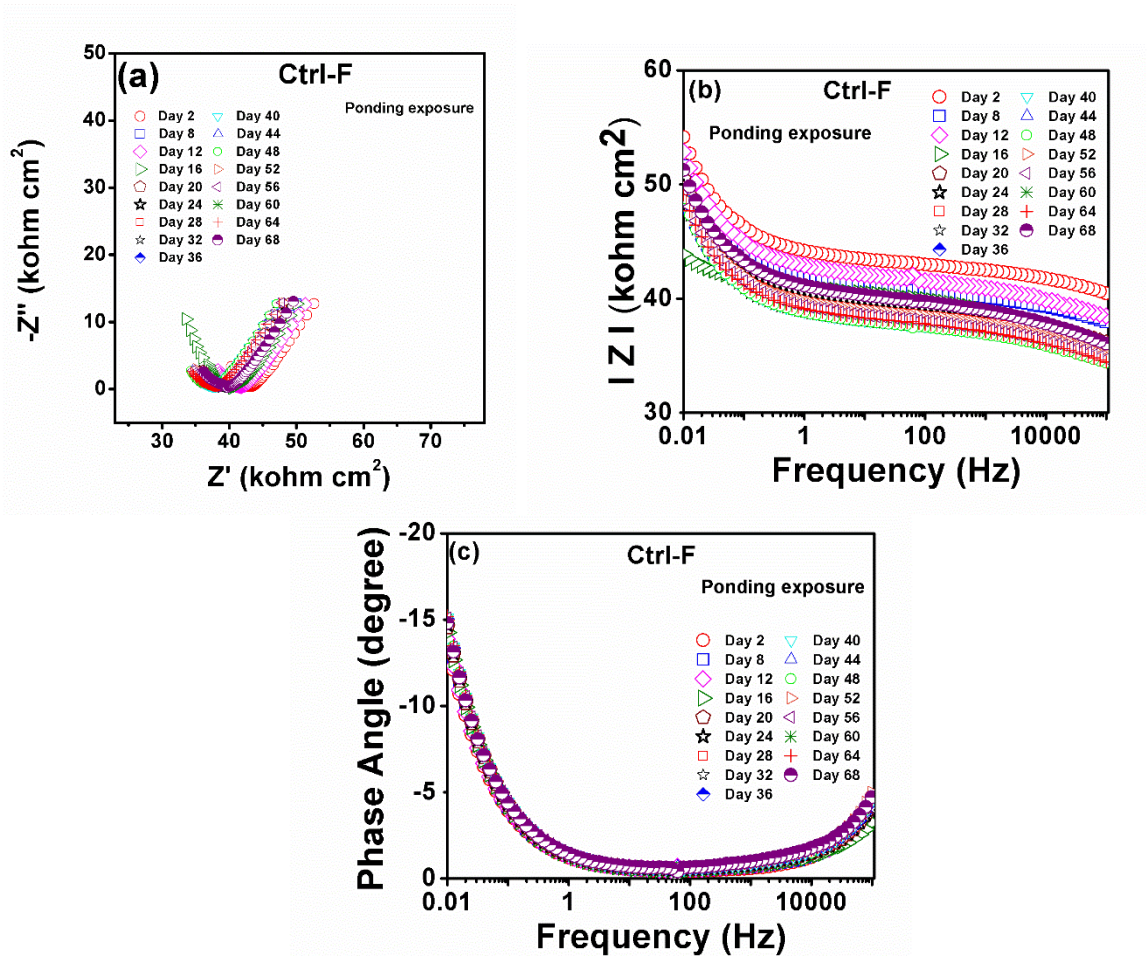

Figure 34. (a) Nyquist, (b) Bode, and (c) phase angle plots for the Control with fiber exposed to Ponding exposure.

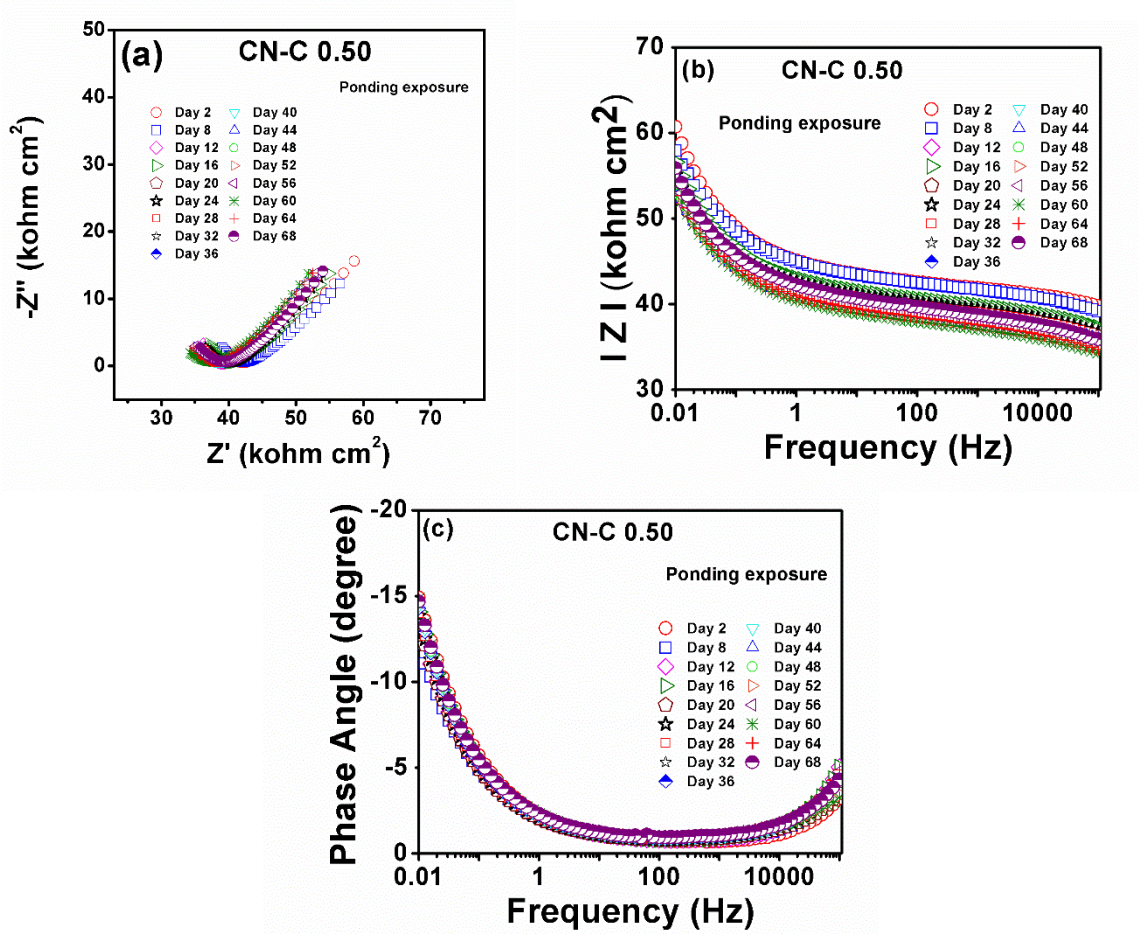

Figure 35. (a) Nyquist, (b) Bode, and (c) phase angle plots for microencapsulated calcium nitrate 0.50% exposed to Ponding exposure.

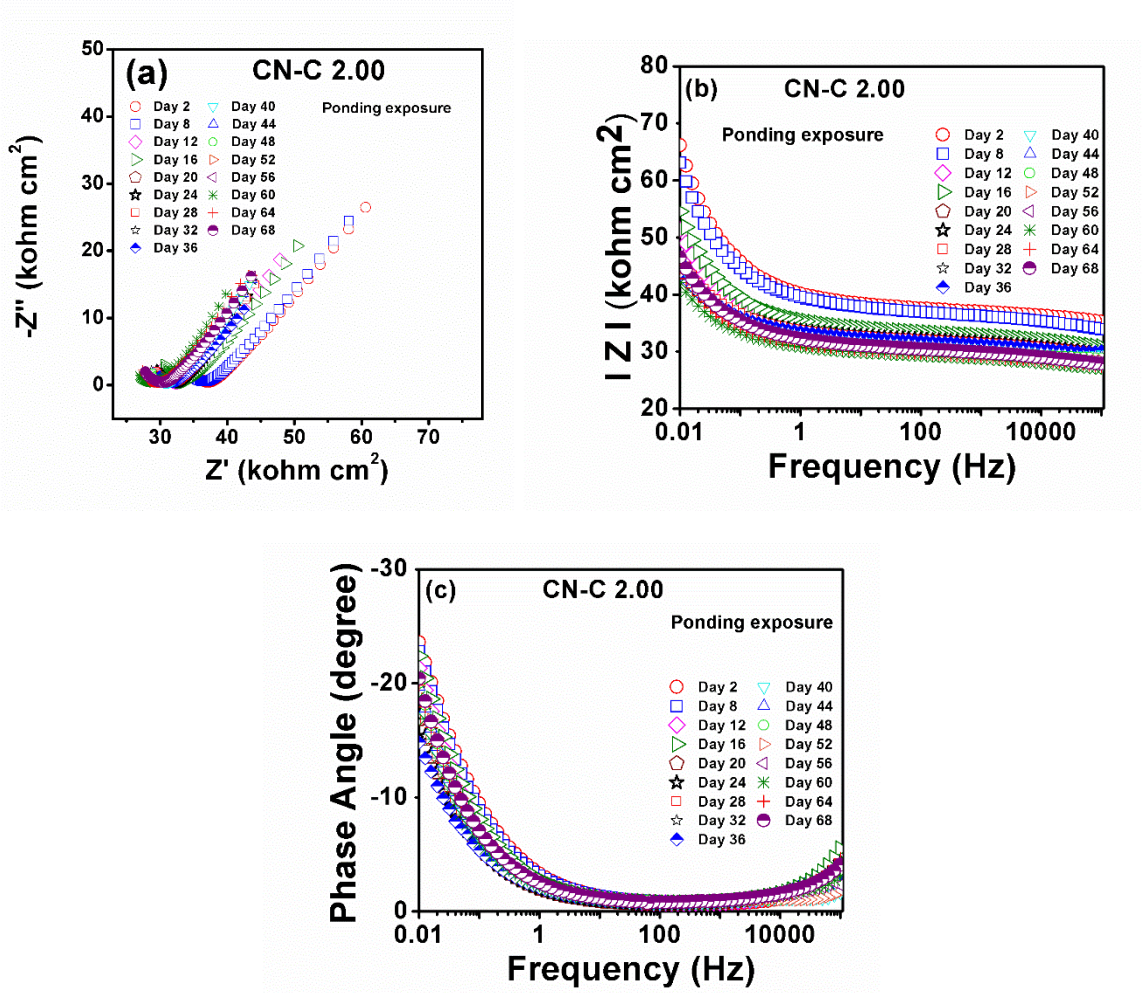

Figure 36. (a) Nyquist, (b) Bode, and (c) phase angle plots for microencapsulated calcium nitrate 2.00% exposed to Ponding exposure.

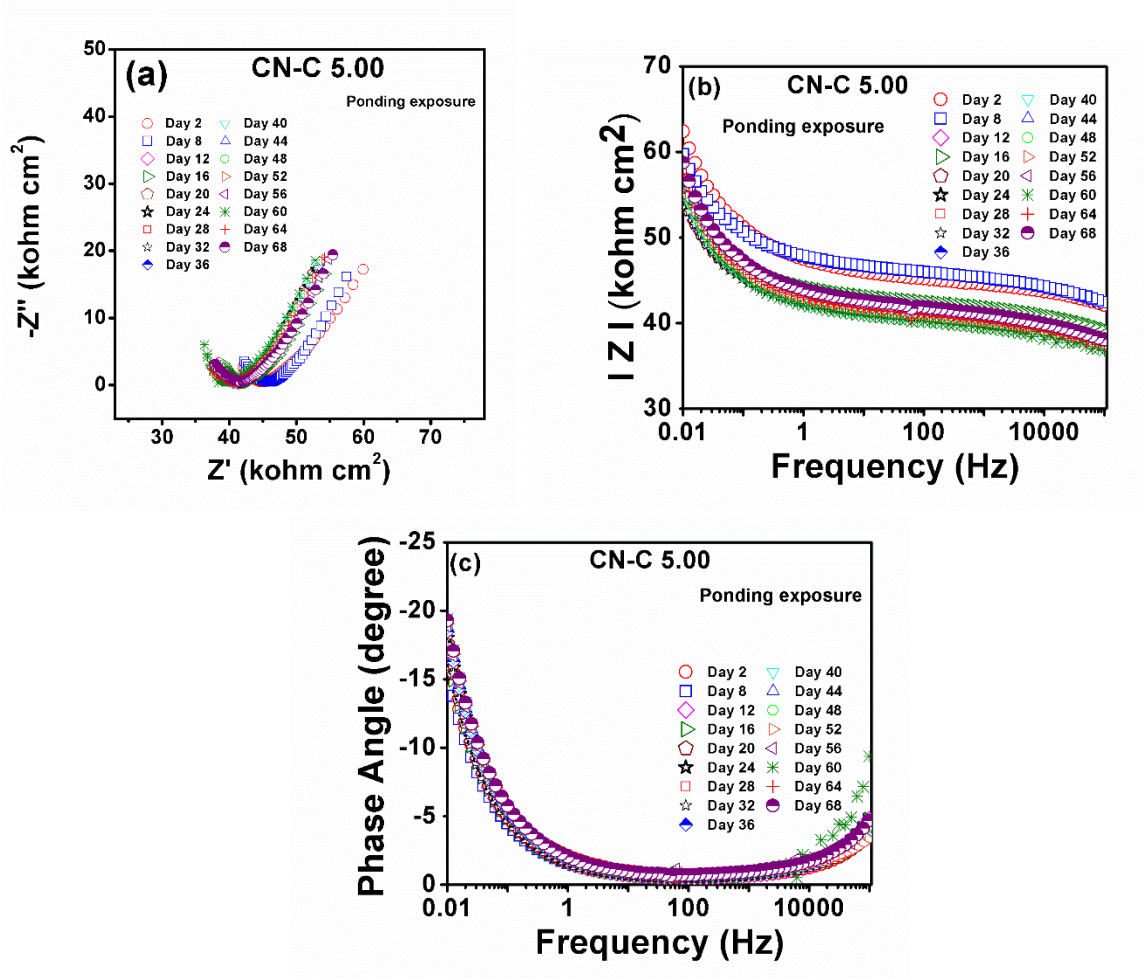

Figure 37. (a) Nyquist, (b) Bode, and (c) phase angle plots for microencapsulated calcium nitrate 5.00% exposed to Ponding exposure.

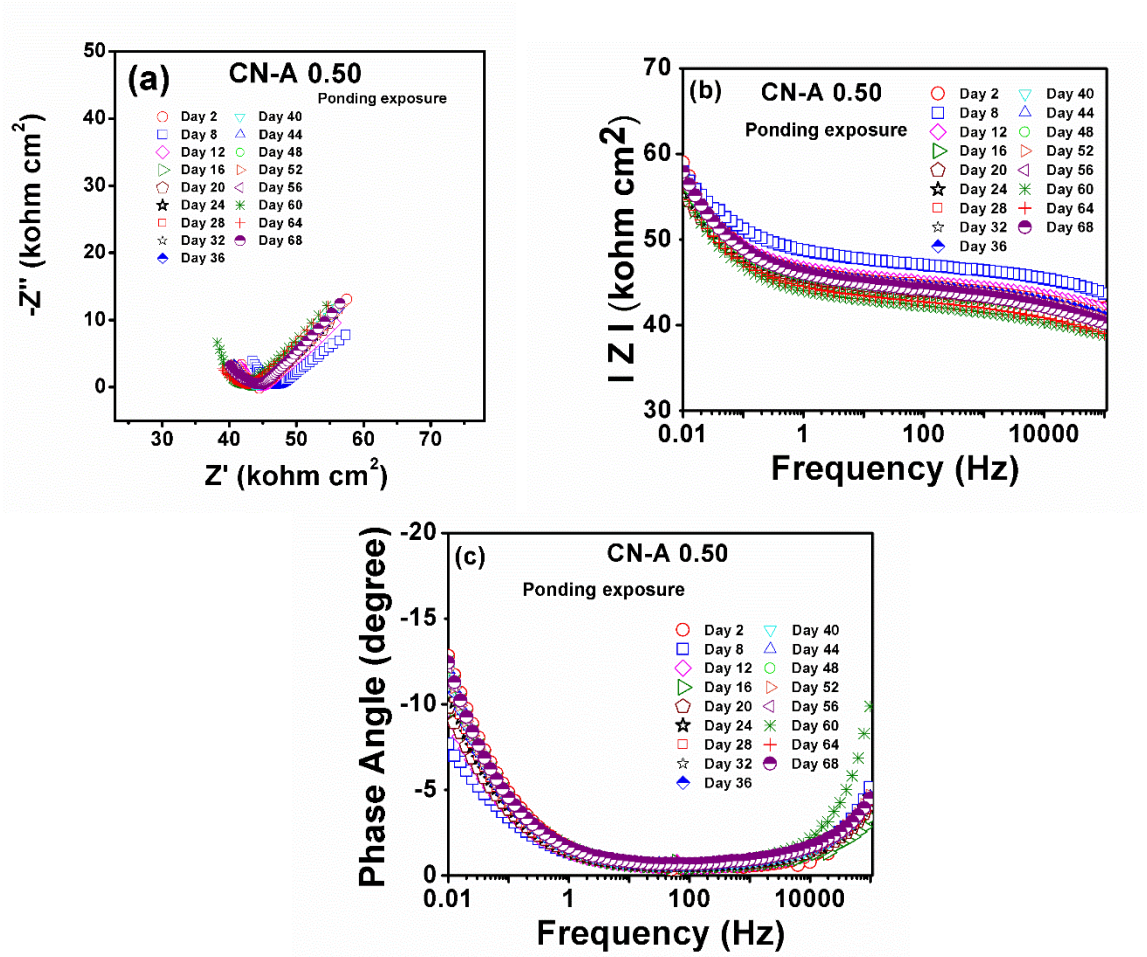

Figure 38. (a) Nyquist, (b) Bode, and (c) phase angle plots for admixed calcium nitrate 0.50% exposed to Ponding exposure.

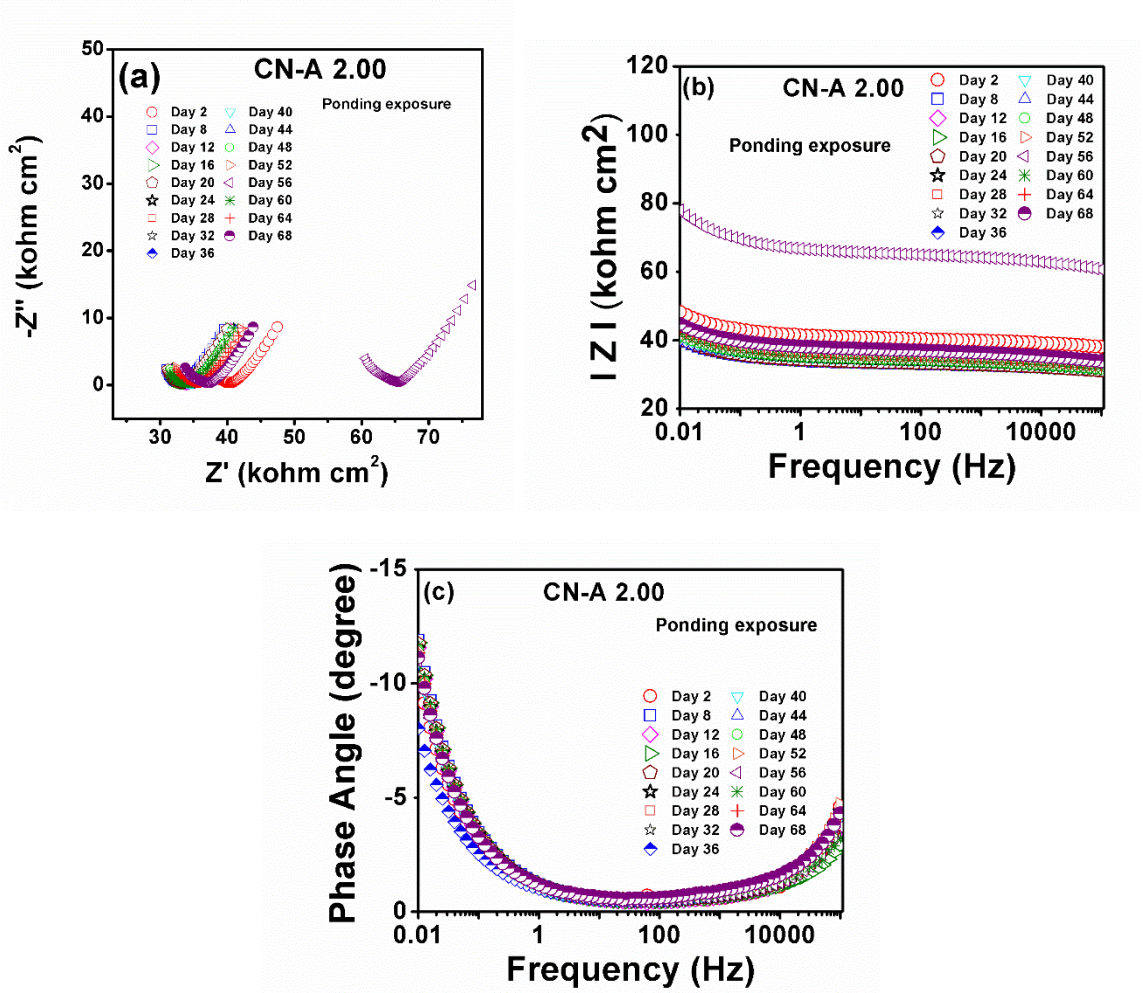

Figure 39. (a) Nyquist, (b) Bode, and (c) phase angle plots for admixed calcium nitrate 2.00% exposed to Ponding exposure.

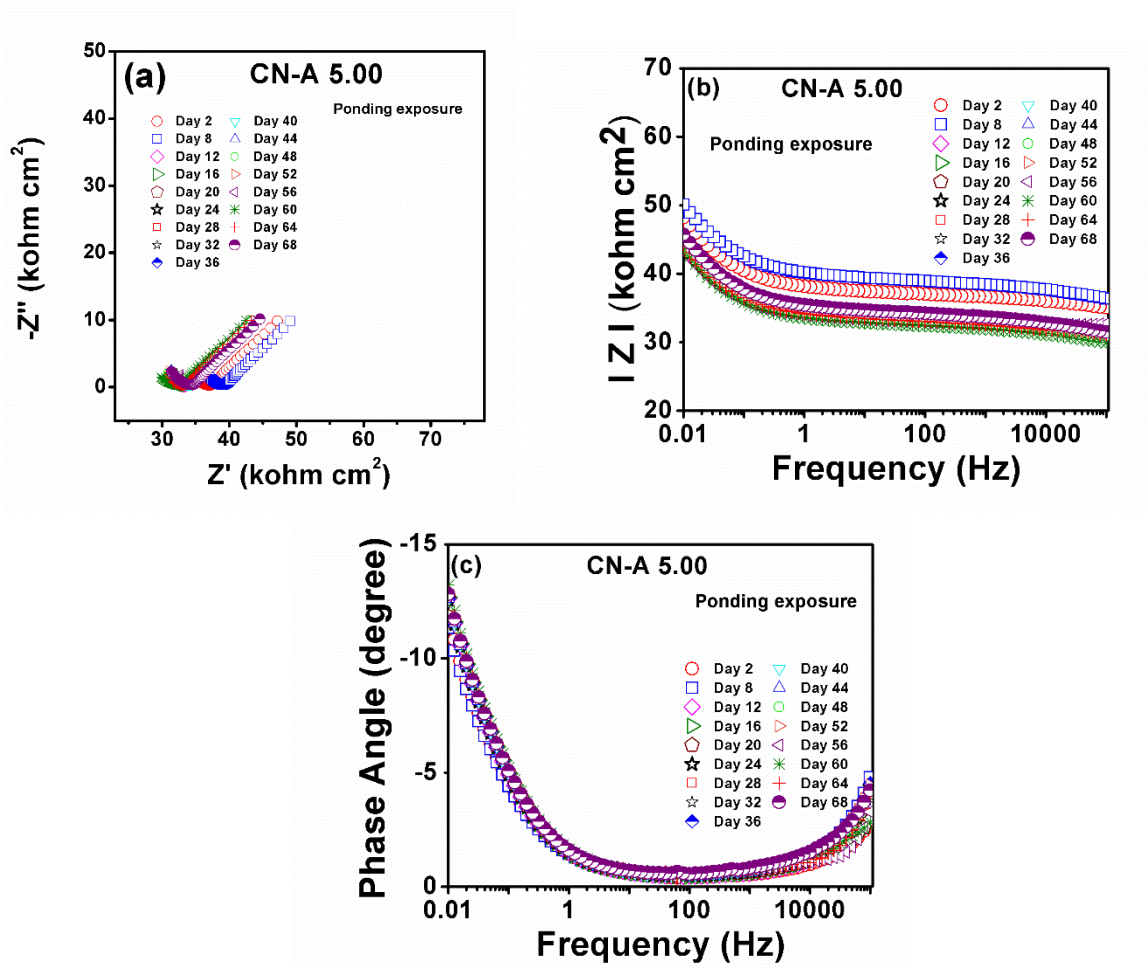

Figure 40. (a) Nyquist, (b) Bode, and (c) phase angle plots for admixed calcium nitrate 5.00% exposed to Ponding exposure.

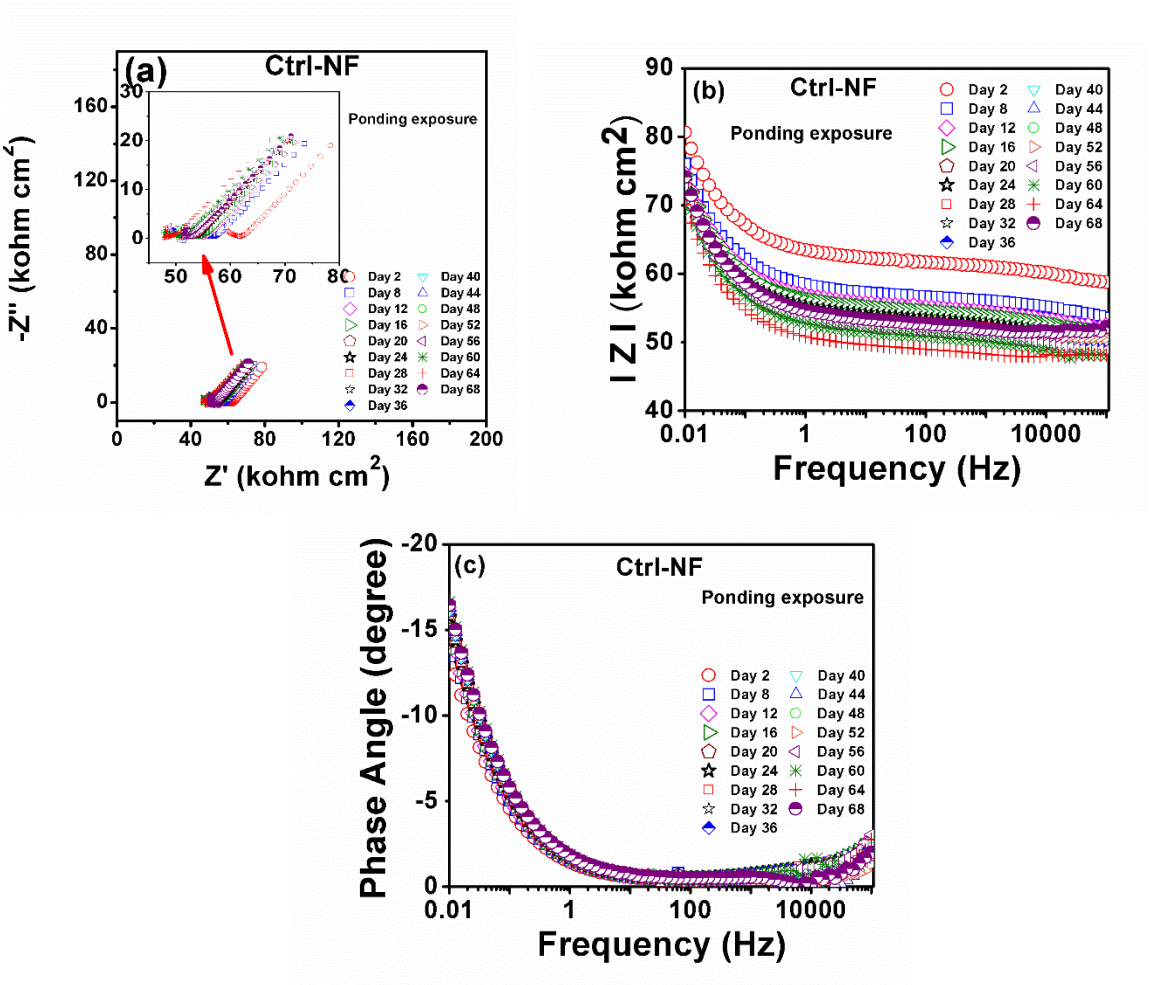

Figure 41. (a) Nyquist, (b) Bode, and (c) phase angle plots for the Control without fiber exposed to Ponding exposure.

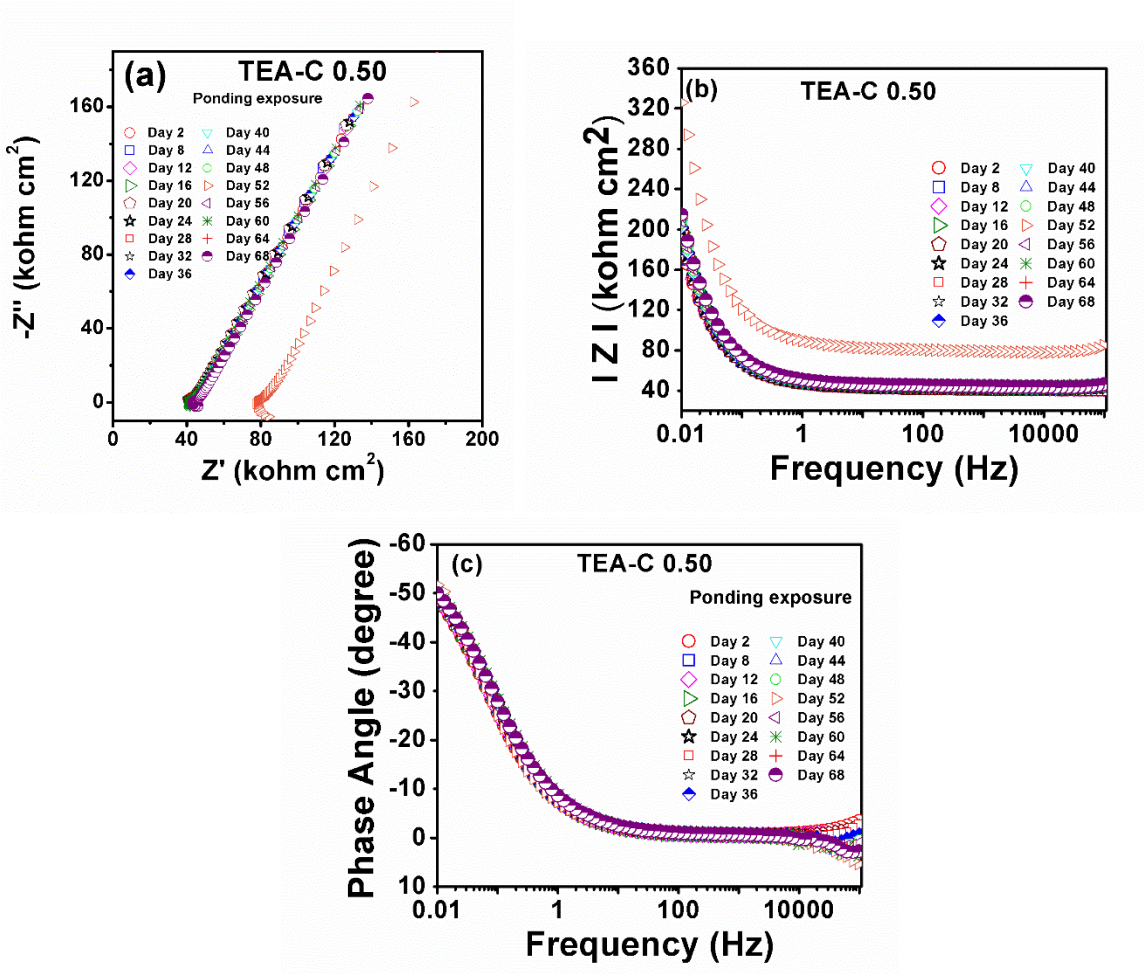

Figure 42. (a) Nyquist, (b) Bode, and (c) phase angle plots for microencapsulated triethanolamine 0.50% exposed to Ponding exposure.

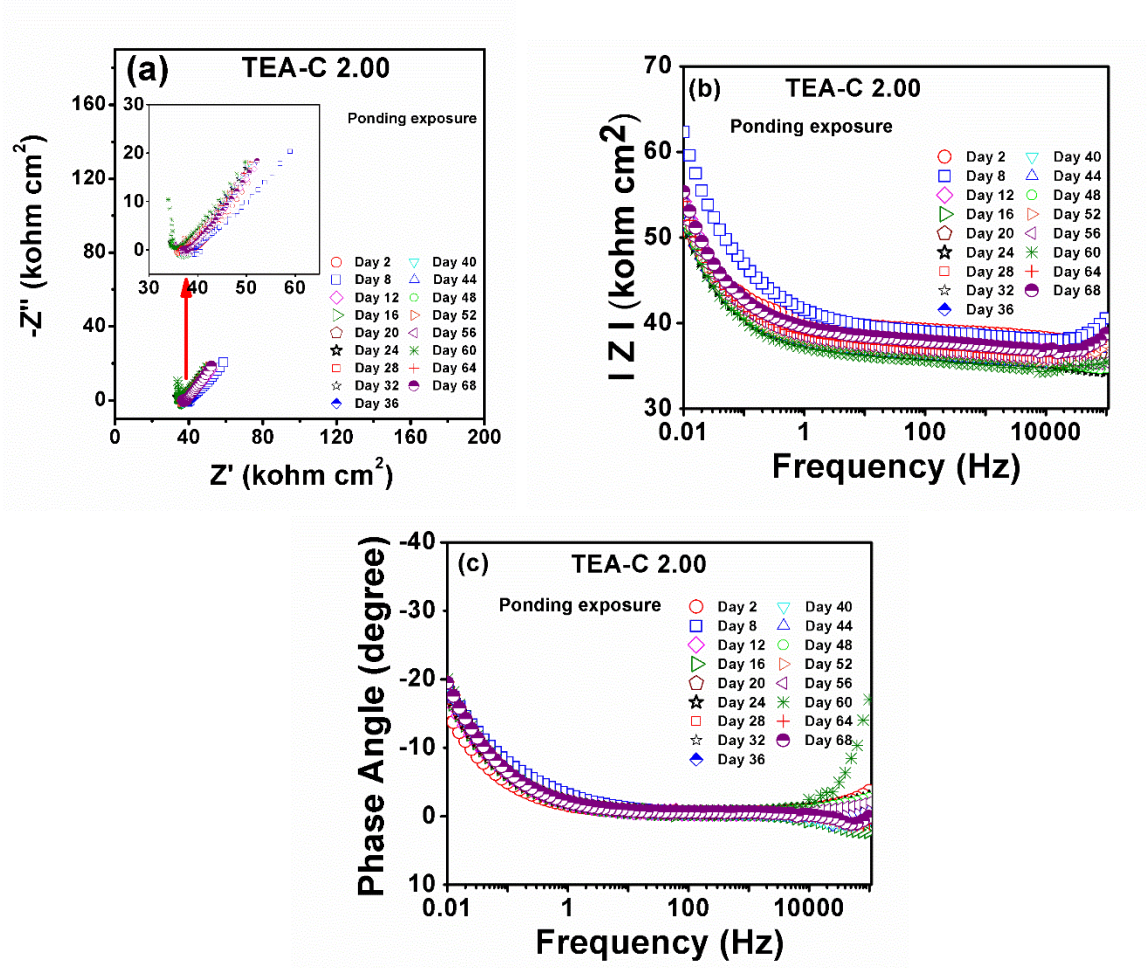

Figure 43. (a) Nyquist, (b) Bode, and (c) phase angle plots for microencapsulated triethanolamine 2.00% exposed to Ponding exposure.

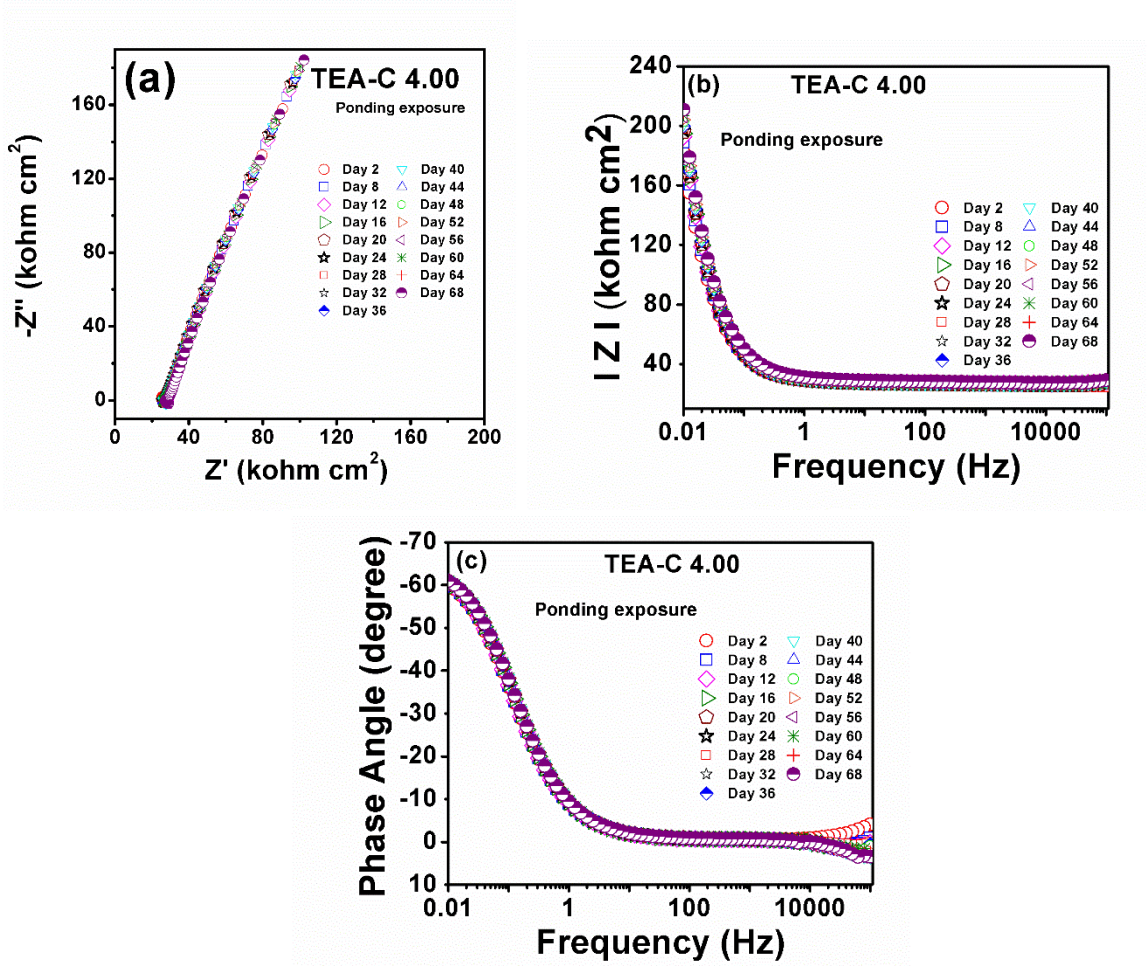

Figure 44. (a) Nyquist, (b) Bode, and (c) phase angle plots for microencapsulated triethanolamine 4.00% exposed to Ponding exposure.

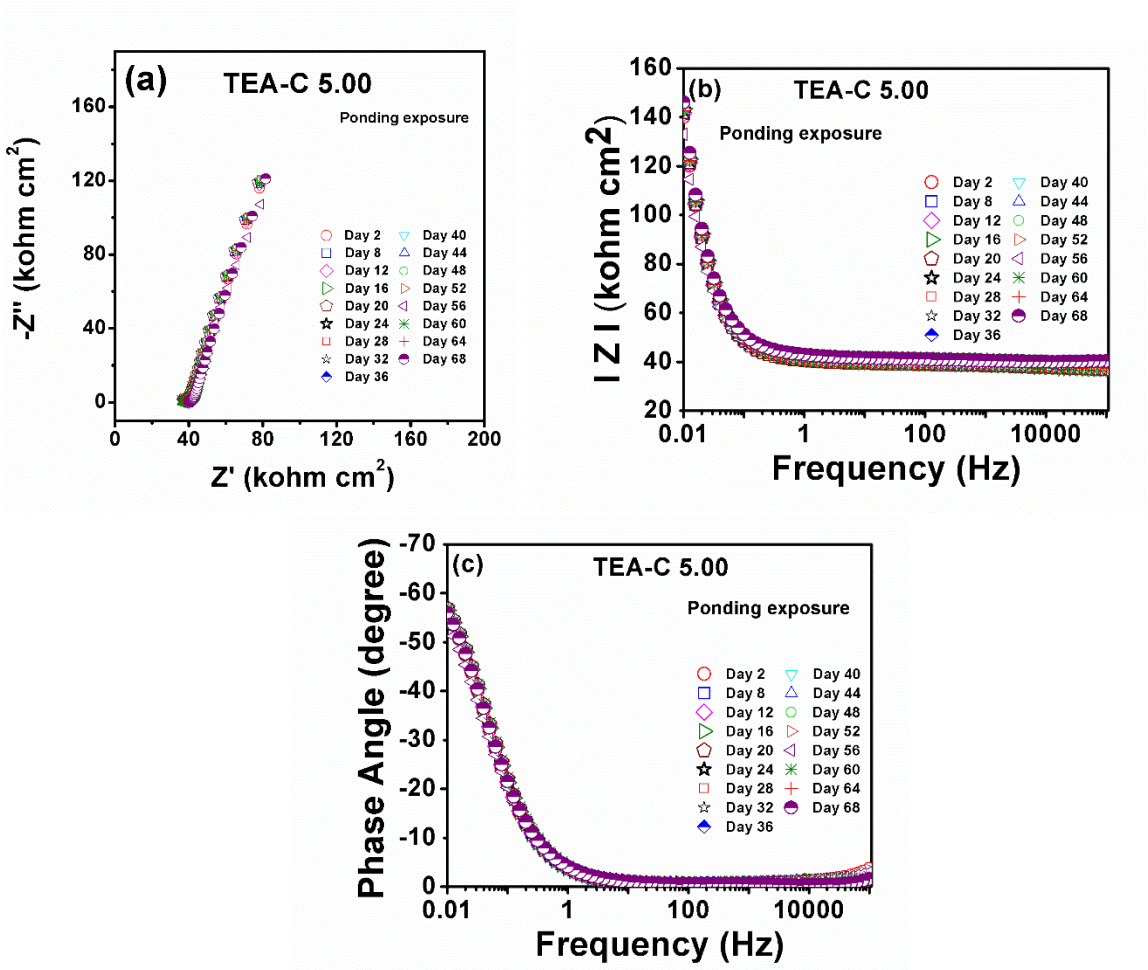

Figure 45. (a) Nyquist, (b) Bode, and (c) phase angle plots for microencapsulated triethanolamine 5.00% exposed to Ponding exposure.

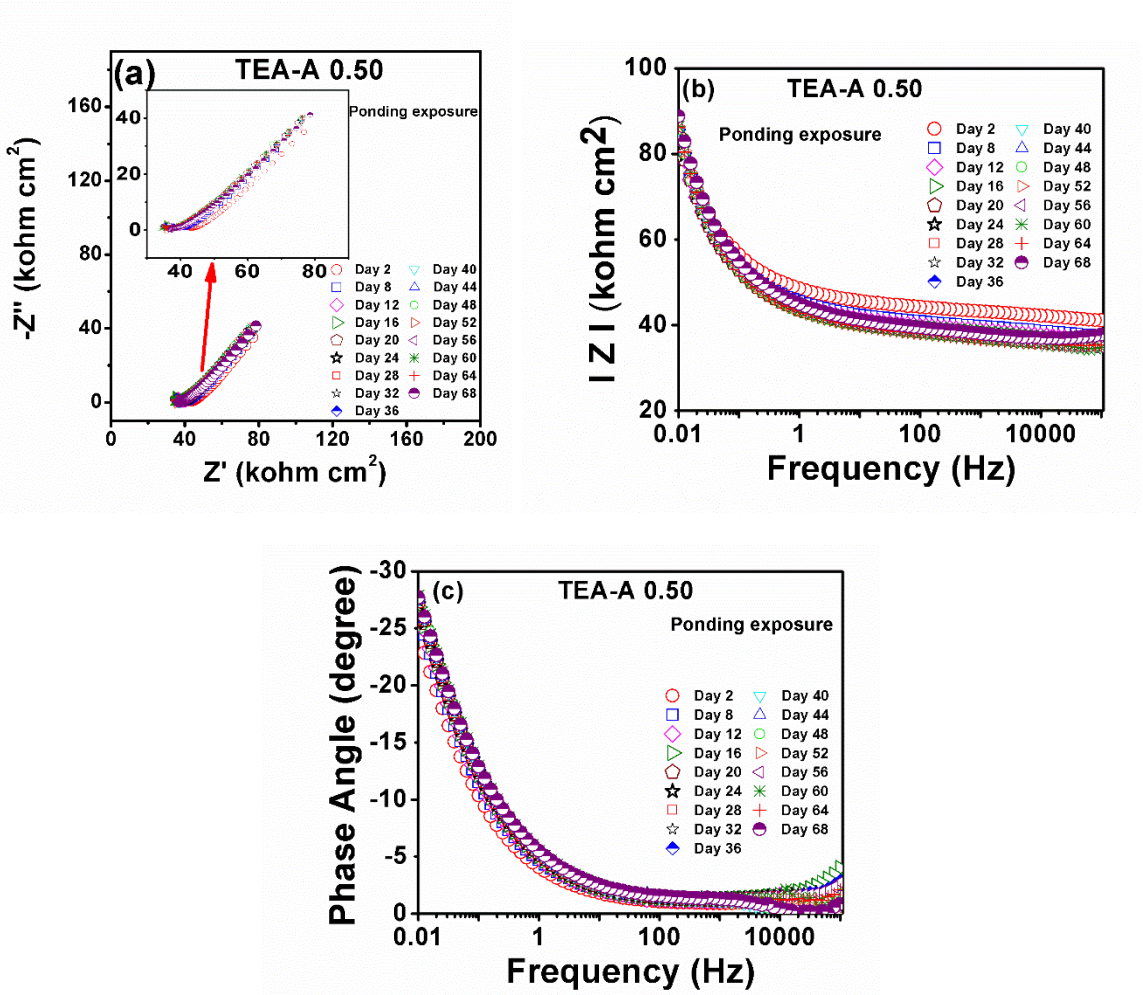

Figure 46. (a) Nyquist, (b) Bode, and (c) phase angle plots for admixed triethanolamine 0.50% exposed to Ponding exposure.

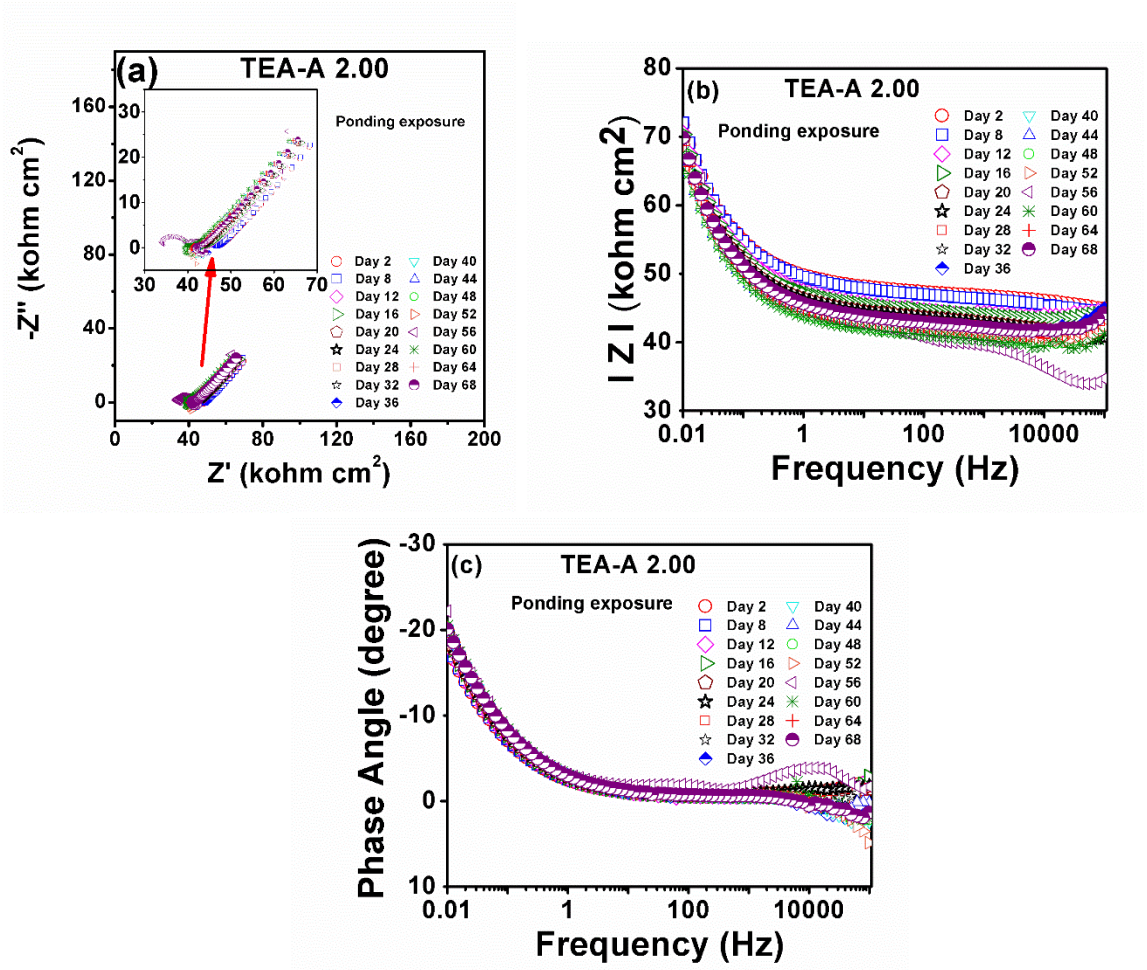

Figure 47. (a) Nyquist, (b) Bode, and (c) phase angle plots for admixed triethanolamine 2.00% exposed to Ponding exposure.

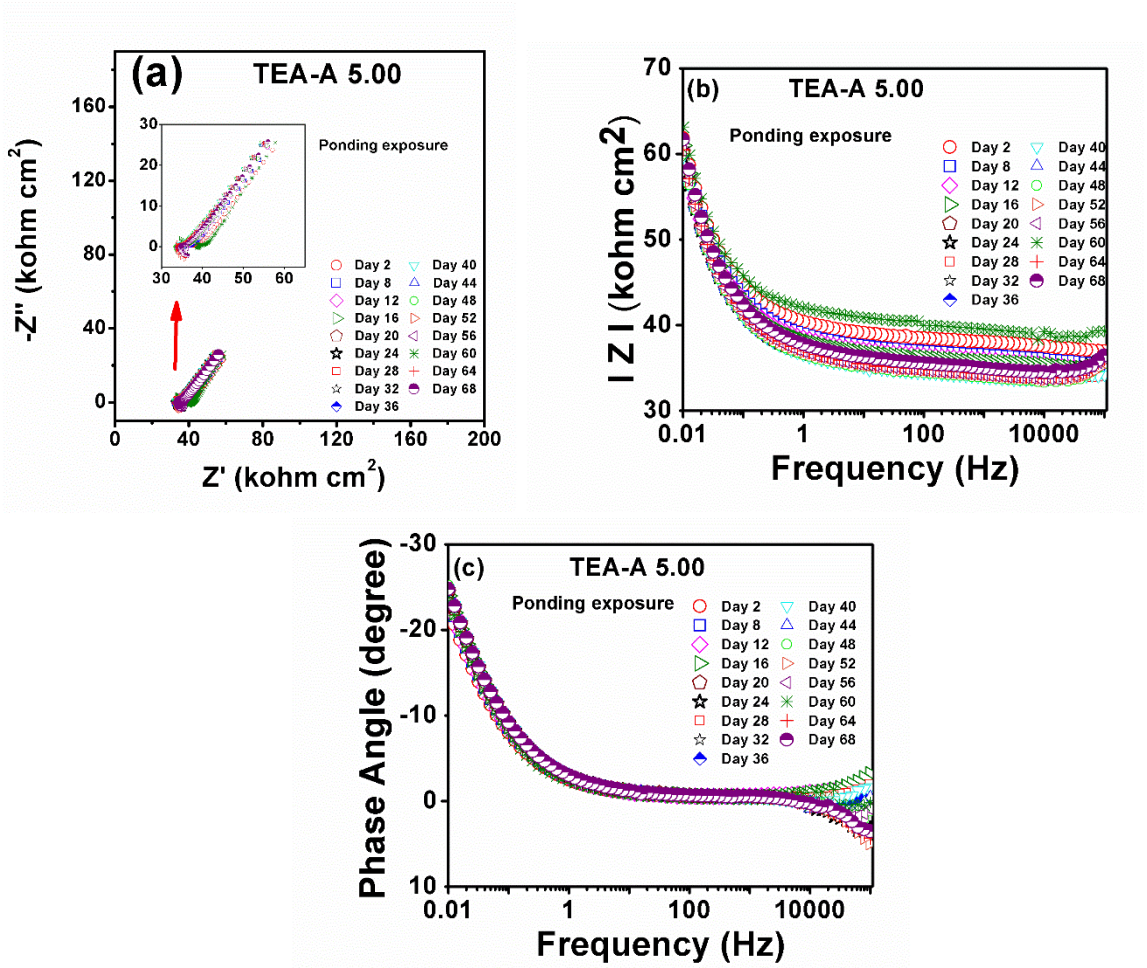

Figure 48. (a) Nyquist, (b) Bode, and (c) phase angle plots for admixed triethanolamine 5.00% exposed to Ponding exposure.

For the CN-A and CN-C samples exposed to the fog chamber exposure, the quarter circles (poorly defined capacitive loops) are observed in the Nyquist plots (Figures 49-55). This characteristic was also found in all types of samples exposed to continuous-then-cyclic, ASTM G109 cyclic, and ponding exposures. The impedance modulus of these samples were lower than the ones observed in the same type of samples exposed to ponding exposure. The modulus values are in the range of 30–40 kΩ-cm^2 in the fog chamber while they are between 40–60 kΩ-cm^2 in the ponding exposure, indicating that corrosion rate of rebars tested in the fog chamber was higher than the one in on the ponding exposure. The impedance modulus values of the Control sample for each exposure are close to the ones of inhibited samples, suggesting that admixed and microencapsulated calcium nitrate did not give a significant corrosion protection to the rebars. A small increase in corrosion resistance with an addition of CN might occur but it cannot be directly observed in the Bode plots. A corrosion rate calculation based on the polarization resistance values obtained from EIS spectra, in this case, could give a more accurate corrosion rate value for each sample.

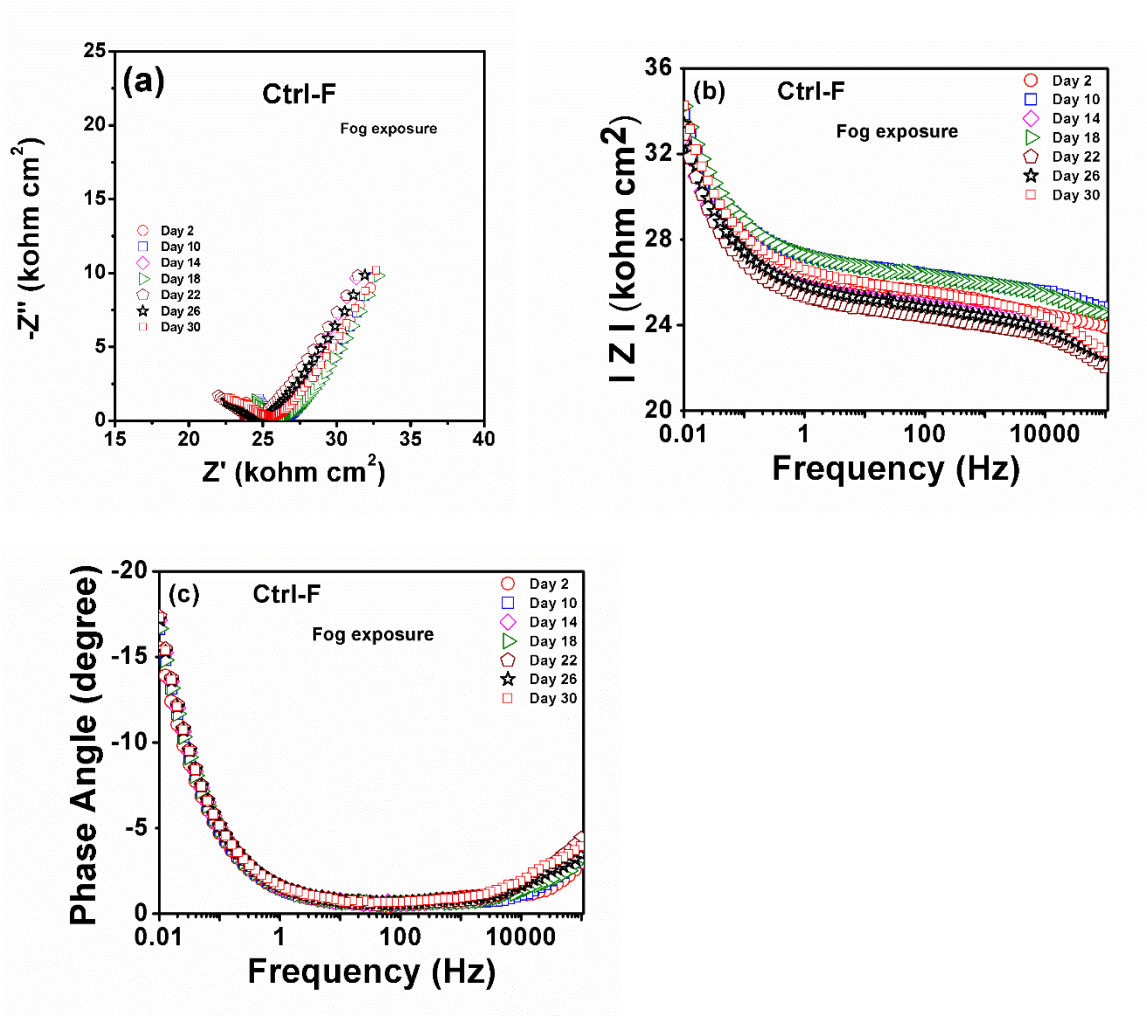

Figure 49. (a) Nyquist, (b) Bode, and (c) phase angle plots for the Control with fiber exposed to fog chamber exposure.

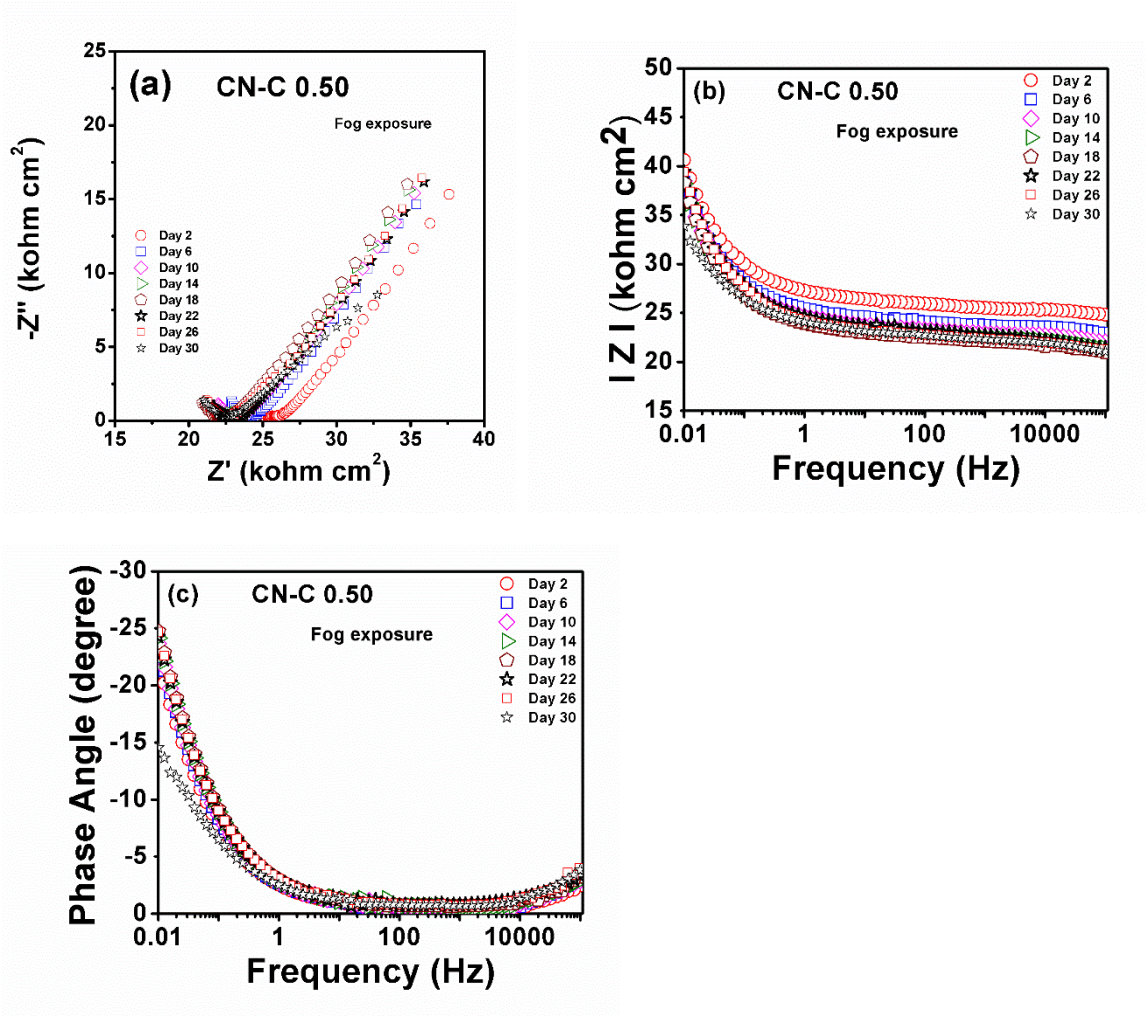

Figure 50. (a) Nyquist, (b) Bode, and (c) phase angle plots for the microencapsulated calcium nitrate 0.50% exposed to fog chamber exposure.

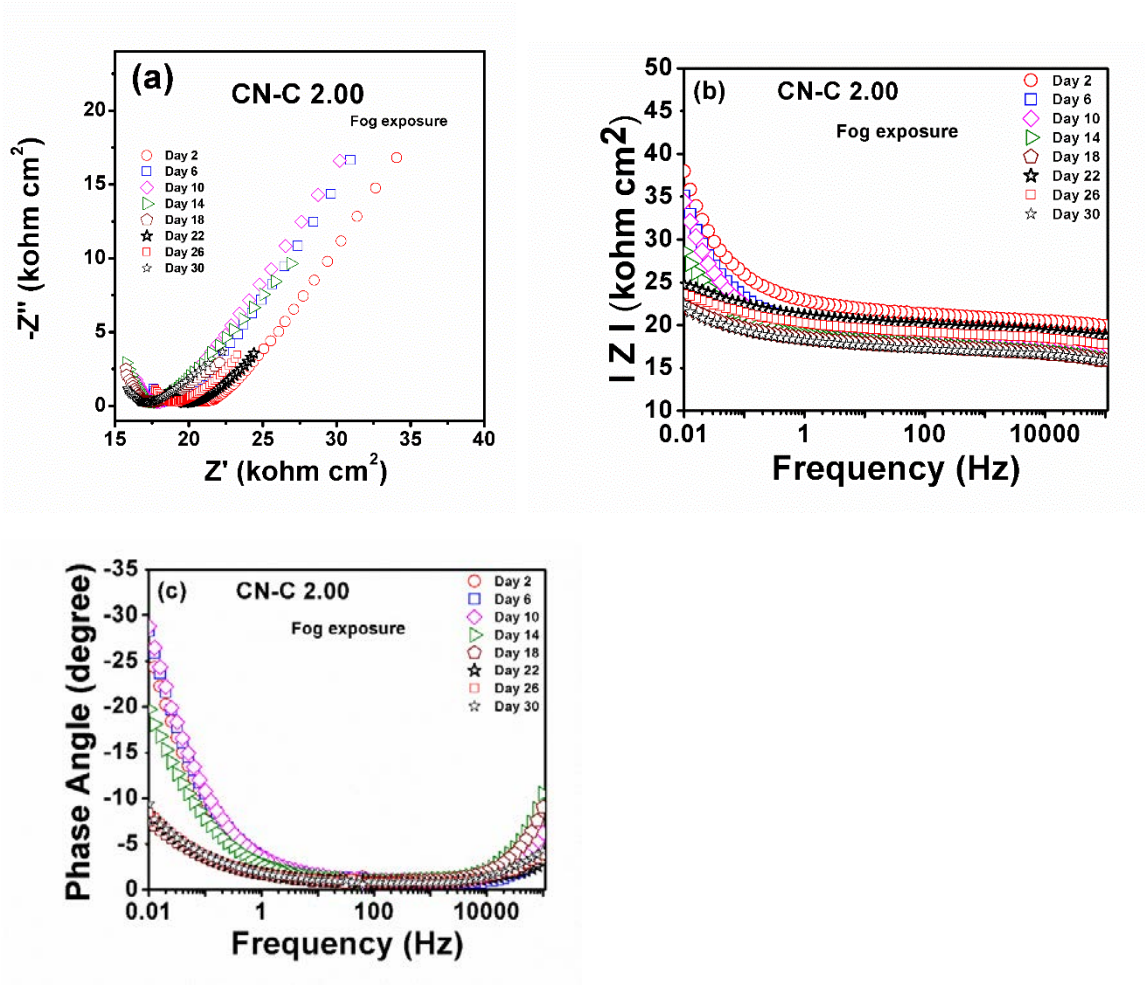

Figure 51. (a) Nyquist, (b) Bode, and (c) phase angle plots for the microencapsulated calcium nitrate 2.00% exposed to fog chamber exposure.

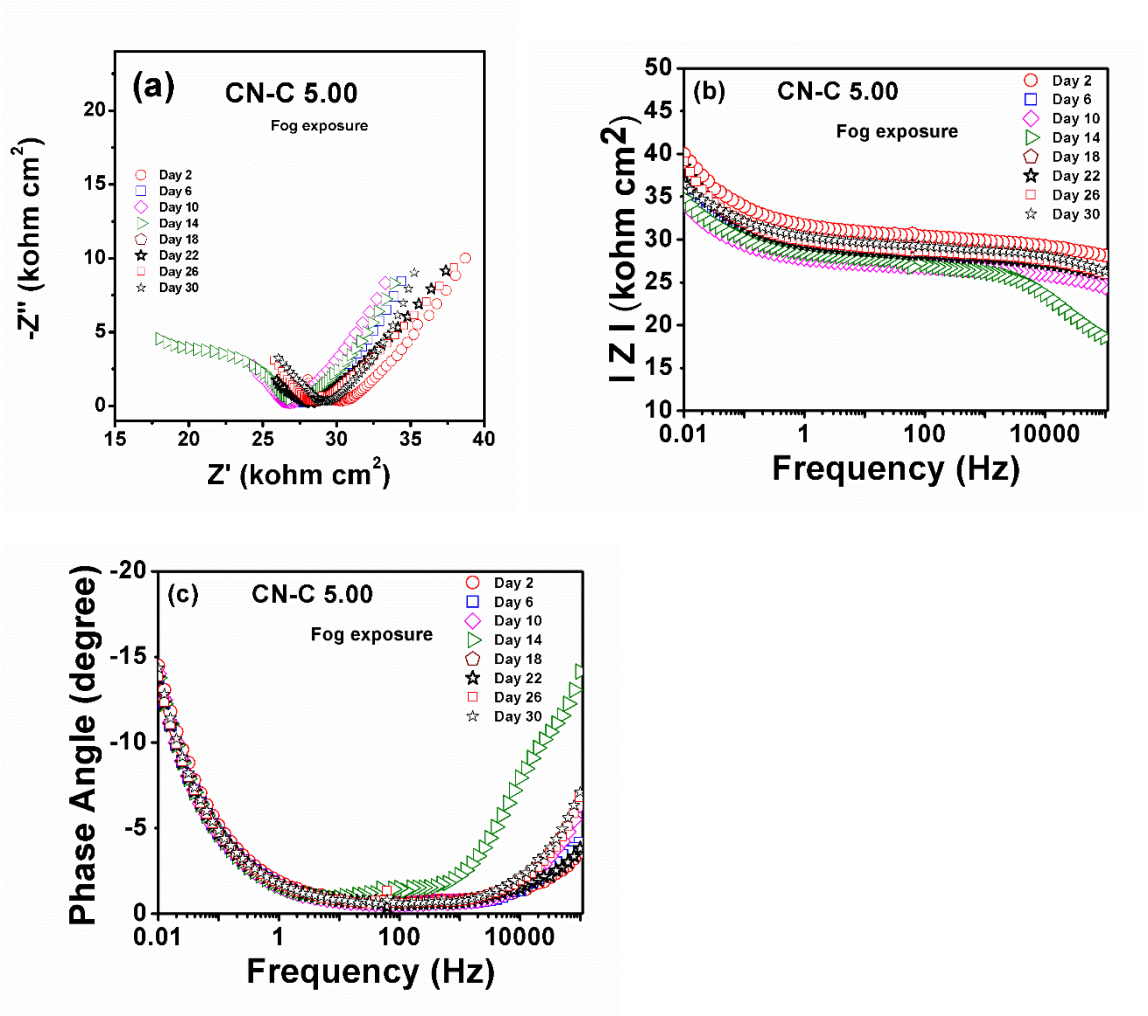

Figure 52. (a) Nyquist, (b) Bode, and (c) phase angle plots for the microencapsulated calcium nitrate 5.00% exposed to fog chamber exposure.

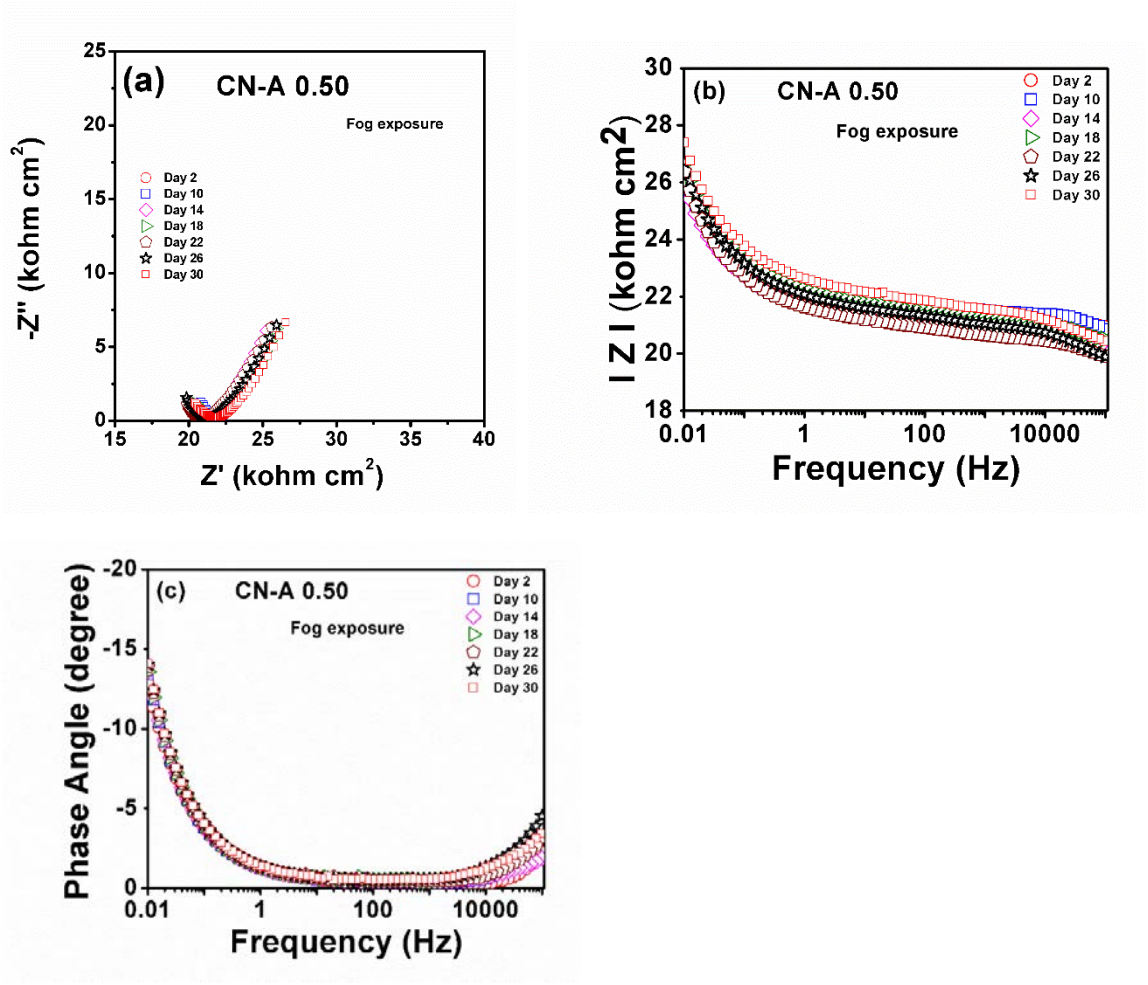

Figure 53. (a) Nyquist, (b) Bode, and (c) phase angle plots for the admixed calcium nitrate 0.50% exposed to fog chamber exposure.

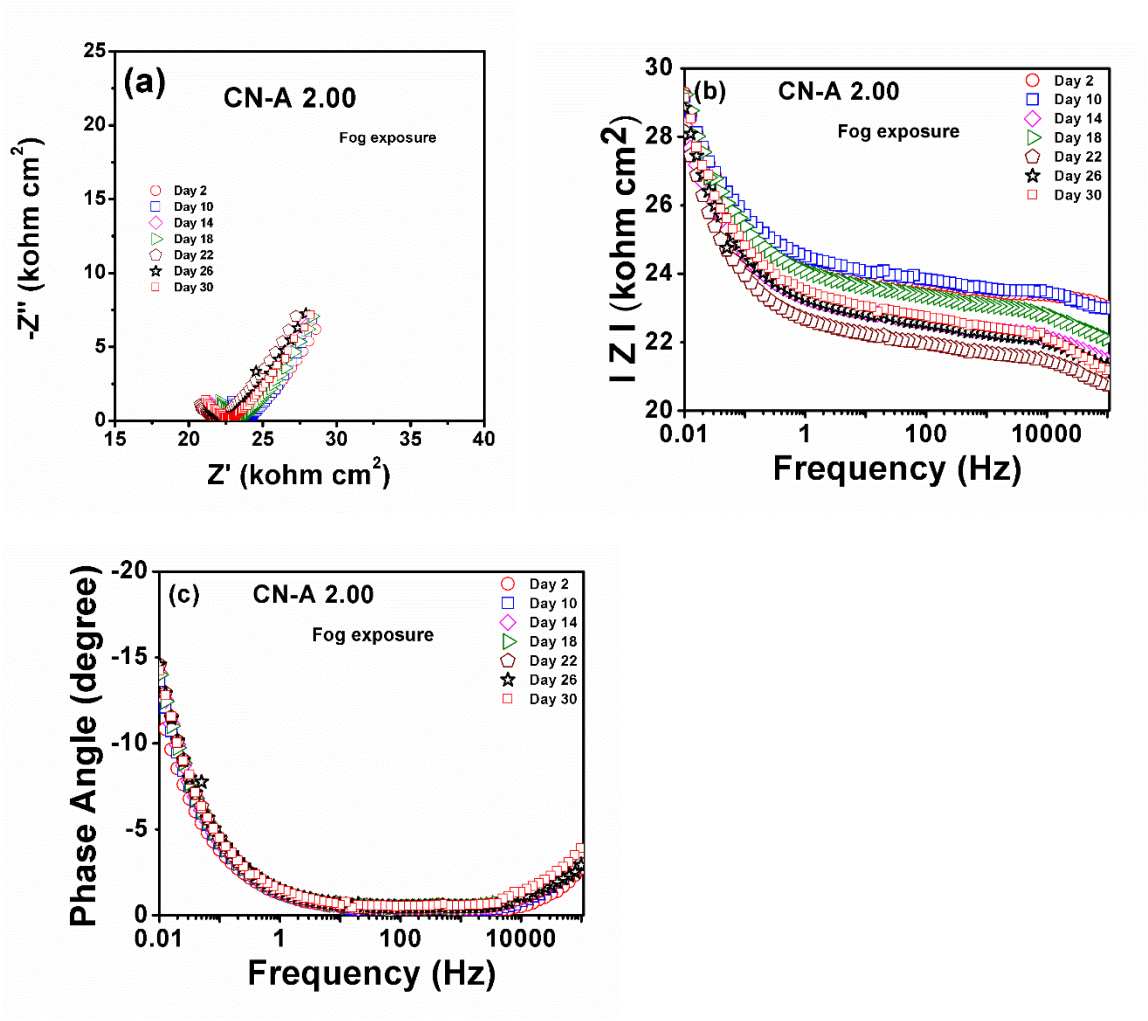

Figure 54. (a) Nyquist, (b) Bode, and (c) phase angle plots for the admixed calcium nitrate 2.00% exposed to fog chamber exposure.

.

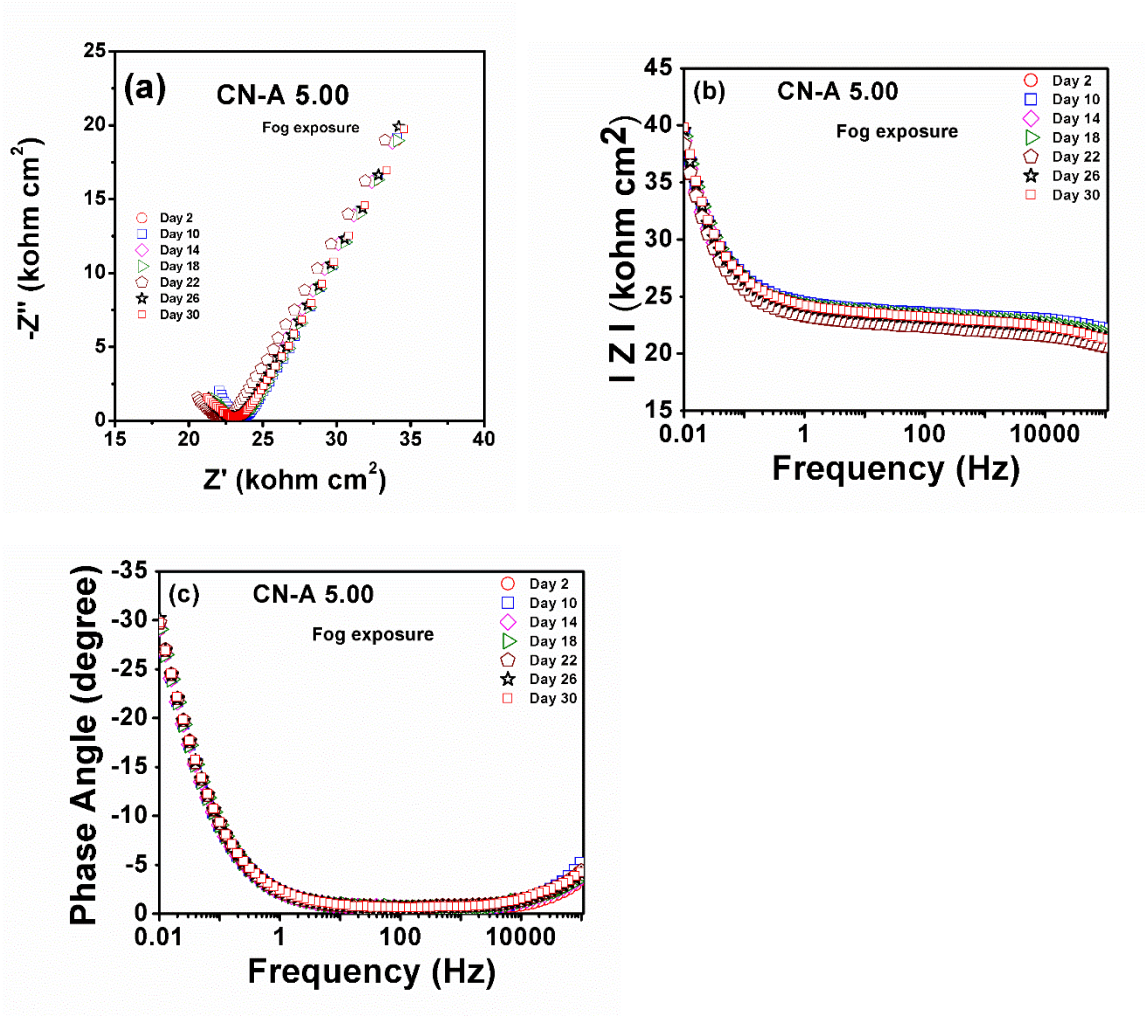

Figure 55. (a) Nyquist, (b) Bode, and (c) phase angle plots for the admixed calcium nitrate 5.00% exposed to fog chamber exposure.

5.3.4. Corrosion Rate and Percent Inhibition

The corrosion rates of samples exposed to different types of exposures are shown in Figures 56-58. In general, the corrosion rates of all samples in all exposures are considered to be insignificant because they are less than 1 mils/year (< 0.0254 mm/year). In general, for CN-I samples, it can be seen that an addition of corrosion inhibitor decreased the corrosion rate compared to the Control (Figure 56). Although there are some variations in the corrosion rates for CN-A and CN-C samples, the corrosion rate of CN-C is generally higher than the one for CN-A (Figure 57a). For TEA samples (Figure 57b), the corrosion rates are very slow, one order of magnitude lower than the ones for CN samples.

The percent of inhibition of all samples, in general, is considered to be low (Figure 59). The fluctuations are observed which are attributed to inconsistent corrosion rate on the Control and inhibited samples. Again, since the corrosion rate is considered to be insignificant, the percent inhibition calculation becomes complex and tends to give more errors.

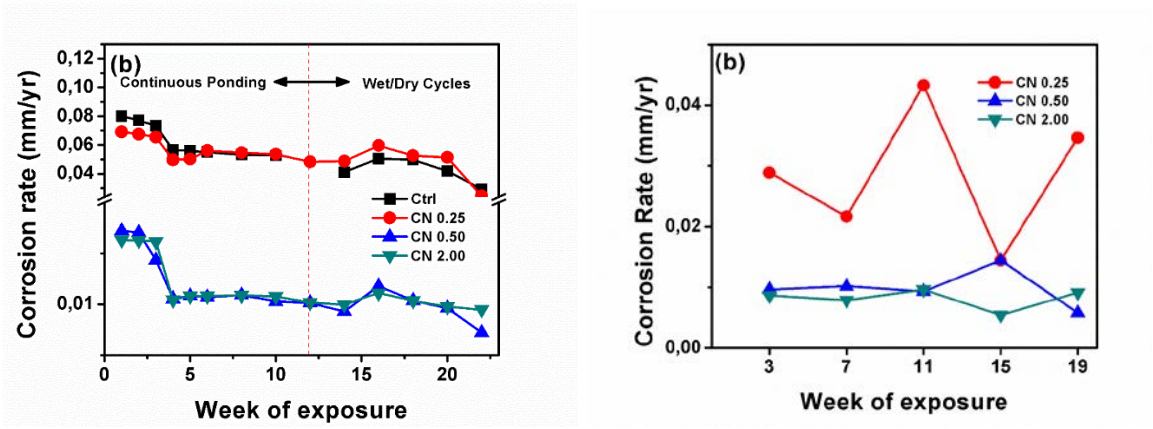

Figure 56. Corrosion rate for: (a) Control and microencapsulated nitrate exposed to continuous-then-cyclic exposure, and (b) only microencapsulated calcium nitrate exposed to ASTM G109 cyclic exposure.

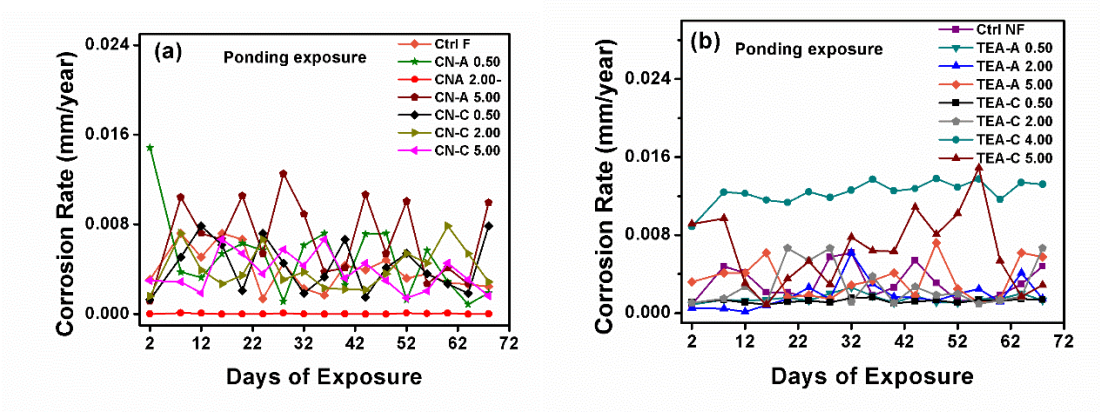

Figure 57. Corrosion rate for: (a) microencapsulated and admixed calcium nitrate and (b) microencapsulated and admixed triethanolamine exposed to ponding exposure.

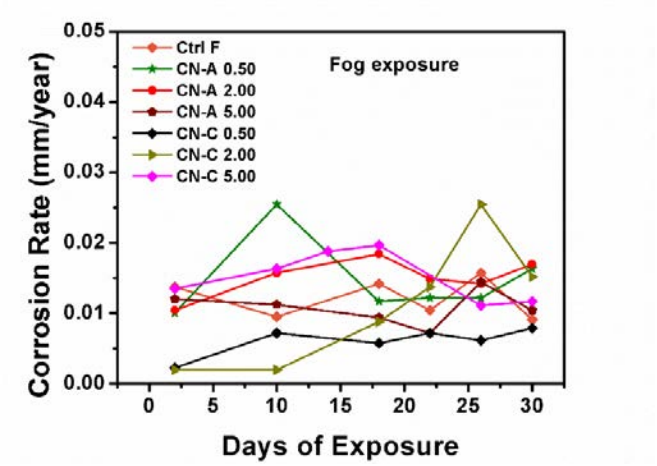

Figure 58. Corrosion rate for microencapsulated calcium nitrate exposed to fog exposure.

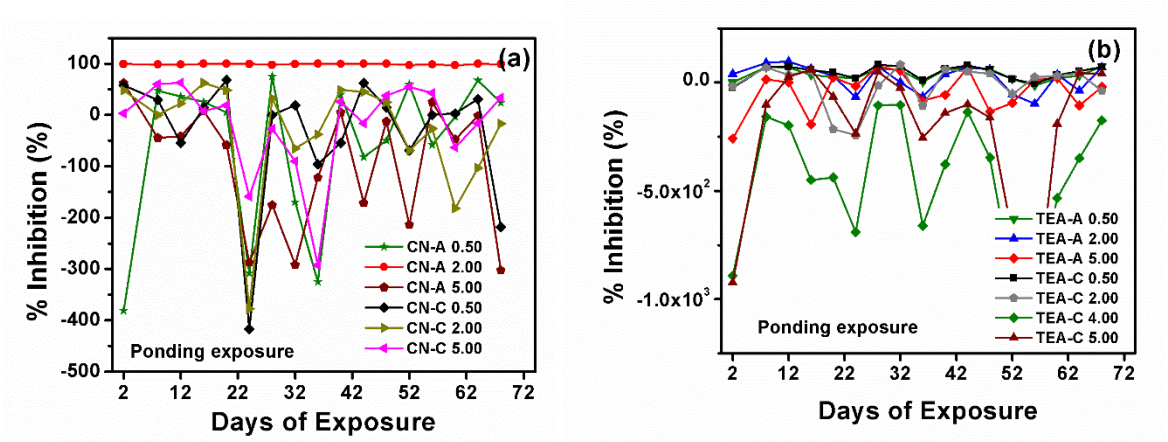

Figure 59. Percent inhibition for: (a) microencapsulated and admixed calcium nitrate, (b) and microencapsulated and admixed triethanolamine exposed to ponding exposure.

6. CONCLUSIONS

The first phase of this study focused on optimizing the procedures to encapsulate calcium nitrate and triethanolamine, and tested their effects on concrete properties, respectively. When varying the agitation rate, sulfonic acid catalyst concentration, and temperature, the morphology of the microcapsules containing calcium nitrate remained consistent, showing spherical capsules with a smooth outer edge. However, the concentration of the sodium bicarbonate wash (used to neutralize the sulfonic acid traces in the microcapsule's shell) was shown to deflate the microcapsules. Therefore, it is recommended to reduce the sodium bicarbonate wash concentration and exposure time to minimize impact on the microcapsule morphology while successfully neutralizing the sulfonic acid traces. With respect to microcapsule size, a variation in temperature did produce significant differences, where a higher temperature corresponded to a smaller mean diameter between those samples produced at 50 °C and those produced at 40 °C and 45 °C. The sulfonic acid concentration also had a significant effect on the mean microcapsule diameter, where a higher sulfonic acid concentration corresponded to a smaller particle size.

The encapsulation of triethanolamine (TEA) involved a four-step process, requiring the production of the seed latex material, the formation of an amphiphilic first shell, the formation of a hydrophobic second shell, and the neutralization of the seed materials with TEA (and thus loading the seed latex particles with TEA). A free radical polymerization process was utilized in order to synthesize the seed latex particles. Seed latex particles were modified at different molecular weights of methacrylic acid and methyl methacrylate to control carboxylic acid content of the seed latex. The carboxylic acid content has a direct impact on the amount of triethanolamine that is infused onto the seed latex particles. The initiator concentration by weight was modified for the solid weight content of the seed latex particles. The introduction of shell particles onto the seed latex particles occurred through a free radical polymerization process as well. Water content of shell particles were altered for a uniform dispersion of nanocapsules throughout the specimen. Sodium hydroxide concentration by weight was changed in order to create an environment with maximal activity amongst monomers.

With the addition of microcapsules admixed into the concrete matrix, it was shown that there is a decrease in the compressive strength for the encapsulated calcium nitrate. The decrease becomes significant with concentrations of microcapsules above 0.5% by weight of the cement. However, when polymer fibers are added onto the concrete matrix, the results did not reflect the same trend, since a higher concentration of microcapsules did not result in a weaker compressive strength (particularly at the 5% level). When triethanolamine capsules were added, nanocapsule concentrations higher than 0.5% resulted in a lower concrete strength. In addition, it should be noted that from all the sample groups tested in this study, those with admixed TEA nanocapsules resulted in significant differences in workability, since the added nanocapsules at higher concentrations dramatically changed since the added microcapsules changed the viscosity of the mixing water. Thus, TEA-C samples resulted in a stiff, dry mix with poor workability and no slump. At the highest nanocapsule concentrations (TEA-C 5.0%), the superplasticizer dosage was doubled to facilitate the concrete casting process. However, even with the use of the vibrating table, the compaction and consolidation of fresh concrete into the beam molds proved to be challenging and the hardened concrete cover's quality was poor, featuring honeycombing. Future research is needed to optimize a mix design that accommodates TEA nanocapsules in concrete.

With respect to the TEA-A group, it was observed that triethanolamine as an admixture is also compatible with concrete as it did not cause any significant differences in compressive strength relative to the control specimens. The only difference was observed with the TEA-A 2% specimen groups, which resulted in a significantly weaker compressive strength (a 10% decrease in strength). These results may not be in agreement with the literature (where triethanolamine as an admixture decreased concrete's compressive strength with higher dosages). This may be attributed to TEA's interaction with the defoaming agent, since the defoamer does strengthen concrete's mechanical properties and its ability to maintain the air content at a low percentage. On the other hand, the CN-A samples had no significant differences in compressive strength when compared to the control samples, with the exception of sample CN-A 2%.

The results of OCP measurements clearly showed that the rebars protected by CN-A were more passive than the ones by CN-C when they are exposed to ponding exposure. The OCP values for the Control were between the ones for CN-A and CN-C. The same trend was observed for TEA samples where the noblest OCP values were found for TEA-A, followed by the Control, and TEA-C. For CN-I samples, an increase in corrosion inhibitor resulted in more noble OCP values for the samples exposed to ASTM G109 cyclic samples, indicating a better corrosion protection. However, for the continuous-then-cyclic exposure, the positive effect of corrosion inhibitor on the corrosion tendency was not obvious due to inconsistent trend.

From EIS spectra results, it is evident that encapsulated TEA (TEA-C) is more effective in inhibiting corrosion than the TEA-A and the Control. This is based on the impedance modulus results, where TEA-C was observed to be four times higher than the TEA-A and Control specimens. The pH change that might be stimulated by wet/dry cycles successfully released and activated the encapsulated TEA. This is also supported by the fact that the phase angle at low frequency for TEA-A is close to zero, indicating that charge transfer reactions that are typical reactions for corrosion were a dominant process at the metal/concrete interface in the admixed samples. For both CN-A and CN-C, the inhibiting effect was found to be minor as suggested by their low impedance modulus difference. However, in general, their values were still higher than the ones for the Control which indicated an improvement in corrosion resistance of rebars with an addition of CN. The phase angle at low frequency indicated that the reaction at the metal/concrete interface in the admixed and microencapsulated samples were similar. Both sample groups had charge transfer reactions dominant at low frequencies. When exposed to the more aggressive environment (fog chamber), corrosion kinetics in both admixed and microencapsulated samples increased as evident by a decrease in the impedance modulus and phase angle.

The corrosion rate that was calculated using polarization resistance data in the EIS spectra, in general, showed that TEA-C samples had the lowest rate. However, since the corrosion rate of all samples are below 1 mils per year (less than 0.0254 mm/year), the difference in percent inhibition of all corrosion inhibitors could not be observed clearly.

From all these corrosion testing results, it can be concluded that TEA-C was more effective in giving a corrosion protection than TEA-A and the Control. In contrast, the corrosion protection performance of both CN-A and CN-C was alike. The corrosion kinetics was slightly reduced on inhibited rebars compared to unprotected rebars (the Control). When comparing TEA-C and CN-C, in the presence of each stimulus (pH changes for TEA-C, cracks for CN-C), TEA-

C protected the rebar better than CN-C did. For the admixture samples (TEA-A and CN-A) that do not need stimuli in the concrete, a stable and better corrosion protection was provided by CN-A.

The corrosion protection trend found in OCP was found to be different from the one in EIS spectra. This might be attributed to the ohmic drop effect across the concrete. This effect normally affects the OCP reading but it does not influence the phase angle reading in EIS. Therefore, the results of phase angle in EIS spectra is more reliable to study the performance of corrosion inhibitor in the good-quality concrete with a high concrete resistance.

6.1 Current Findings

We present the preparation and inhibition behavior of rebar in the presence of microencapsulated calcium nitrate (CN) with concentrations of 0.5, 2.0, and 5 wt.% in concrete. From both open circuit potential (OCP) and electrochemical impedance spectroscopy spectra, it was found that an addition of CN corrosion inhibitor-containing microcapsules into concrete beams successfully repassivated or maintained the passivity of the rebar when the concrete was cracked. This corrosion inhibitor healed the rebar by forming a passive layer on the rebar surface under the crack. This healing process was evident by an increase of OCP values to more positive values or by stable OCP values at around -100 mV vs SCE. An increase in phase angle after corrosion activation for CN C 2% clearly showed this healing process. The optimum concentration for maintaining the passivity on rebar in the cracked concrete was found to be 5 wt.%.

6.1.1 Encapsulation of Calcium Nitrate

The microencapsulation procedure was adapted from a previous study *(10)*. The process is based on a water-in-oil suspension polymerization reaction of polyurea-formaldehyde, where a 25% calcium nitrate solution (by weight) was encapsulated as the core material. The suspension polymerization reaction was enabled by heating at an elevated temperature (40 °C) in the presence of an acid catalyst (sulfonic acid) for 2 hours. The sulfonic acid concentration used was of 0.25% by wt. of organic solvent. Once the microcapsules were synthesized, any trace of sulfonic acid on the microcapsules' surface was neutralized by washing the microcapsule slurry with a 1% sodium bicarbonate solution. The microcapsules were then recovered through a vacuum filtration.

6.1.2 Concrete Mix Design

A water-cement ratio of 0.48 was selected through preliminary laboratory tests. The nominal maximum aggregate size was 19 mm for the coarse aggregate, and 4.76 mm for the fine aggregate, respectively. The microcapsules were embedded at varying concentrations of microencapsulated corrosion inhibitors by weight of cement to determine the minimal dosage required to mitigate corrosion considerably. A superplasticizer was added to increase the workability of the concrete mix. A defoaming agent was also added at a dosage of 0.1% by weight of cement to counter the increases in air voids caused by the addition of microcapsules in concrete. The details of the concrete mix design are shown in Table 13.

Table 13. Concrete mix design.

Material Description	Proportions (kg/m^3)
Aggregate 1: Sand, Southern Aggregates, LA	744
Aggregate 2: #67 Limestone, Pine Bluff	1151
Cement: Holcim Type I	297
Water: Mixing water	142
Air (%)	5.0
50 mm Polymer Fibers**	1.8
Admixture 1: Adva 195 (ml/100kg)	195
Admixture 2: Microcapsules* (%)	0%, 0.5%, 2.0%, 5.0%
Admixture 3: TEGO Antifoam MR 1015* (%)	0.10

Table 14 shows the characteristics of the specimens used in this study, where two 75 mm x 150 mm cylinders were poured per specimen group. Given that the microcapsules need to be ruptured during cracking to release the calcium nitrate, it was important to damage the concrete specimens in a controlled manner. As such, polymer fibers were added to increase the ductility of concrete, so as to prevent sudden failure when cracking the specimens. After 14 days of curing in a 95% relative humidity chamber, the specimens were subjected to a splitting tensile test, where a displacement rate (0.005 in/min) was applied until a crack was induced. The crack size was around 0.3 mm.

Table 14. Samples tested in current results.

Sample ID	Corrosion Inhibitor	Mechanism of Protection	Microcapsule Concentration (% by wt. of cement)	Corrosion Inhibitor Concentration (% by wt. of cement)	Fiber Reinforced?	Pre-Cracked?
CTRL	Control	N/A	0.00 %	0.00 %	Y	Y
CN C 0.50	Calcium Nitrate	Microcapsule	0.50 %	0.11 %	Y	Y
CN C 2.00	Calcium Nitrate	Microcapsule	2.00 %	0.44 %	Y	Y
CN C 5.00	Calcium Nitrate	Microcapsule	5.00 %	1.10 %	Y	Y

6.1.3 Exposure of Concrete Samples

The cylindrical concrete beams were pre-cracked before the exposure to release the calcium nitrate from the microcapsules. For the corrosive environment a 5% by weight NaCl brine was used to simulate an aggressive marine environment. Before exposure the top and bottom of the cylindrical samples were sealed with an epoxy to limit the exposure area of the rebar to that in the middle of the sample. To determine the effectiveness of the corrosion inhibitors, the electrochemical tests were performed as follow.

6.1.4 Electrochemical Testing

During exposure of the concrete samples, electrochemical tests were performed for 10 days. The electrochemical tests performed were open circuit potential (OCP) and electrochemical impedance spectroscopy (EIS). All tests were performed with a three-electrode system with saturated calomel electrode as the reference electrode, and a graphite rod as the counter electrode (Figure 60). The EIS testing was carried out from 10 kHz to 0.01 Hz with an amplitude of 10 mV.

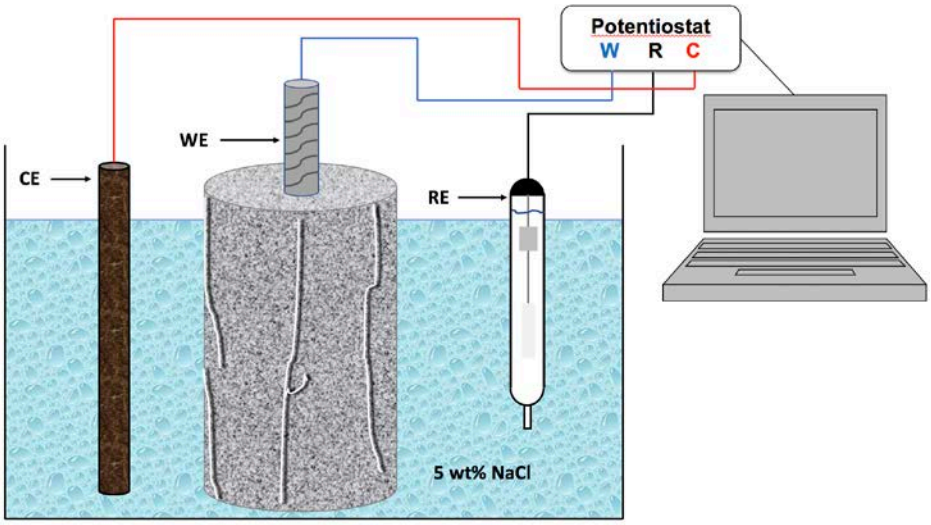

Figure 60. Experimental set-up for open circuit and electrochemical impedance spectroscopy measurement.

6.1.5 Discussion

Figure 61 shows an evolution of OCP values during 10 days of testing. In general, the control sample (without the microcapsule) showed the most active corrosion process compared to the microcapsule samples, as indicated by its lowest OCP values. It is also observed that the sample with 0.5 wt.% of microcapsules (CN C 0.5%) followed the similar trend found in the control sample, but the OCP value of CN C 0.5% decreased more gradually at more positive values. This may indicate there was a release of corrosion inhibitor from the capsule due to crack but the concentration was not sufficient to passivate the rebar surface under the crack.

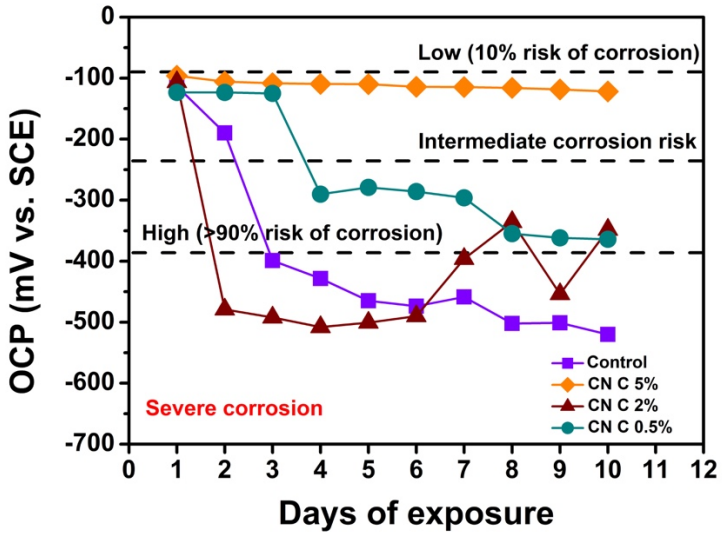

Figure 61. OCP change over the experimental period.

The sample with 2 wt.% of microcapsules (CN C 2%) showed the OCP trend that reflects the effect of inhibitor. The OCP values decreased during the first 4 days, but they then tend to be increased to be more positive as the inhibitor was released and activated. The last OCP value of this sample which was -350 mV vs. SCE indicated that corrosion inhibitor could not give

adequate corrosion protection regardless a passivation effect that can be seen from day 6 to 10. The sample with 5 wt.% microcapsule (CN C 5%) showed a better inhibiting performance compared to any other samples as its OCP values were far more positive than control and other inhibited samples. This suggests an addition of 5 wt.% microcapsule into the concrete is adequate to provide a corrosion protection to rebar.

Figures 62-63 show the comparison of the EIS results between the control sample and 2 wt.% microcapsule sample. Nyquist plots for the control (Figure 62a) and CN C 2% (Figure 62b) present the similar magnitude of real part of impedance (X-axis) but the imaginary part showed that the impedance for CN C 2% is higher. The semicircle Nyquist plot is observed more clearly in the Nyquist plot of CN C 2% from day 2 - 9. The final impedance found in CN C 2% sample was found to be higher than the one for the control sample, indicating better corrosion resistance in CN C 2% sample.

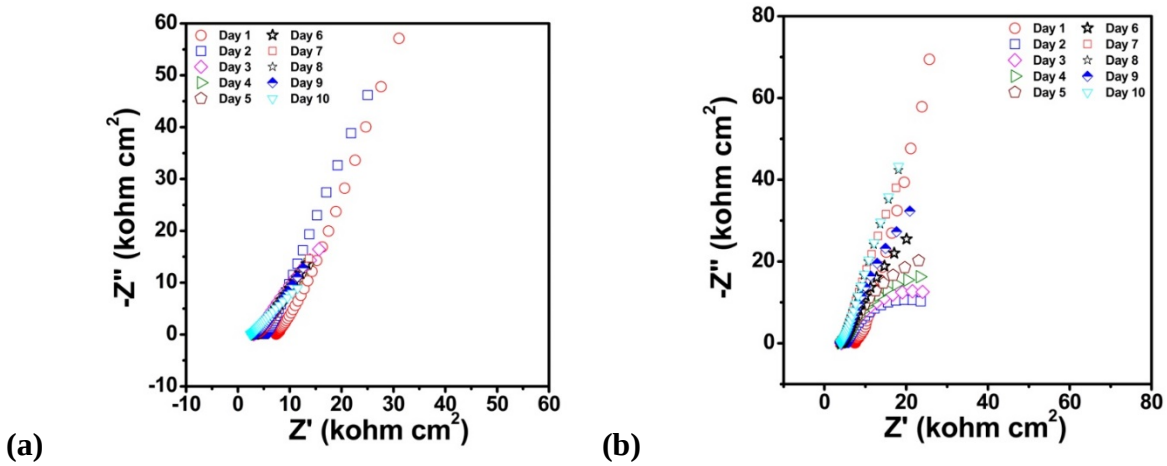

Figure 62. Nyquist plots for (a) Control and (b) CN C 2%.

From the Bode plots shown in Figure 63, the modulus of impedance for the control sample (Figure 63a) was lower than the one for the sample with CN C 2% (Figure 63b), indicating a lower corrosion resistance for the control sample. The modulus of impedance was found to be decreased from 65 to 15 kohm·cm^2 for the control sample, whereas it was 100 to 30 kohm·cm^2 for CN C 2%. The Phase angle plots for the control sample and CN C 2% are presented in Figure 5. Unlike the control sample (Figure 64a) that showed a continuous corrosion activation, CN C 2% sample (Figure 64b) showed a passive-active-repassivation transition behavior during 10 days of testing. This transition is clearly shown by a change in the number in time constant at the lowest frequency in CN 2 wt.% sample. At day 1, there was only one time constant, indicating the rebar was still passive. However, at day 2, the phase angle dropped from 70 to 20° which indicated a change from semi capacitive to resistive behavior. This decrease in phase angle was accompanied by the presence of second time constant at the low frequencies which corresponded to active corrosion process. From day 3 – 9, the phase angle increased from 30 to 60° and the second time constant gradually disappeared. At day 10, the second time constant almost disappeared and the phase angle reached almost 70°, which was the same as the phase angle at day 1. The disappearance of the second time constant is attributed to the repassivation of rebar by corrosion inhibitor.

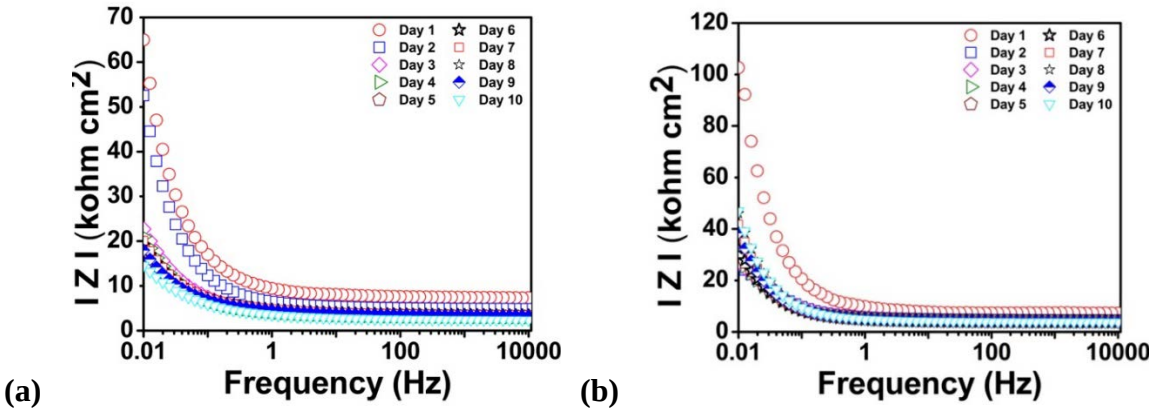

Figure 63. Bode plots for (a) Control and (b) CN C 2%.

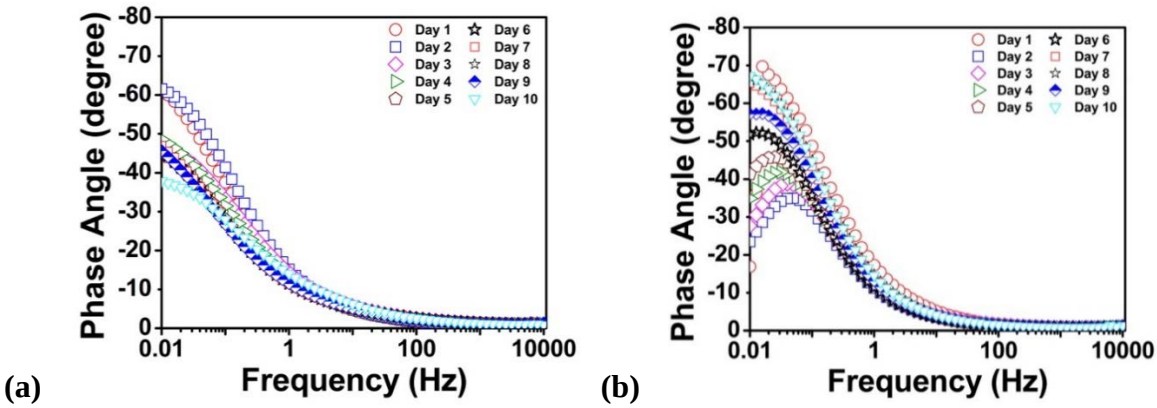

Figure 64. Phase angle plots for (a) Control and (b) CN C 2%.

The effect of encapsulated corrosion inhibitors in the concrete matrix was experimentally characterized in this study. From both OCP values and EIS spectra, it was found that an addition of calcium nitrate corrosion inhibitor-containing microcapsules into cracked concrete beams successfully repassivated or maintained the passivity of the rebar when the concrete is damaged. This corrosion inhibitor healed the rebar by forming a passive layer on the rebar surface under the crack. This healing process was evident by an increase of OCP values to more positive values or by stable OCP values at around -100 mV vs SCE during corrosion testing. An increase in phase angle after corrosion activation for CN C 2% clearly showed this healing process due to corrosion inhibitor. These results suggest that calcium nitrate encapsulated in polyurea-formaldehyde is a good candidate for anticorrosion self-healing system in the concrete. The optimum concentration of microcapsule containing calcium nitrate for maintaining the passivity on rebar in the cracked concrete was found to be 5 wt.%.

7. RECOMMENDATIONS

The innovative in-situ EIS measurements clearly demonstrated the reliability of the proposed technique to measure the EIS signatures in the fog chamber. This successful technique offers fast and reliable in-situ electrochemical measurements in the fog chamber for any systems, not only for the concrete. A natural continuation of this work would involve long-term corrosion testing, and possibly testing of other encapsulated corrosion inhibitors before moving towards field testing, where environmentally-friendly inhibitors will be highly desired. In addition, microcapsules that feature a pH controlled release behavior are recommended, as this can ensure the corrosion inhibition mechanism to occur precisely when needed.

REFERENCES

1. Hartt, W. H., R. G. Powers, V. Leroux, and D. K. Lysogorski. Critical Literature Review of High-Performance Corrosion Reinforcements in Concrete Bridge Applications: Final Report.*Fhwa-Hrt-04-093*, No. July, 2004, .

2. ASCE. 2017 Infrastructure Report Card. 2017, Available at: https://www.infrastructurereportcard.org/.

3. Zuo, J. et al. Preparation of metal hydroxide microcapsules and the effect on pH value of concrete.*Constr. Build. Mater.*, Vol. 155, 2017, pp. 323–331. Available at: http://www.sciencedirect.com/science/article/pii/S0950061817314988.

4. Dong, B. et al. Electrochemical impedance study on steel corrosion in the simulated concrete system with a novel self-healing microcapsule.*Constr. Build. Mater.*, Vol. 56, 2014, pp. 1–6. Available at: http://www.sciencedirect.com/science/article/pii/S0950061814001044.

5. Østnor, T. A., and H. Justnes. Anodic corrosion inhibitors against chloride induced corrosion of concrete rebars.*Adv. Appl. Ceram.*, Vol. 110, No. 3, 2011, pp. 131–136. Available at: http://www.tandfonline.com/doi/full/10.1179/1743676110Y.0000000017.

6. White, S. R. et al. Autonomic healing of polymer composites.*Nature*, Vol. 409, No. 6822, 2001, pp. 794–797. Available at: http://dx.doi.org/10.1038/35057232.

7. Choi, H., Y. K. Song, K. Y. Kim, and J. M. Park. Encapsulation of triethanolamine as organic corrosion inhibitor into nanoparticles and its active corrosion protection for steel sheets.*Surf. Coatings Technol.*, Vol. 206, No. 8–9, 2012, pp. 2354–2362. Available at: http://dx.doi.org/10.1016/j.surfcoat.2011.10.030.

8. Ghosh, S. K. *Functional Coatings*, 2006. Available at: http://dx.doi.org/10.1002/3527608478.ch1.

9. Rodson, M., and H. B. Scher. Water-in-oil microencapsulation process and microcapsules produced thereby. 2000, Available at: https://www.google.com/patents/US6113935.

10. Milla, J., M. H. Marwa, and T. Rupnow. Evaluation of Self-Healing Concrete with Microencapsulated Calcium Nitrate.*J. Mater. Civ. Eng.*, Vol. 29, No. 12, 2017, pp. 4017235. Available at: https://doi.org/10.1061/(ASCE)MT.1943-5533.0002072.

11. Hassan, M. M., J. Milla, T. Rupnow, M. Al-Ansari, and W. H. Daly. Microencapsulation of Calcium Nitrate for Concrete Applications.*Transp. Res. Rec. J. Transp. Res. Board*, Vol. 2577, 2016, pp. 8–16. Available at: http://dx.doi.org/10.3141/2577-02.

12. Choi, H., K. Y. Kim, and J. M. Park. Encapsulation of aliphatic amines into nanoparticles for self-healing corrosion protection of steel sheets.*Prog. Org. Coatings*, Vol. 76, No. 10, 2013, pp. 1316–1324. Available at: http://dx.doi.org/10.1016/j.porgcoat.2013.04.005.

13. The Editors of Encyclopaedia Britannica. Polymerization.*Encycl. Br.*, 2016, Available at: https://www.britannica.com/science/polymerization.

14. Tuutti, K. *Corrosion of Steel in Concrete*. Swedish Cement and Concrete Research Institute, Stockholm, 1982.

15. Grubb, J. A., H. S. Limaye, and A. M. Kakade. Testing pH of Concrete.*Concr. Int.*, Vol. 29, No. 4, 2007, .

16. Söylev, T. A., and M. G. Richardson. Corrosion inhibitors for steel in concrete: State-of-the-art report.*Constr. Build. Mater.*, Vol. 22, No. 4, 2008, pp. 609–622. Available at: http://www.sciencedirect.com/science/article/pii/S0950061806002959.

17. Al-Amoudi, O. S. B., M. Maslehuddin, A. N. Lashari, and A. A. Almusallam. Effectiveness of corrosion inhibitors in contaminated concrete.*Cem. Concr. Compos.*, Vol. 25, No. 4, 2003, pp. 439–449. Available at: http://www.sciencedirect.com/science/article/pii/S0958946502000847.

18. Vaysburd, A. M., and P. H. Emmons. How to make today's repairs durable for tomorrow — corrosion protection in concrete repair.*Constr. Build. Mater.*, Vol. 14, No. 4, 2000, pp. 189–197. Available at: http://www.sciencedirect.com/science/article/pii/S0950061800000222.

19. Montes, P., T. W. Bremner, and D. H. Lister. Influence of calcium nitrite inhibitor and crack width on corrosion of steel in high performance concrete subjected to a simulated marine environment.*Cem. Concr. Compos.*, Vol. 26, No. 3, 2004, pp. 243–253. Available at: http://www.sciencedirect.com/science/article/pii/S095894650300043X.

20. El-Jazairi, B. et al. *The use of calcium nitrate as a corrosion inhibiting admixture to steel reinforcement in concrete*. Elsevier, London, 1990.

21. Berke, N., F. Gianetti, P. G. Tourney, and Z. G. Matta. *4th international conference on deterioration and repair of reinforced concrete in the Arabian Gulf*, 1993.

22. Osial, M., and D. Wiliński. Organic substances as corrosion inhibitors for steel in concrete – an overview.*J. Build. Chem.*, Vol. 1, 2016, pp. 42–53.

23. Perez, J. P. et al. Why TIPA Leads to an Increase in the Mechanical Properties of Mortars Whereas TEA Does Not.*Spec. Publ.*, Vol. 217, .

24. Dodson, V. H. *Concrete Admixtures*. Springer Science & Business Media, 2013.

25. Ramachandran, V. S. Action of triethanolamine on the hydration of tricalcium aluminate.*Cem. Concr. Res.*, Vol. 3, No. 1, 1973, pp. 41–54. Available at: http://www.sciencedirect.com/science/article/pii/0008884673900604.

26. Ramachandran, V. S. Influence of triethanolamine on the hydration characteristics of tricalcium silicate.*J. Appl. Chem. Biotechnol.*, Vol. 22, No. 11, 1972, pp. 1125–1138. Available at: https://doi.org/10.1002/jctb.5020221102.

27. Corrosion Inhibition in Reinforced Concrete.No. European Patent Application No. 86304383.2, .

28. Ormellese, M., L. Lazzari, S. Goidanich, G. Fumagalli, and A. Brenna. A study of organic substances as inhibitors for chloride-induced corrosion in concrete.*Corros. Sci.*, Vol. 51, No. 12, 2009, pp. 2959–2968. Available at: http://www.sciencedirect.com/science/article/pii/S0010938X09003692.

29. Wang, Y. et al. Self-immunity microcapsules for corrosion protection of steel bar in reinforced concrete.*Sci. Rep.*, Vol. 5, 2015, pp. 18484. Available at: http://www.ncbi.nlm.nih.gov/pmc/articles/PMC4682076/.

30. Dong, B. et al. Smart releasing behavior of a chemical self-healing microcapsule in the stimulated concrete pore solution.*Cem. Concr. Compos.*, Vol. 56, 2015, pp. 46–50. Available at: http://www.sciencedirect.com/science/article/pii/S0958946514002121.

31. Dong, B., Y. Wang, N. Han, and F. Xing. *Proceeding of fourth international conference for self-healing materials*, 2013.

32. Dong, B., Y. Wang, N. Han, and F. Xing. *Proceeding of fourth international conference for self-healing materials*, 2013.

33. Milla, J., M. M. Hassan, T. Rupnow, M. Al-Ansari, and G. Arce. Effect of Self-Healing Calcium Nitrate Microcapsules on Concrete Properties.*Transp. Res. Rec. J. Transp. Res. Board*, Vol. 2577, 2016, pp. 69–77. Available at: http://dx.doi.org/10.3141/2577-09.

34. Broomfield, J. P. *Corrosion of steel in concrete: Understanding, investigation and repair*. Taylor & Francis, London, 2007.